

Norges miljø- og
biovitenskapelige
universitet

Master's Thesis 2016 30 ECTS

Department of Mathematical Sciences and Technology

Effect of Soiling on the Performance of Photovoltaic Modules in Kalkbult, South Africa

Mari Benedikte Øgaard

Environmental Physics and Renewable Energy

Preface

This study is investigating the effect of soiling on the performance of photovoltaic modules in Kalkbult, South Africa, and is based on an initiative promoted by Institute for Energy Technology (IFE), in collaboration with Stellenbosch University and Scatec Solar.

Calling the process of writing a master thesis an adventure is overused and a cliché. However, this semester has led me across the world, into the deepest deserts and up medium tall mountains. I have eaten antelope, been defrauded, met incredible nice and interesting people, I got to test my more practical engineering skills by fixing a car with a rope in the middle of nowhere, and I almost died a few times because I never got used to cars driving on the wrong side of the road. And I have learned a lot. So, I will discard my reluctance towards pompous language, and call it an adventure anyway.

This adventure would not have been so fun and interesting if it had not been for all the people assisting me along the way.

First of all, I want to thank Josefine Selj, my supervisor at IFE, for optimistic support and excellent guidance. I would also like to thank my supervisor at NMBU, Arne Auen Grimenes, for his enthusiasm, invaluable advices and time.

I have to thank Armand du Plessis, Carmen Lewis and Tashriq Pandy for interesting discussions, answering all my questions regarding the test station and measuring equipment, and for support during my experiments at the test station in Kalkbult. Your assistance before and during my stay in South Africa was invaluable, and I will be forever grateful that you introduced me to South African hospitality. I would also like to thank Johann Strauss for assistance in Stellenbosch regarding measurement equipment, and I have to thank OREEC and IFE for supporting my trip to Stellenbosch and Kalkbult financially.

I am also very grateful for the opportunity to get to know the research environment at IFE. To follow the work of the dedicated and enthusiastic researches at the Department for Solar Energy has been truly inspirational. I am very thankful for your interest in my research and results. Especially I want to thank Lenny Enström for helping me with measurement equipment, Halvard Haug for assisting me in the use of the *IV*-fit program, and Ashenafi Weldemariam for introducing me to the test site and the project.

Finally, I want to thank my mother, Anne Falk Øgaard, for good advices in the beginning of the process of writing my master thesis, and for reading and commenting my final result.

Kjeller, 09.12.2016

Mari Benedikte Øgaard

Sammendrag

Med høy solinnstråling, vidstrakte landområder som er lite utnyttet på grunn av tørt klima, og gode økonomiske og politiske forhold for investeringer i fornybar energi, har Sør-Afrika et stort potensiale for utnyttelse av solenergi. En ulempe med områder hvor det er tørt klima og lite regn, er at lyset som treffer solcellene kan bli redusert på grunn av støv som samler seg på modulooverflaten. Om det innkommende lyset blir redusert, vil også den leverte effekten bli mindre.

Formålet med denne oppgaven er å undersøke i hvor stor grad tilsmussing av overflaten på fotovoltaiske moduler reduserer generert effekt i et område i Northern Cape-regionen i Sør-Afrika. Effekten av støv på overflaten av modulene er estimert gjennom analyse av måledata fra et testanlegg ved Scatec Solars solpark i Kalkbult. Ytelsen til regelmessig vaskede og uvaskede solcellemoduler er sammenlignet, og påvirkningen av støv er undersøkt for både polykrystallinske silisiumsolceller og kadmium tellurid tynnfilmceller. Forskjellige vasketeknikker og virkningen av et anti-støvprodukt er også testet. Dataanalysen er supplementert med en eksperimentell del utført ved testanlegget, hvor det ble gjort målinger for å kvantifisere støvmengden på modulene og endringene i transmittans gjennom modulglassene som følge av tilsmussing.

I tidsperioden dekket av dataanalysen (04.05.2016 – 04.11.2016) var effekttap som kan forklares med tilsmussing av modulooverflaten bare signifikant i vintermånedene mai-juli. Tynnfilmmodulene opplevde større tap enn silisiummodulene, og modulene med anti-støvproduktet samlet mot forventning mer støv enn modulene uten. I juli, når tapene på grunn av tilsmussing var på sitt høyeste, var det gjennomsnittlige effekttapet på grunn av støv 1 % for silisiummodulene uten anti-støvprodukt, 2 % for silisiummodulene med anti-støvprodukt, og 4 % for tynnfilm-modulene med anti-støvprodukt.

For silisiummodulene ble det vist at kraftig nedbør vasket modulooverflaten godt nok til at ytelsen til modulene gikk tilbake til det nivået den var på når modulene var rene. For tynnfilmmodulene ble ytelsen også økt etter regn. Det kan derimot virke som overflaten til tynnfilmmodulene ikke ble vasket godt nok, og fortsatt opplevde støvrelaterte tap etter kraftig nedbør.

Kvantifiseringen av støvmengden på modulene antydte en daglig støvakkumulering på 13 – 22 mg/m² i oktober. Dette er lavt sammenlignet med resultater fra andre studier, og bekrefter at oppsamling av støv på modulooverflaten skjer langsomt i vårmånedene. Dette kan forklare at det ikke ble påvist noen signifikante tap på grunn av støv i perioden fra august til oktober.

Transmittansmålingene bekrefter at to og en halv dag med naturlig oppsamling av støv i Kalkbult i oktober ikke er nok til å signifikant redusere det innkommende lyset som treffer solcellene.

Abstract

With high irradiance, widespread semi-dry, unexploited areas of land, and fortunate economic and political conditions for investments in renewable energy, the potential for utilizing solar energy in South Africa is large. However, in semi-dry areas with little precipitation, dust may accumulate on the module surface, reducing the light reaching the solar cell, and the performance of photovoltaic modules may be reduced.

The purpose of this study is to investigate the effect of soiling on the power output from photovoltaic modules for an area in the Northern Cape region in South Africa. The effect of soiling is estimated through analysis of data from a test station at Scatec Solar's solar park in Kalbult, where the performance of regularly cleaned and uncleaned polycrystalline silicon and CdTe thin film modules is compared. Different cleaning techniques and the effect of an anti-soiling product are also investigated. The data analysis is supplemented by experiments conducted at the test station, including quantification of dust accumulation and measurements of changes in the transmittance through module glass.

In the time period considered in this analysis (04.05.2016 – 04.11.2016), it may seem like the losses due to soiling are only significant in the winter months May – July, and that thin film modules are more affected by soiling than polycrystalline silicon modules. The applied anti-soiling product seemed to work against its purpose and increase the dust accumulation on the module surface. In July, when the losses for the recorded data were at their highest, the average power loss due to soiling was 1 % for poly Si-modules without anti-soiling treatment, 2 % for poly Si-modules with anti-soiling treatment, and 4 % for thin film modules with anti-soiling treatment.

For the poly Si-modules, it was shown that heavy rainfall cleaned the module surface to the extent that the performance was recovered. For the thin film modules, the performance also increased after heavy rain, although it may seem like the module surface was not completely cleaned.

The measurements of the soiling levels suggest a daily dust accumulation of 13 – 22 mg/m² in October. Compared with results from other studies, this confirms that the soiling levels in the spring months are low, and is an explanation for why there was not observed any significant reduction in performance in the period from August to October.

The transmittance measurements confirm that two and a half days with soiling in October is not enough to significantly reduce the incoming light on the solar cells.

Nomenclature

Symbols

A	Areal	m^2
D	Duty cycle	%
E	Energy	J
FF	Fill factor	-
G_t	Global tilted irradiance	W/m^2
I	Current	A
I_L	Solar irradiance	W/m^2
I_{L0}	Reference solar irradiance	W/m^2
m	Mass	G
P	Power	W
P_{in}	Incoming available power at PV-module surface	W/m^2
P_{max}	Maximum power point (MPP)	W
P^*	Temperature corrected power output	W
R	Resistance	Ω
S_R	Soiling ratio	%
T_{amb}	Ambient temperature	$^{\circ}C$
T_c	Solar cell temperature	$^{\circ}C$
T_m	Back-surface module temperature	$^{\circ}C$
ν	Frequency	Hz
V	Voltage	V
Y_R	Yield ratio	%
η	Efficiency	%
η^*	Temperature corrected efficiency	%

α	Solar altitude angle	°
β	PV-module tilt angle	°
γ	PV-module temperature coefficient	%/°C
γ_m	PV-module orientation angle	°
γ_s	Solar azimuth angle	°
θ	Angle of incidence	°
θ_z	Zenith angle	°

Abbreviations

<i>AM</i>	Air mass	-
<i>PV</i>	Photovoltaic	-
<i>RH</i>	Relative humidity	%
<i>WS</i>	Wind speed	m/s

Subscripts

<i>C</i>	Conduction band
<i>f</i>	Final
<i>G</i>	Bandgap
<i>i</i>	Initial
<i>in</i>	Input
<i>MPP</i>	Maximum power point
<i>OC</i>	Open circuit
<i>out</i>	Output
<i>ph</i>	Photon
<i>SC</i>	Short circuit
<i>STC</i>	Standard test conditions

V Valence band

Constants

h Planck constant $6.626\,069 \cdot 10^{-34}$ Js

k_B Boltzmann constant $1.380\,649 \cdot 10^{-23}$ JK⁻¹

q Elementary charge $1.602 \cdot 10^{-19}$ C

Contents

Preface	I
Sammendrag	II
Abstract.....	III
Nomenclature.....	IV
1 Introduction	1
2 Theoretical prerequisites	3
2.1 Solar radiation.....	3
2.1.1 Solar resource.....	3
2.1.2 Solar spectrum.....	4
2.1.3 Time and location dependent changes in light intensity	5
2.2 Relevant angles for tilted PV-modules.....	6
2.3 Photovoltaic solar cell technology	6
2.3.1 Operational principles of a solar cell.....	6
2.3.2 Solar cell parameters	8
2.3.3 The equivalent circuit.....	9
2.3.4 Solar cell efficiency.....	10
2.3.5 Standard test conditions.....	11
2.3.6 Solar cell technologies.....	12
2.4 Soiling	12
2.4.1 The effect of PV-system design on the accumulation of dust and soiling losses.....	12
2.4.2 The effect of climatic conditions on the accumulation of dust	13
2.4.3 The effect of local environment on the accumulation of dust.....	14
3 Experimental and analytical methodology.....	15
3.1 Test station.....	15
3.1.1 Layout and surroundings	15
3.1.2 Insolation at test station	17
3.1.3 Weather conditions at test station.....	18
3.1.4 Measurements at the test station.....	21
3.2 Cleaning strategy	24

3.2.1	Regularly cleaning.....	24
3.2.2	Additional cleaning	26
3.2.3	Cleaning techniques and anti-soiling product	26
3.3	Data analysis.....	26
3.3.1	Data selection.....	27
3.3.2	Data correction.....	28
3.3.3	Presentation of results.....	33
3.3.4	Summary of analysis procedure	34
3.4	Experimental methodology.....	35
3.4.1	Quantified accumulation of dust	35
3.4.2	Transmittance measurements.....	37
4	Results and discussion	39
4.1	Analytical estimation of the effect of soiling.....	39
4.1.1	Changes in yield ratio	39
4.1.2	Estimation of the effect of soiling on PV-module performance.....	43
4.1.3	Effect of cleaning	53
4.2	Irradiance dependence and temperature effects.....	58
4.3	Quantified dust accumulation	60
4.3.1	Verification of weighing method	60
4.3.2	Soiling level measurements	62
4.3.3	Summary of subsection.....	64
4.4	Transmittance measurements.....	64
4.4.1	Measurements and uncertainty discussion.....	64
4.4.2	Summary of subsection.....	66
4.5	Summary of results in a non-site-specific perspective.....	66
5	Conclusions	68
6	Further work.....	69
7	References.....	70
8	Appendix.....	73
	Appendix A.....	74
	Appendix B.....	78
	Appendix C.....	81

Appendix D.....	84
Appendix E.....	86

1 Introduction

At the UN Climate Change Conference in Paris in 2015, negotiators from all over the world made an agreement where one of the formulated goals was to avoid a rise in the global temperature above 2 °C compared to pre-industrial levels. The motivation for this target is that scientists all over the world agree that the atmosphere of the Earth is getting warmer due to emissions of greenhouse gasses caused by human activity, and that an increase in temperature over 2 °C can lead to dangerous changes in the global climate. (*More details about...* 2015)

Reaching this target demands a transformation of the energy sector, as current energy trends are not sustainable. About two-thirds of the greenhouse gas emissions caused by human activity are related to energy production and consumption. (IEA 2015) In 2014, 66 % of the global electrical energy generation was based on fossil fuels. (The Shift Project)

According to the International Energy Agency (IEA) photovoltaic (PV) energy, generating electrical energy from solar insolation, is one of the most promising emerging technologies to reduce the greenhouse gas emissions from the energy sector. The technology development and the fast deployment of photovoltaic technology in recent years have resulted in substantial price reductions. From 2008 to 2014 the cost of photovoltaic modules was divided by five. (Philbert 2014) In 2014, IEA predicted that by 2050 16 % of the global electrical energy generation will be covered from PV-technology.

South Africa is a country with high potential for photovoltaic energy generation, because of high solar irradiance and large areas of land. In 2010 the South African Renewable Energy Independent Power Producer Procurement Programme (REIPPPP) was introduced, with the aim of installing 3.7 GW of renewable energy. In the five first years, the programme led to private investments of 12 billion dollars in renewable energy, about half of the investments in large solar parks. A result of this is that the cost of solar power has fallen below the cost of electrical energy generation from coal. (Barstad 2016)

Power production using PV-technology is dependent of the incoming solar radiation. In a natural environment, accumulation of dust and bird droppings on the PV-modules will occur, reducing the transmittance of sunlight. At some locations, there have been observed 50 % loss due to soiling. (Adinoyi & Said 2013) In large solar parks, dust and dirt on the module can consequently lead to considerable power losses. In some cases, it may be economically beneficial to clean the PV-modules, particularly in dry areas where there is little precipitation causing natural cleaning. Because cleaning might be costly and water is scarce in arid areas, a fundamental understanding of the soiling process and the effect soiling has on the PV-module performance is important to determine how often it is necessary to clean. Insight in the soiling process and effect may also lead to financial gains by reducing the uncertainty in the expected total production from solar parks.

Previous research on the effect of soiling shows that the accumulation of dust on the PV-modules is dependent on both climatic conditions and the local environment, and that how much the dust is affecting the power production depends on the properties of the dust. (Mani & Pillai 2010) The amount of soiling and its effect on the PV-modules is because of this largely dependent of location.

With fortunate economic and climatic conditions for installing solar parks, and large semi-dry areas, it is interesting to investigate the effect of soiling on solar energy generation in South Africa. In this thesis, the effect of dust accumulation on the power output from PV-modules and the necessity of cleaning are investigated for an area in the Northern Cape region. This is conducted through analysis of data from a test station at Scatec Solar's solar park in Kalkbult, where the performance of regularly cleaned and uncleaned polycrystalline silicon and CdTe thin film modules is compared. Different cleaning techniques and the effect of an anti-soiling product are also investigated. The results from the analysis are supported by additional measurements at the test station, including quantification of dust accumulation and measurements of changes in the transmittance through module glass. The losses due to soiling are also related to local weather conditions, mainly amount of precipitation. Wind and humidity conditions are also discussed, respectively limited to the wind speed and relative humidity. Wind direction and dew formation are not included.

2 Theoretical prerequisites

The theory in section 2.1 – 2.3 is mainly based on *Solar Energy - The physics and engineering of photovoltaic conversion technologies and systems* (Jäger et al. 2016) and PVEDucation.org (Honsberg & Bowden 2014). Additional sources are specified.

2.1 Solar radiation

2.1.1 Solar resource

In the centre of the Sun, approximately 4 million tons of mass are converted into energy through nuclear fusion every second. This gives a total power of about $3.8 \cdot 10^{26}$ W. Most of the energy is released as electromagnetic radiation. The solar surface has a temperature of about 6000 K, and is the source of the radiation that hits the Earth. The energy emitted from the solar surface is spread over a sphere, as illustrated in Figure 2.1. As the distance from the Sun increases, the energy density decreases. Because of this, the power received by the Earth is only a small part of the power at the Sun's surface. Outside the Earth's atmosphere, the average solar radiation is approximately 1361 W/m^2 . This value is the *solar constant*, and applies for a plane perpendicular to the direction of the Sun at the mean distance between the Earth and the Sun. The resulting average insolation at the surface of the Earth is approximately $1500 \text{ kWh/m}^2/\text{year}$. (Goswami & Besarati 2013)

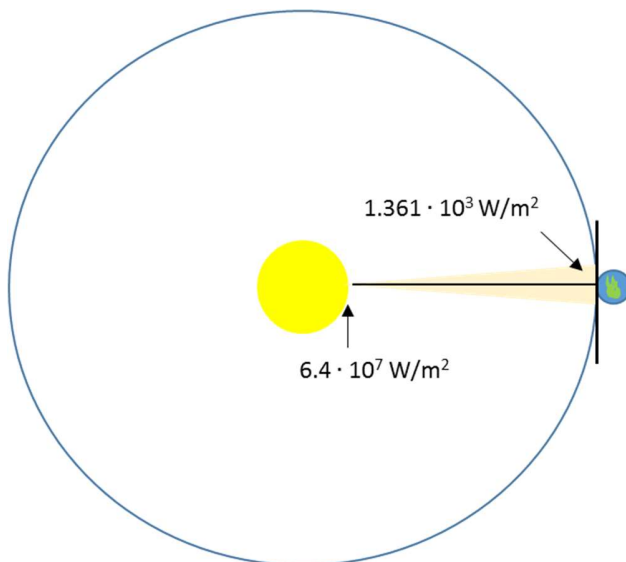


Figure 2.1: The radiation from the surface of the Sun compared to the irradiance outside the atmosphere (the solar constant).

2.1.2 Solar spectrum

At the same time as light has the properties of an electromagnetic wave, it also shows the properties of particles. These particles are called photons, and according to Planck's law their energy is proportional to the frequency of the light:

$$E_{ph} = h\nu \quad (1)$$

where E_{ph} is the energy of the photon, h is Planck's constant and ν is the frequency.

The energy of the solar radiation has a spectral distribution, and the energy in the incoming light is consequently different at different wavelengths. The solar spectrum may be defined as the energy of the photons given as a function of the wavelength of the light.

Through the atmosphere, the solar radiation is attenuated due to scattering and absorption by air molecules, aerosols, and dust particles. Because of this, the distance the sunlight travels through the atmosphere influence the solar irradiance reaching the surface of the Earth, and the solar spectrum at the surface will change through the day. Optical air mass (AM) represents the ratio of the distance the sunlight travels in the atmosphere to the distance when the Sun is at zenith, i.e. the shortest possible path through the atmosphere:

$$AM = \frac{1}{\cos\theta_z} \quad (2)$$

where θ_z is the Sun's angle with the zenith, as illustrated in Figure 2.2. The spectrum outside the atmosphere is called AM0, because no atmosphere is traversed.

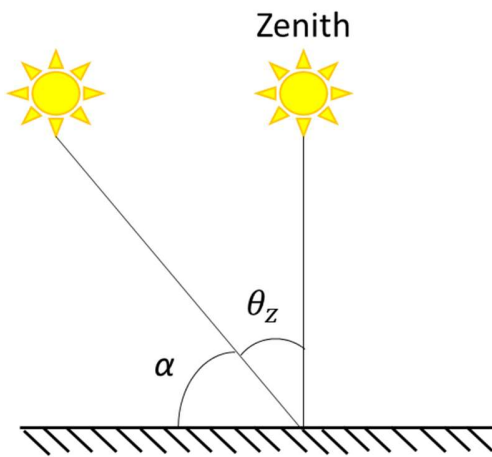


Figure 2.2: Angles describing the position of the Sun. θ_z is the zenith angle and α is the solar altitude angle.

The absorption of the sunlight in the atmosphere by water vapour (H_2O), oxygen (O_2) and carbon dioxide (CO_2) causes especially large changes in the solar spectrum. The absorption is dependent of wavelength, resulting in gaps in the solar spectrum, as presented in Figure 2.3. Clouds and other local atmospheric conditions will change the spectrum even more.

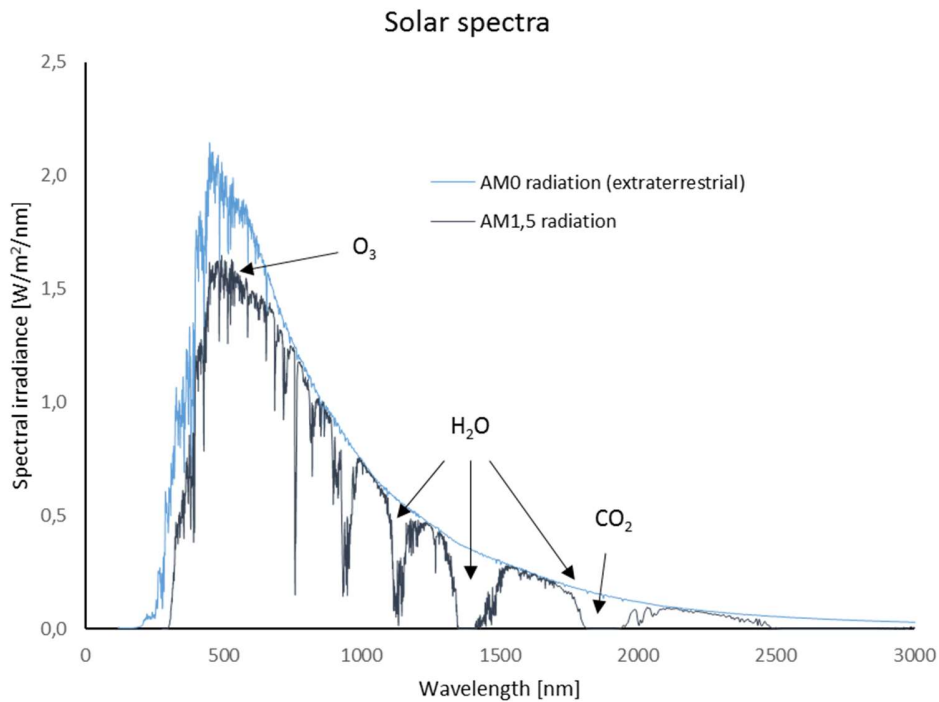


Figure 2.3: The AM0 spectrum outside the atmosphere and the standard AM1.5 spectrum. The gaps in the AM1.5 spectrum are caused by absorption by gases in the atmosphere. As shown for four of the largest gaps, different gases absorb light at different wavelengths. (Cook 2013)

2.1.3 Time and location dependent changes in light intensity

The Earth's motion relative to the Sun results in daily and annual variation in the solar irradiance at a specific location. When the sunlight hits the Earth with an increasing zenith angle, the sunrays are spread over a larger area, as illustrated in Figure 2.4. (NASA) This gives a reduction in light intensity from equator to the poles, from midday to evening and from summer to winter. With low solar altitude angles, the sunlight is additionally attenuated because of the longer path through the atmosphere, as discussed earlier.

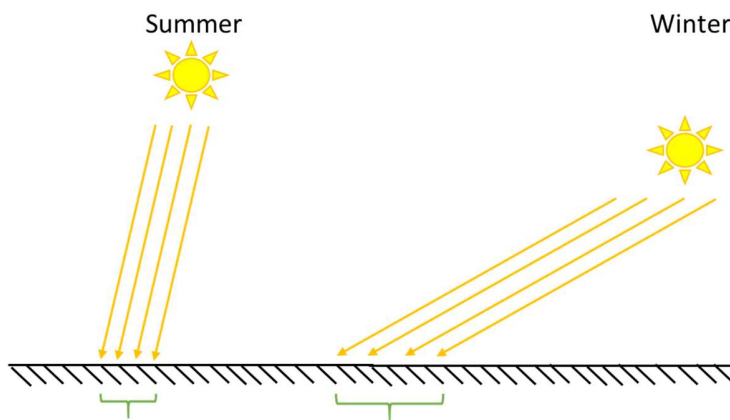


Figure 2.4: Variation in irradiance due to motion of the Earth relative to the Sun leading to different angles of incidence.

2.2 Relevant angles for tilted PV-modules

An illustration of the angles necessary to describe the orientation of the PV-module and how the solar radiation hits its surface is given in Figure 2.5. The tilt angle (β) and the orientation angle (γ) are used to describe the orientation and mounting of the module. The solar azimuth angle (γ_s) and the angle of incidence (θ) are used to describe the position of the Sun relative to the module.

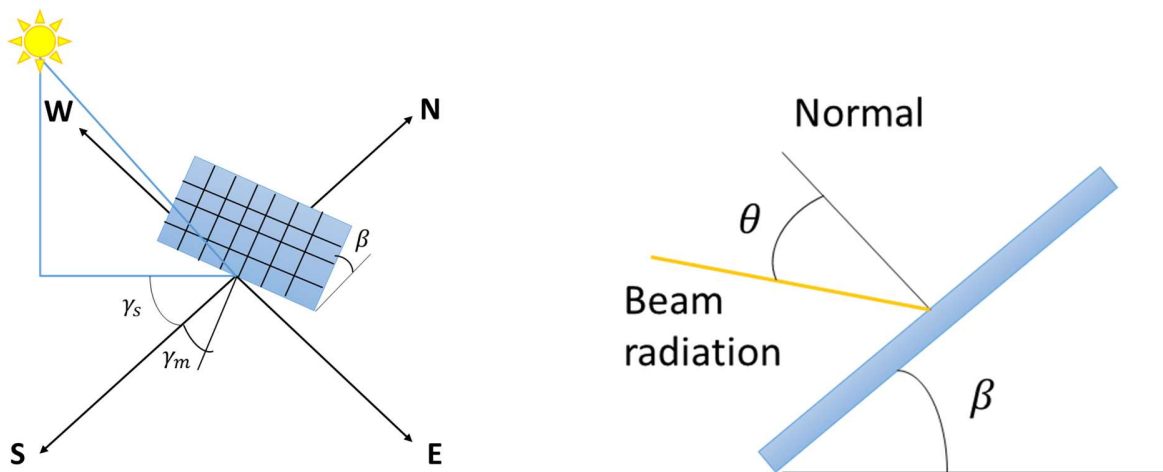


Figure 2.5: Angles describing the orientation of a PV-module and how the solar irradiance hits the surface. Left: the tilt angle of the module (β), the module orientation (γ_m), and the solar azimuth angle (γ_s). Right: the angle of incidence of solar radiation (θ) and the tilt angle of the module (β). From: Pedersen (2015).

2.3 Photovoltaic solar cell technology

2.3.1 Operational principles of a solar cell

Most photovoltaic solar cells consist of a positive (p) doped and a negative (n) doped semiconductor material, forming a pn-junction. Doping is a technique where atoms of another element is added to the semiconductor, leading to a surplus (negative) or deficit (positive) of electrons in the material. An important principle in the operational process of a solar cell is the *photovoltaic effect* which occurs when electrons excited to a higher energy level by incoming light is transferred between the two semiconductor materials, generating a potential difference between the materials.

The first part of the process leading to the photovoltaic effect is the generation of charge carriers in the solar cell materials due to absorption of the photons in the incoming light. When photons are absorbed in a semiconductor material, electrons are excited from an initial energy level E_i to a higher energy level E_f . In an ideal semiconductor, the electrons have energy levels either in the *valence band* or in the *conduction band*. It is not possible for the electrons to have energies in the *band gap* between the valence band and the conduction band. A photon with higher energy than the band gap energy will have the capability to excite an electron from the valence band to the conduction band. When an electron is excited to a higher energy

level, a so-called hole (a particle with the behaviour of a positive elementary charge) is created at the initial energy level. The process of creating an electron-hole pair is illustrated in Figure 2.6.

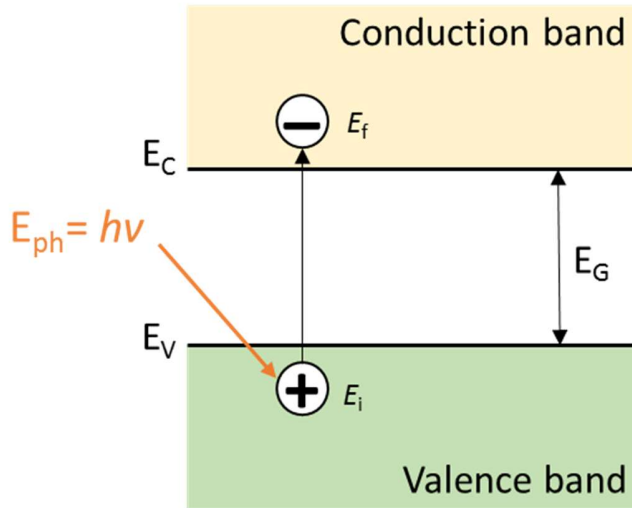


Figure 2.6: The absorption of a photon with energy (E_{ph}) larger than the band gap energy (E_G), leading to the generation of an electron-hole pair. E_C is the minimum energy of the conduction band, and E_V is the maximum energy of the valence band.

In a pn-junction the positive doped and the negative doped semiconductor materials create an internal electric field. The function of this field is to separate the electron-hole pair and avoid immediate recombination. The pn-junction in a solar cell is illustrated in Figure 2.7.

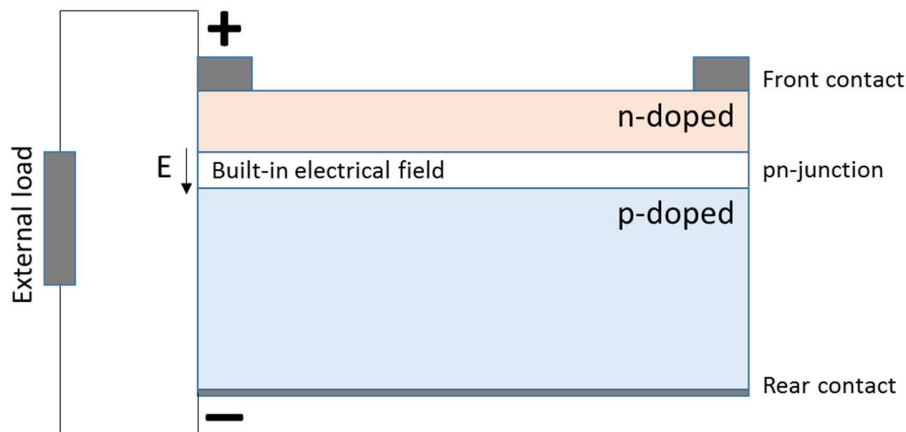


Figure 2.7: Sketch of the solar cell and its pn-junction.

When the solar cell is an open circuit, the numbers of electrons in the n-material and holes in the p-material will increase. This creates an electric field at the junction in the opposite direction of the original internal electric field, reducing the net electric field. Due to the reduced electric field a diffusion current is generated to balance out the surplus of carriers in the two materials, a new equilibrium is established and a voltage is

generated over the pn-junction. At open circuit conditions, an equilibrium is reached where the light generated current is balanced by the diffusion current, and there is no net current. The voltage over the pn-junction in this situation is called the *open-circuit voltage*.

To generate power, a current is necessary in addition to the voltage. If the solar cell is connected to an external circuit, as illustrated in Figure 2.7, the carriers will exit the solar cell, generating a current, because of the potential difference in the solar cell. When a solar cell is short-circuited, the carriers exit the pn-junction and recombine as soon as they are generated, and there is no build-up of potential difference. This current is called the *short circuit current*.

2.3.2 Solar cell parameters

To characterize the performance of solar cells, the following parameters from an IV -curve of an illuminated solar cell are mainly used (illustrated in Figure 2.8):

- Short circuit current, I_{SC}
- Open circuit voltage, V_{OC}
- Maximum power point (MPP), P_{max} .
- Fill factor, FF

The short circuit current is determined by the flux and energy of the photons incident on the solar cell, and is thus dependent of the solar spectrum, the surface area, and the optical properties of the cell. As explained in the previous section, the open circuit voltage is the voltage over the pn-junction when the diffusion current compensates the light generated current. V_{OC} is therefore dependent of the light generated current. The generated power is the product of the current and the voltage ($P = V \cdot I$), the current and voltage pair on the IV -curve giving the maximum power point (P_{max}) is further denoted as I_{MPP} and V_{MPP} . The fill factor is the ratio between the maximum power and the product of V_{OC} and I_{SC} :

$$FF = \frac{I_{MPP}V_{MPP}}{I_{SC}V_{OC}} \quad (3)$$

The efficiency of the solar cell is calculated from the incoming light on the module (P_{in}) and output power:

$$\eta = \frac{P_{max}}{P_{in}} = \frac{I_{MPP}V_{MPP}}{P_{in}} = \frac{I_{SC}V_{OC}FF}{P_{in}} \quad (4)$$

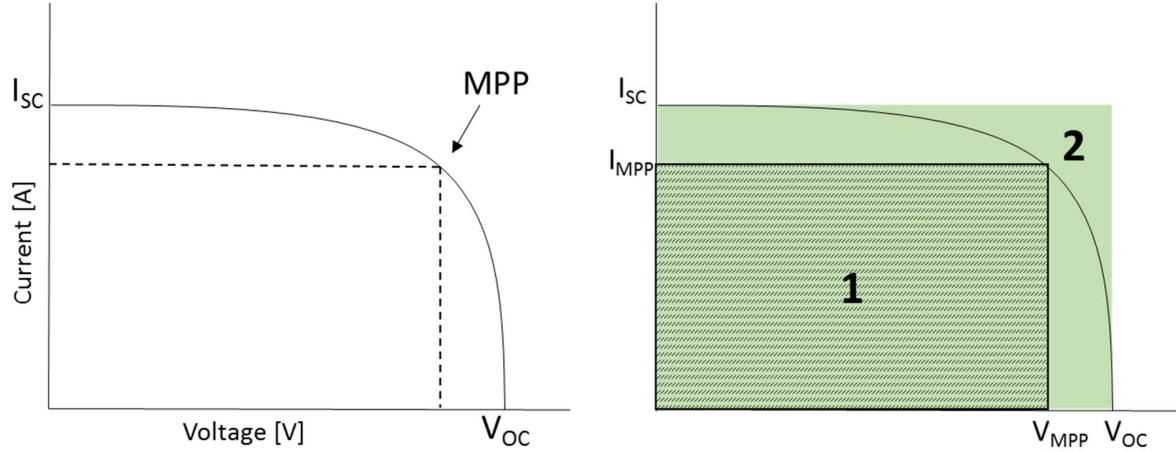


Figure 2.8: The figure on the left side shows an IV-curve where the short circuit current, the open circuit voltage and the maximum power point are indicated. The fill factor is the ratio between the hatched area (1) and the green area (2) on the figure on the right side.

Another important parameter of the solar cell, is the cell temperature. This parameter is not easily measured in an automated set up. Assuming one-dimensional heat conduction through the module materials behind the cell, the cell temperature can be estimated from the measured back-surface module temperature from the following equation (King et al. 2004):

$$T_c = T_m + \frac{I_L}{I_{L0}} \Delta T \quad (5)$$

where T_c is the cell temperature, T_m is the measured back-surface module temperature, I_L is the measured solar irradiance on the module (W/m^2) and I_{L0} is the reference solar irradiance equal to $1000 \text{ W}/\text{m}^2$. ΔT is the difference between the cell temperature and the back-surface module temperature at an irradiance level of $1000 \text{ W}/\text{m}^2$.

Honsberg and Bowden (2014) suggest a method where the cell temperature is estimated from the ambient temperature, irradiance and the nominal operating cell temperature (NOCT), given by the following equation:

$$T_c = T_{amb} + \frac{NOCT - 20^\circ\text{C}}{800 \text{ W}/\text{m}^2} \cdot I_L \quad (6)$$

where T_{amb} is the ambient temperature and $NOCT$ is the cell temperature when the irradiance is $800 \text{ W}/\text{m}^2$, the ambient temperature is 20°C , the wind speed equal to $1 \text{ m}/\text{s}$ and the module is mounted with open back side.

2.3.3 The equivalent circuit

2.3.3.1 The two-diode model

The behaviour of a solar cell can be described by a circuit with a diode and a current source connected in parallel. The diode is representing the pn-junction. In a non-ideal solar cell, the fill factor will be influenced

by internal resistances, represented by a series resistance R_s and a shunt resistance R_p . In practice, there will be recombination in the pn-junction resulting in additional losses. To compensate for the diode in the model not being ideal, two diodes can be used to present the pn-junction, where one is ideal and one is non-ideal. In the model this is described with an ideality factor, describing how closely the diode follows the ideal diode equation. An ideal diode has an ideality factor equal to one, and a non-ideal diode has a factor greater than one. The equivalent circuit of a real solar cell using the two-diode model is shown in Figure 2.9. For this circuit the relation between the current (I) and the voltage (V) is given by the following equation:

$$I = I_{ph} - I_{d1} - I_{d2} - I_p = I_{ph} - I_{01} \left\{ \exp \left[\frac{q(V-IR_s)}{n_1 k_B T} \right] - 1 \right\} - I_{02} \left\{ \exp \left[\frac{q(V-IR_s)}{n_2 k_B T} \right] - 1 \right\} + \frac{V-IR_s}{R_p} \quad (7)$$

where T is the cell temperature in kelvin, n_1 and n_2 are the ideality factors of the diodes, k_B is the Boltzmann constant, q is the elementary charge, I_{01} and I_{02} are the saturation currents of the diodes, and I_{ph} is the light generated current. I_{d1} and I_{d2} is the currents through the diodes and I_p is the current through the shunt resistance.

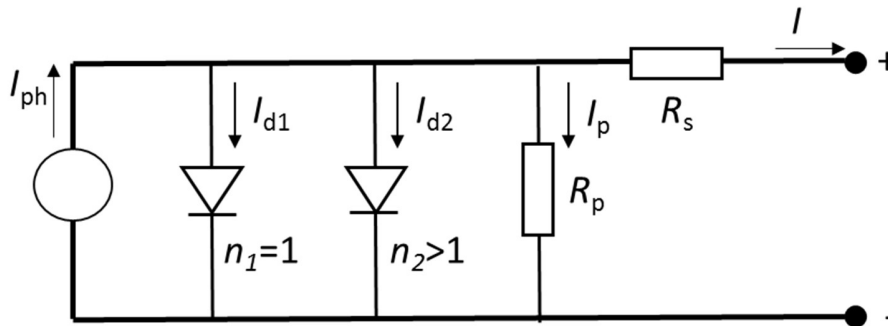


Figure 2.9: The equivalent circuit of a solar cell, based on the two-diode model.

2.3.3.2 Internal resistances

The series resistance in the two-diode model is the sum of the resistance of the top and rear metal contacts, the contact resistance between the semiconductor and the metal contacts and the resistance in the semiconductor itself.

The main impact of the series resistance is reduction of the fill factor, but it may also reduce the short circuit current at high values.

The shunt resistance in the solar cell is typically representing power losses due to manufacturing defects providing an alternate path for the light-generated current. This reduces the current through the pn-junction and the voltage over the junction is reduced. This effect is dominating at low light, when there is less light-generated current.

2.3.4 Solar cell efficiency

Cell temperature, light intensity and angle of incidence are important factors influencing the efficiency of a solar cell, and are more closely discussed in the following subsections.

2.3.4.1 Temperature effect

The cell temperature is the most significant parameter affecting the performance of a PV-system. (Woyte et al. 2014)

In a semiconductor, an increase in temperature will increase the energy of the electrons in the material. A result of this is a reduction of the band gap in the semiconductor, less energy is required to excite the electrons to the conduction band, and the thermally excited electrons will dominate the electrical properties of the semiconductor. The parameter that is most affected by this in a solar cell, is the open circuit voltage. Because the intrinsic carrier concentrations will increase due to the lower bandgap, the diffusion current will increase, and V_{OC} will decrease. I_{SC} will increase slightly at higher temperatures, but not enough to compensate for the reduction in V_{OC} .

The effect of temperature on solar cell is well known, and many different models to explain this correlation are proposed. Most of the models of the temperature corrected power output (the expected power output if the cell temperature was 25 °C) have a linear form where the only difference between the numerical values of the material and system dependent parameters. (Skoplaki & Palyvos 2009) One example is the following model (Herteleer 2015):

$$P^* = \frac{P_{max}}{1 + \gamma(T_c - T_{STC})} \quad (8)$$

where P_{max} is the measured maximum power, T_c is the cell temperature, $T_{STC} = 25$ °C, and γ is a material dependent constant.

2.3.4.2 Effect of light intensity

Variation of the light intensity incident on a solar cell is affecting both I_{SC} , V_{OC} , FF , the efficiency, and the impact of the internal resistances.

The shunt resistance is especially affecting the losses at low light intensity. At low light, the current through the solar cell is low, and the fraction of the current flowing through the shunt resistance increases. At high light intensities, the series resistance has a greater effect on the losses, because of increased currents.

2.3.4.3 Effect of angle of incidence

When the solar angle of incidence is increased, the reflectance on the glass surface of the PV-module will increase, reducing the irradiance reaching the solar cell. King et al. (2004) showed that these optical losses is negligible until the angle of incidence (θ , illustrated in Figure 2.5) is approximately 55°.

2.3.5 Standard test conditions

To compare different solar cell technologies and producers, a set of standard test conditions (STC) is defined. STC requires irradiance of 1000 W/m², a cell temperature of 25 °C and an AM1.5 spectrum. The standard AM1.5 spectrum defined in the International Standard IEC 60904-3 is the AM1.5 spectrum at a plane tilted 37° to the horizontal, faced towards the Sun.

2.3.6 Solar cell technologies

The solar cell market today is dominated by PV-technology based on crystalline silicon semiconductors. There are two different types of crystalline silicon solar cells, monocrystalline and polycrystalline. The first is made from one single crystal, the second is composed of multiple smaller crystals. In 2016 the maximum efficiency was 23.8 % for a monocrystalline module, and 19.5 % for a polycrystalline module. (Green et al. 2016)

Thin film solar cells are referred to as the second-generation PV-technology, and are much thinner than the traditional silicon solar cells. In these solar cells, the active semiconductor layer is sandwiched between a transparent conductive oxide layer and the electric back contact. In this analysis cadmium telluride thin film modules are used. The max efficiency of this type of module in 2016 was 18.6 %. (Green et al. 2016)

2.4 Soiling

Because of dust in the air, lifted from the ground by wind, traffic, volcanic eruptions and pollution, PV-modules are exposed to soiling.

There are many factors influencing the accumulation of dust on PV-module surfaces (Mani & Pillai 2010):

- Characteristics of the PV-system: tilt angle, height of installation, surface texture.
- Climatic conditions: precipitation, wind speed and direction, ambient temperature, humidity.
- Local environment: vegetation, traffic, air pollution, type of dust (chemical, biological, and electrostatic properties, size, shape, and mass)

The effect of soiling on PV-modules is consequently highly dependent on location. A study performed in Dhahran in Saudi Arabia, showed a 50 % decrease in power output after six months without cleaning and precipitation. (Adinoyi & Said 2013) Data from Flanders in Belgium showed that at a tilt angle of 35° the decrease in transmittance saturated between 3 and 4 % after five weeks of exposure. (Appels et al. 2013) In Malaga in Spain the monthly average energy losses are 2 %, except for the summer months with little precipitation when the monthly average losses may exceed 15 %. (Zorilla-Casanova et al. 2011) At Kjeller, Norway, it was shown that the decrease in efficiency due to soiling saturated after one week of exposure. The maximum reduction in efficiency for a week was 0.3 percentage points. (Pedersen 2015)

2.4.1 The effect of PV-system design on the accumulation of dust and soiling losses

When the tilt angle (β , shown in Figure 2.5) of the PV-module is increased, the accumulation of dust on the module surface decreases due to gravity. Cano (2011) showed that during three months in Mesa, Arizona, for tilt angles of 0°, 23° and 33° the losses due to soiling were respectively 2.02 %, 1.05 % and 0.96 %.

The direction of the PV-modules influence the losses due to soiling. When the PV-modules are clean, the total losses are approximately constant during the day. For the dirty modules the losses are dependent of the angle of incidence of the incoming light. (Zorilla-Casanova et al. 2011) This is because the optical losses, caused by absorption and reflection due to dust, increases when the angle of incidence increases. A

consequence is that the losses due to soiling is at its minimum at solar noon. This means that with a tracking system, where the modules follow the direction of the sun, the losses due to the accumulated soil will be reduced. On cloudy days, the irradiance is mainly diffuse, and the losses does not change in the same way through the day.

2.4.2 The effect of climatic conditions on the accumulation of dust

2.4.2.1 *Precipitation*

Research on the cleaning effect of precipitation on PV-modules gives different results. Data from Spain shows that rain cleans the surface if the daily precipitation is above 4 - 5 mm (Garcia et al. 2011), other studies show that rainfall of 1 mm is enough to clean the surface and restore the performance. (Caron & Littmann 2013; Zorilla-Casanova et al. 2011) It is also shown that rain has a limited effect on small dust particles (2 – 10 μm) and larger dust particles are easier washed off. (Appels et al. 2013)

Comparing studies on the cleaning effect of rain is challenging, as it is difficult to conduct this kind of research under controlled conditions. The size and properties of the particles, and to which extent they stick to the surface might be factors leading to variation in the results. The same applies to the conditions under the rainfall, like the wind speed and direction and the rain intensity, i.e. mm precipitation per time. How clean the modules were after the rainfall may also be difficult to compare.

2.4.2.2 *Wind*

The wind speed and direction are influencing both the accumulation and removal of dust. In general, low wind speed will increase the soiling on PV-modules, while high wind speed will reduce the soiling by having a cleaning effect on the modules. (Guo et al. 2015; Mani & Pillai 2010) Goossens and Van Kerschaever (1999) showed that for wind speeds in the range 0.63 – 2.59 m/s, the dust accumulation was higher for lower wind speeds than for higher wind speeds. However, the dust pattern created at the lower wind speeds reduced the light transmittance in greater extent than the dust pattern created at higher wind speeds.

The wind direction will also affect the dust accumulation, but in a larger PV-system this can vary at different locations dependent on the geometry of the system. The increase and decrease of soiling due to wind speed and direction, is also dependent of the mass and size of the dust particles. (Mani & Pillai 2010)

It is important to notice that turbulence of the air will be different on the edge than in the center of the module, leading to a nonhomogeneous distribution of dust on the surface.

A special case of dust accumulation due to wind, is dust storm. The soiling levels caused by one single dust storm can reduce the power output by 20 %. (Adinoyi & Said 2013)

2.4.2.3 *Relative humidity*

An increase in relative humidity is shown to increase the accumulation of dust. (Guo et al. 2015; Naeem et al. 2015) An explanation for this is that higher humidity may increase the probability for the dust particles to stick to the module surface, and also reduce the probability that the particles are removed by wind. At high relative humidity, the particles in the air may get heavier and more likely fall down on the module surface. Because of the water content of the particles, they will more likely stick to the surface. (Naeem et al. 2015) On the other hand, if the high relative humidity is leading to formation of

dew on the surface, this may cause partial cleaning of the module surface. (Caron & Littmann 2013) The partial cleaning effect is dependent on the dew to roll of the surface, and that it does not evaporate, or remains on the surface, making it easier for dust particles to stick to module glass.

2.4.3 The effect of local environment on the accumulation of dust

In dry areas, the activity in the local environment may have an important impact on the accumulation of dust. In the Central Valley region in California, it was shown that the soiling rate, i.e. how quickly dust accumulates on the modules, was below 1 % per month in low desert regions, and the peak value for the heavy agricultural regions was 11.5 % per month. (Caron & Littmann 2013)

3 Experimental and analytical methodology

The losses due to soiling in Kalkbult are determined by comparing the performance of regularly cleaned modules and uncleaned modules. In the first part of this chapter the test station with the modules, its climatic conditions and measurement equipment, and the cleaning strategies are described. Then the steps in the analysis of the data from the test site are presented. In the last section, the methodology of the experiments conducted at the test site to support the analytical results is described.

3.1 Test station

3.1.1 Layout and surroundings

The test station is co-located with Scatec Solar's 75 MW PV-park in Kalkbult, South Africa (latitude: - 30.2, longitude: 24.1), and consists of a weather station, a pyranometer, and 24 PV-modules facing north and with a tilt angle of 30°. 16 of the modules are 255 W Virtus II Modules from Rene Sola (polycrystalline silicon), and 8 are 100 W thin film modules from First Solar (cadmium telluride). Four of the thin film modules are of type FS-4100A, covered by an anti-reflective coating. The other four are of type FS-4100 and without coating. Figure 3.1 shows the set-up and numbering of the modules. Close-ups of the two different types of modules are presented in Figure 3.2. The solar park is located at the east side of the test station. On the west side, there are train tracks and a gravel road, both with low traffic. There is also a substation with lightning rods on the western side, which could cause shading of the modules. However, because of the distance between the substation and the modules, this will only be a problem in the evening. The vegetation in the area is low, and the only agricultural activity is livestock farming. There are some birds in the area, meaning there is a risk of bird droppings on the module surfaces. The impact on the analysis is nevertheless minimal, as the module surfaces are checked every day, and bird droppings are removed.

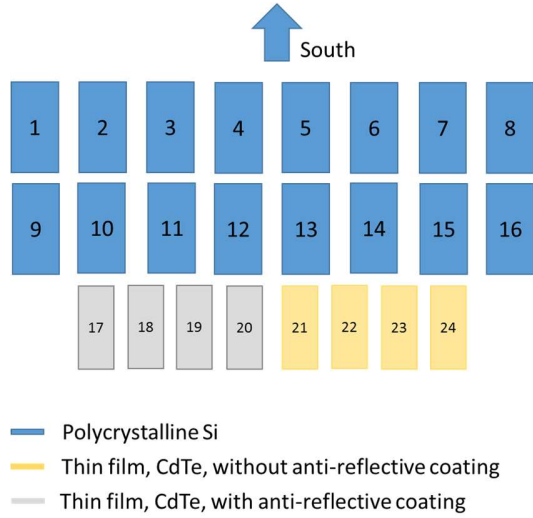


Figure 3.1: The set up and numbering of the three different types of modules on the test site. Behind the three rows of modules used in the analysis is a row with modules charging batteries that provide power to the measuring equipment. The weather station is located behind the fourth row.

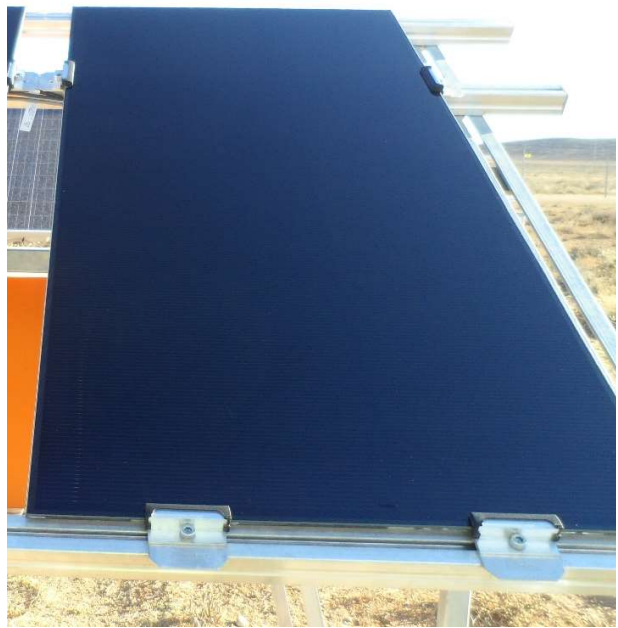


Figure 3.2: Left: The Rene Sola polycrystalline silicon module. Right (Armand du Plessis, by permission): The First Solar cadmium telluride module.

3.1.2 Insolation at test station

Kalkbult is located in the Northern Cape region, close to De Aar. This area in South Africa receives an average annual insolation of about 2 MWh/m² (Figure 3.3). For a surface in Kalkbult with the same orientation and tilt angle as the PV-modules at the test station, the average annual insolation is 2480 kWh/m². This value is based on interpolation of long-term measurements from different weather stations logged in the solar radiation database PVGIS-CMSAF. (JRC EC 2016) The insolation distribution through the year is illustrated by the total monthly insolation and the daily insolation per month in Figure 3.4.



Figure 3.3: The average annual insolation in the southern part of Africa. The approximately location of Kalkbult is marked with a black dot. From GHI Solar Map © 2016 Solargis. (Solargis 2016)

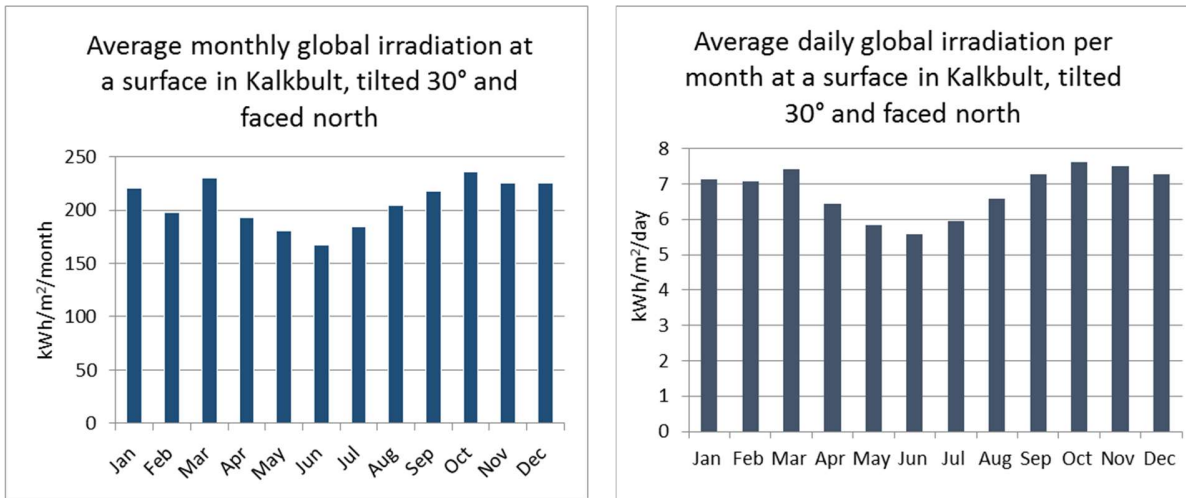


Figure 3.4: The average monthly global insolation and the daily average for each month at the test station in Kalkbult for a surface tilted 30°, faced north. The averages are given from long-term measurements from the solar radiation database PVGIS-CMSAF. (JRC EC 2016) The given values are based on interpolation between weather stations in the area.

3.1.3 Weather conditions at test station

In the Northern Cape, there are more days with precipitation in the summer than in the winter, as shown in Figure 3.5. The measured amount of precipitation at the test station in the period 25.03 – 21.11 in 2016 is given in Figure 3.6.

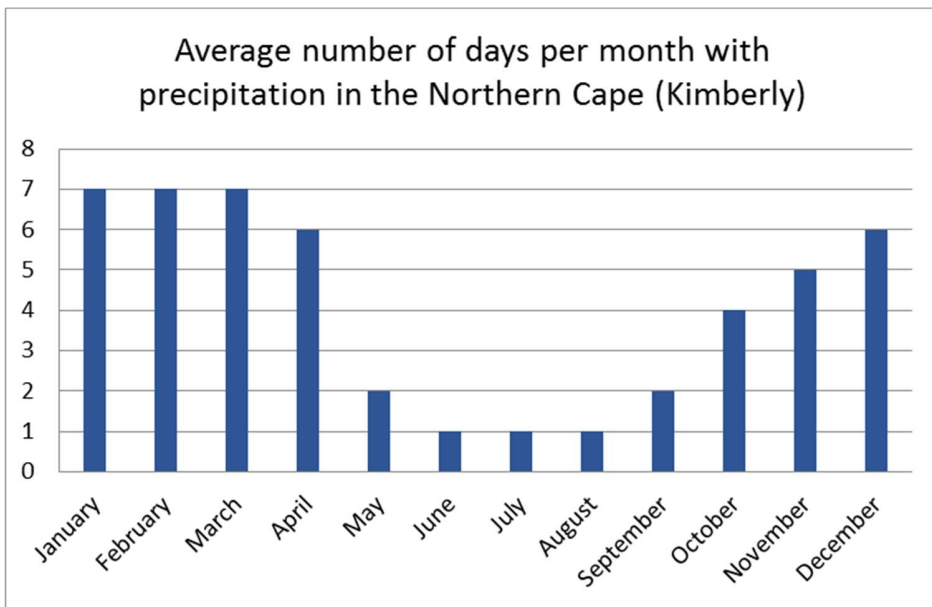


Figure 3.5: Average number of days per month in the Northern Cape (Kimberly) with precipitation over 1 mm. Average calculated from 1961-1990. (Veret som var... 2016)

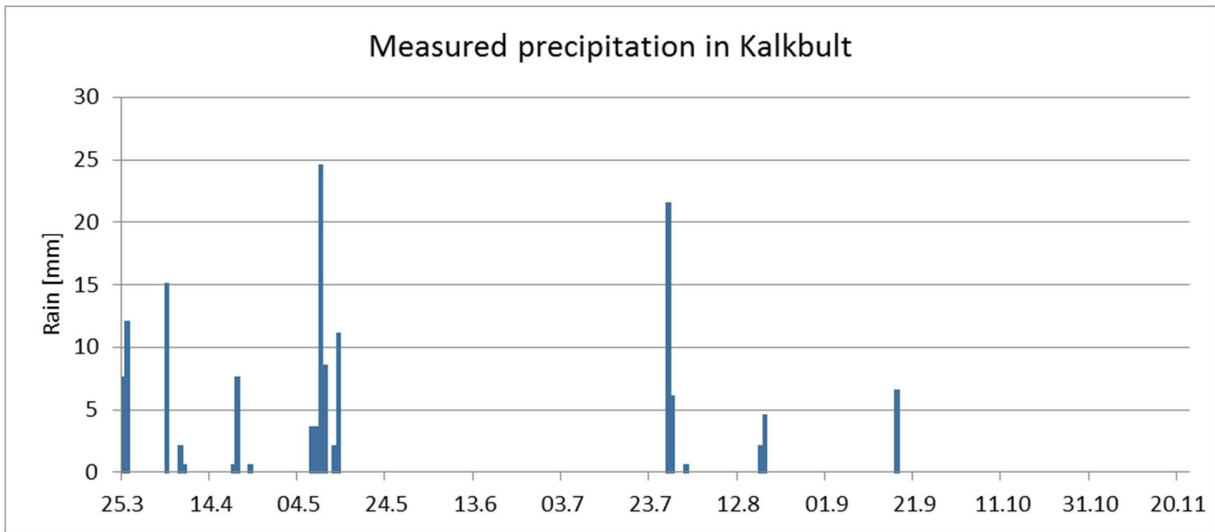


Figure 3.6: Measured daily precipitation in Kalkbult in the period 25.03.2016 – 21.11.2016.

The daily averages of wind speed, relative humidity and temperature measured at the test station 25.03 - 21.11 in 2016 are presented in Figure 3.7 - Figure 3.9.

Dust storms do occur in Kalkbult, but in the 16 months the test station has been active, this has only happened once.

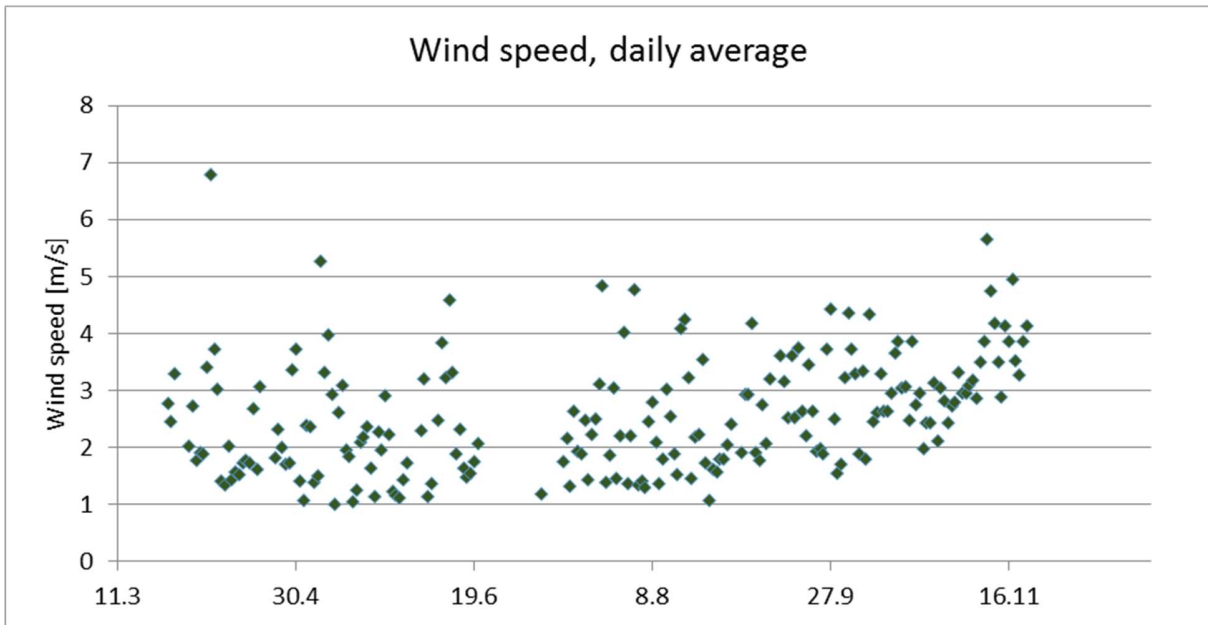


Figure 3.7: The daily average of the wind speed in the period 25.03.2016 – 21.11.2016 measured at the test station in Kalkbult.

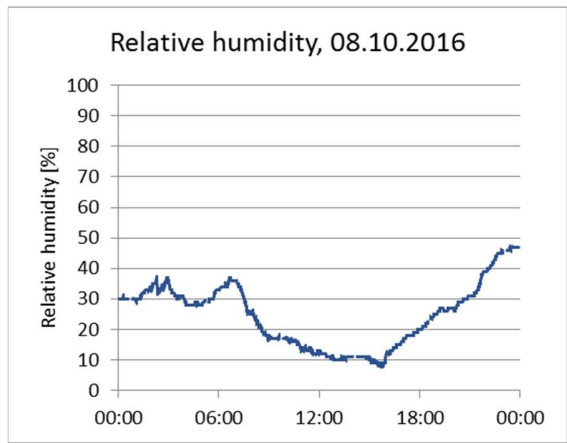
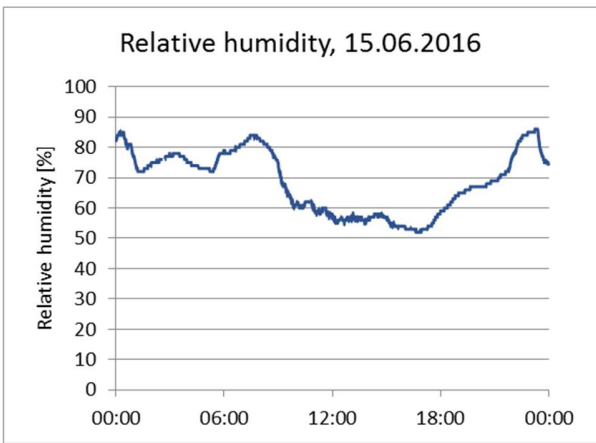
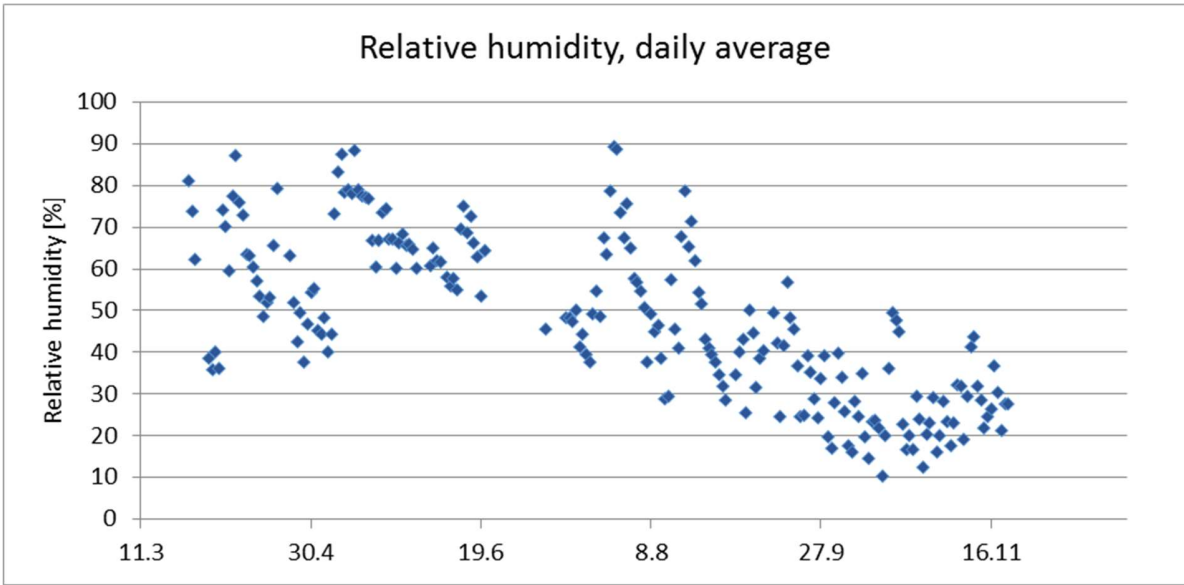


Figure 3.8: Top: The daily average of relative humidity in the period 25.03.2016 – 21.11.2016 measured at the test station in Kalkbult. Bottom: The changes in relative humidity through the day on a day in the middle of June where the daily average is high and a day in October where the daily average is low.

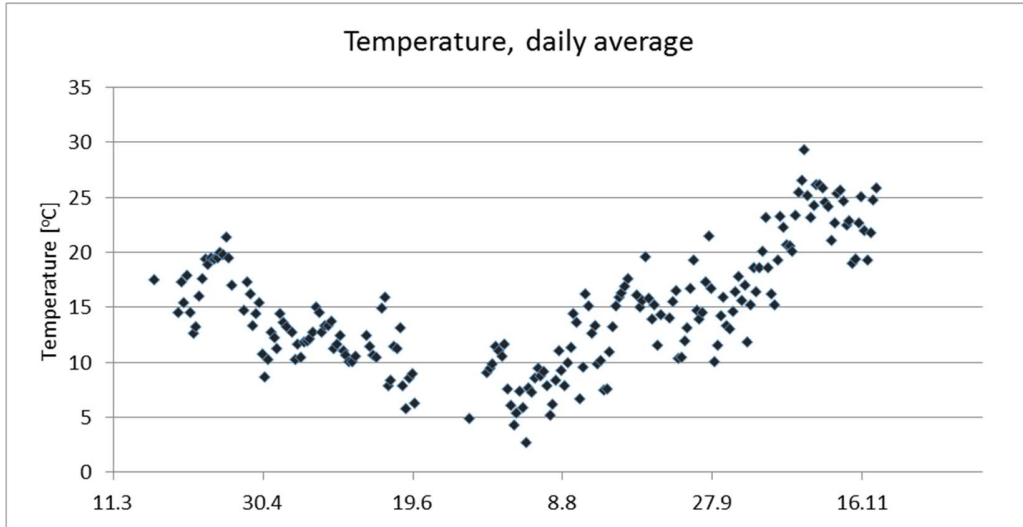


Figure 3.9: The daily average of the temperature in the period 25.03.2016 – 21.11.2016 measured at the test station in Kalkbult.

3.1.4 Measurements at the test station

Every tenth minute, for all the modules, 20 *IV*-pairs and the temperature at the rear side of the module is measured and logged. Every fifth second the irradiance is measured by the pyranometer. For every minute the maximum, minimum is logged, as well as the instantaneous value in the end of the minute. The weather station is measuring the wind speed and direction, ambient temperature, pressure, and relative humidity every fifth second. For every minute the maximum, minimum and average value is logged. The amount of precipitation is measured and logged every minute. The instruments were installed in the field May–November 2015, and have not been calibrated after they were installed. The calibration validity is 12 – 24 months for the weather station and 24 months for the pyranometer. Each instrument has their own clock, but the time is synchronized at least once a month for all devices.

3.1.4.1 *IV*-pairs

The 20 *IV*-pairs are measured within two seconds for every module, and are used to make an *IV*-curve and find the maximum power point of the modules. The measurements are conducted using an intelligent device with the ability to vary the resistance seen by the module. The device is an active load with a design based on the principle of a DC-DC switch mode converter for power control. (Ndapuka 2015) The following equations describe the operational principle:

The output voltage (V_{out}) and the input voltage (V_{in}) in the active load are related by the duty cycle (D):

$$V_{out} = DV_{in} \quad (9)$$

The output power can hence be expressed as:

$$P_{out} = V_{out}I_{out} = DV_{in}I_{out} \quad (10)$$

Neglecting the losses in the active load, the input power is equal to the output power ($P_{in} = V_{in}I_{in} = P_{out}$), and the average output current (I_{out}) can be expressed as a function of the duty cycle:

$$I_{out} = \frac{I_{in}}{D} \quad (11)$$

The resistance of a fixed resistor connected to the active load and the resistance seen by the source are consequently related by the duty cycle the following way:

$$R_{out} = \frac{V_{out}}{I_{out}} = \frac{DV_{in}}{\frac{I_{in}}{D}} = D^2 \frac{V_{in}}{I_{in}} = D^2 R_{in} \rightarrow R_{seen\ by\ source} = \frac{1}{D^2} R_{resistor} \quad (12)$$

Each poly-Si module is connected to its own active load. For the thin film modules, two modules share one active load. The active load is connected to a 750 W, 1 Ω resistor where the power from the module is dumped. The IV -pairs is measured starting with an open circuit voltage and then the resistance seen by the module is reduced by discretely increasing the duty cycle. The relationship between the resistance seen by the module, the duty cycle and the resistance of the resistor is given by the following equation, based on equation 12:

$$R_{seen\ by\ module} = \frac{1}{D^2} R_{resistor} \quad (13)$$

This gives an exponential decrease in resistance for the measurement points taken, giving more measurements on the IV -curve close to the short circuit current.

3.1.4.2 Irradiance

A Kipp-Zonen SMP10 Smart Pyranometer (Figure 3.10), installed at the same angle as the tilt angle of the modules, is used to measure irradiance. This is a Secondary Standard pyranometer, with a response time of < 2 s for 95 % of the response, and a temperature response of < 1 %. The maximum uncertainty of the instrument for total hourly radiation is 3 %.

A pyranometer has a 180° view angle, and is consequently measuring the global irradiance, including both the direct normal irradiance and the diffuse horizontal irradiance. (PVPMC 2014) As the pyranometer is installed with the same tilt angle as the modules, the measured value is denoted as tilted global irradiance (G_t).

Until 13.07.2016, the irradiance was logged with a five second delay relative to the measurements on the PV-modules and from the weather station. In the period 21.06.2016 – 12.07.2016 there are no measurements from the pyranometer. To compensate for this, measurements from a pyranometer at the solar park are added to the dataset. This pyranometer is also measuring the irradiance at an angle of 30°. However, because it is of another standard and on a different location, the readings from this pyranometer will differ from the readings of the pyranometer at the test site. The percentage difference between the pyranometers is calculated for a period of clear days with available data from both pyranometers, and used to correct the data from the Scatec Solar pyranometer. The reliability of the calculations based on irradiance in the period before 13.07.2016, will consequently be reduced.

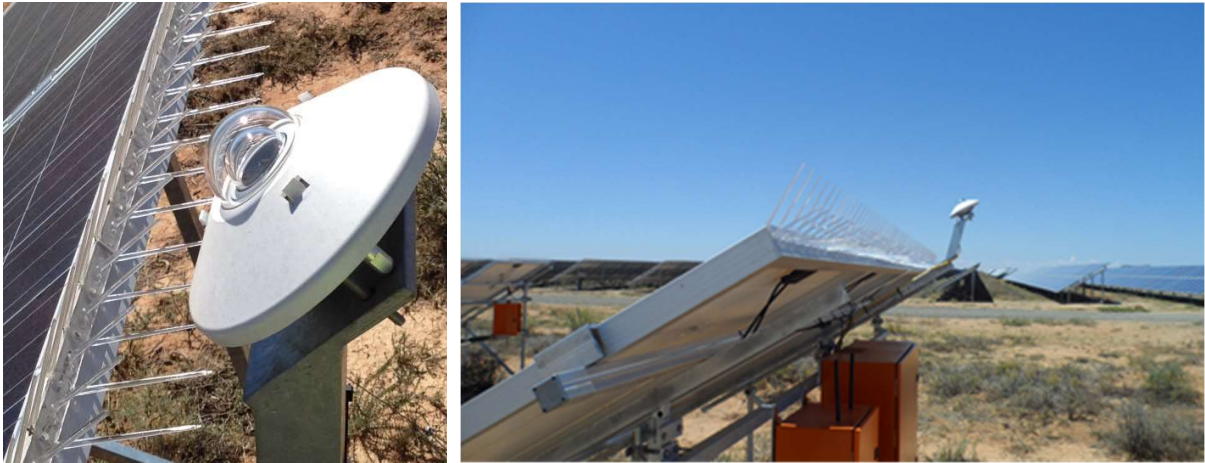


Figure 3.10: The Kipp-Zonen SMP10 Smart Pyranometer mounted at the same angle as the modules.

3.1.4.3 Back-surface module temperature

The rear side temperature of the module is measured using an ADT7310 temperature sensor from Analog Devices. The accuracy of the sensor is $\pm 0.5\text{ }^{\circ}\text{C}$, lifetime drift included. The temperature sensor and its position on the module are shown in Figure 3.11. The temperature sensor is fastened on an aluminum plate which is directly mounted on the polymer sheet on the back-surface, approximately in the middle of the module. The aluminum plate conducts heat towards the temperature sensor, as well as protecting the sensor. Heat-paste is used between the sensor and the aluminum plate to obtain uniform contact.



Figure 3.11: The ADT7310 temperature sensor, mounted at the back side of the module. Left (Armand Du Plessis, by permission): mounting of temperature sensor. Right: position of the sensor on the module.

3.1.4.4 Weather station

The weather station is a Met Station One provided by Met One Instruments, and measures wind speed and direction, ambient temperature, pressure, relative humidity, and amount of precipitation. In this analysis, the wind speed, ambient temperature, relative humidity and amount of precipitation are used. The wind speed is measured using a three-cup anemometer and a lightweight vane tail, with a resolution of 0.1 m/s, accuracy of $\pm 2\%$, and a range of 0 – 50 m/s. The temperature and humidity sensors are built into a temperature shield to reduce errors due to solar heating. The temperature is measured with a resolution of 0.1 °C, an accuracy of $\pm 0.4\text{ °C}$, in a range from - 40 °C to + 60 °C. The relative humidity measurements are given in the range 0 – 100 %, with a resolution of 1 % and an accuracy of $\pm 4\%$. A rain gauge with a logging resolution of 0.25 mm is used to measure the precipitation. The weather station is installed about 3 meters above the ground, and is located behind the PV-modules at the test site, as shown in Figure 3.12.

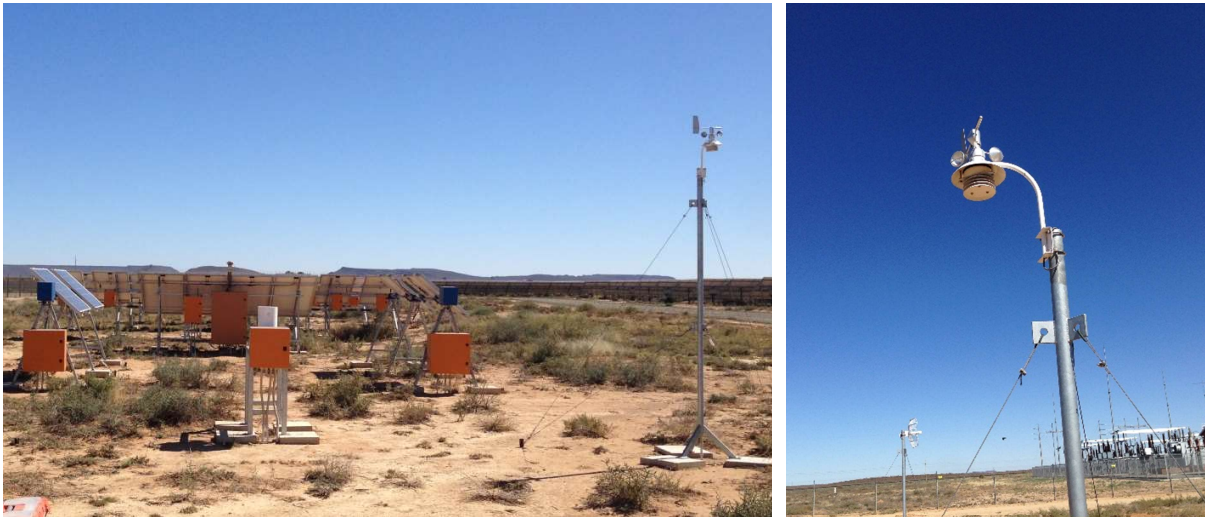


Figure 3.12: Left: the test site with the weather station located behind the PV-modules. Right: the Met One Instruments weather station.

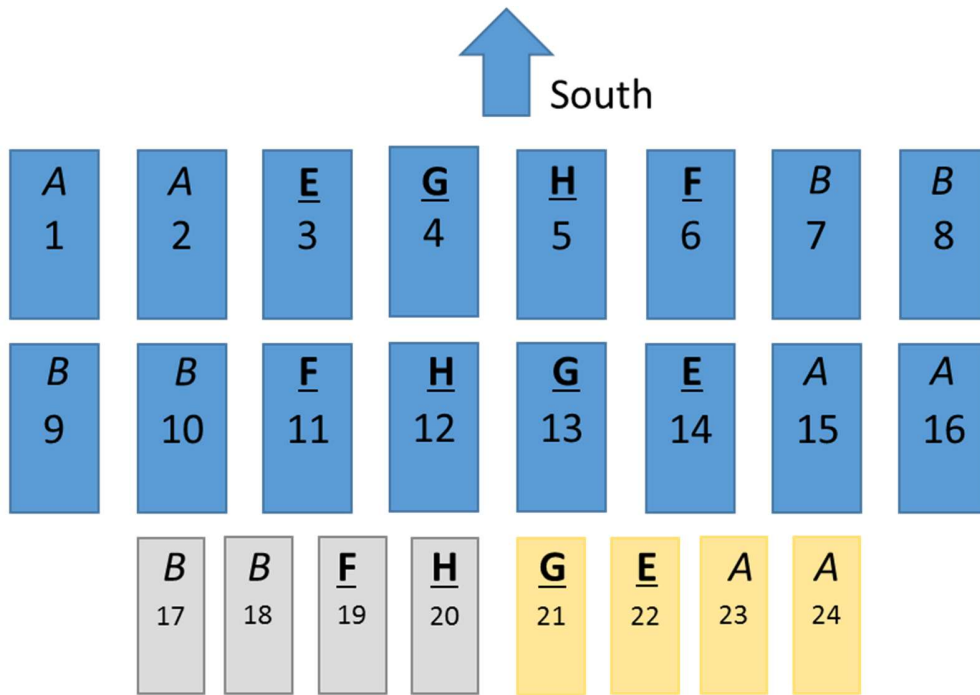
3.2 Cleaning strategy

3.2.1 Regularly cleaning

To investigate the effect of an anti-soiling product and the effect of dry cleaning and cleaning with distilled water, there are implemented four different cleaning strategies and two different reference strategies, denoted by letters explained in Table 3-1 and Figure 3.13. Half of the modules at the test site are used as references, and are left uncleaned. Initially, all the modules were cleaned with distilled water 21.01.2016, and for half of the modules (A, E, G) an anti-soiling product was applied 16.02.2016. The cleaned modules (E, F, G, H) are cleaned every second week from 20.04.2016.

Table 3-1: Description of the cleaning strategies and the corresponding module numbers. The letter denoting the cleaning strategy for the regularly cleaned modules are underlined and bold to separate them from the reference modules. Illustrated in Figure 3.13.

Cleaning strategy	Description	Poly Si-modules	Thin film modules
<i>A</i>	Anti-soiling treatment, reference	1, 2, 15, 16	23, 24
<i>B</i>	No anti-soiling treatment, reference	7, 8, 9, 10	17, 18
<u>E</u>	Anti-soiling treatment, wet cleaning	3, 14	22
<u>F</u>	No anti-soiling treatment, wet cleaning	6, 11	19
<u>G</u>	Anti-soiling treatment, dry cleaning	4, 13	21
<u>H</u>	No anti-soiling treatment, dry cleaning	5, 12	20



● **CLEANED MODULES** ● REFERENCE MODULES

- Thin film, CdTe, without anti-reflective coating
- Polycrystalline Si
- Thin film, CdTe, with anti-reflective coating

Figure 3.13: The distribution of cleaning strategies for all the modules. The different cleaning strategies are denoted by letters explained in Table 3.1. The letter denoting the cleaning strategy for the regularly cleaned modules are underlined and bold to separate them from the reference modules.

3.2.2 Additional cleaning

3.2.2.1 *Increased cleaning frequency*

On 17.10.2016, four of the regularly cleaned poly Si-modules (poly3 – 6) were cleaned after only one week of exposure to soiling. From this, the effect of cleaning is attempted isolated by comparison with the other regularly cleaned modules.

3.2.2.2 *Long-term cleaning*

On 28.10.2016, four of the reference modules (poly2, poly7, poly10 and poly15) were cleaned for the first time since 21.01.2016, to investigate the effect of long term cleaning.

3.2.3 Cleaning techniques and anti-soiling product

For both the wet and dry cleaning a microfiber cloth is used. For the dry cleaning a dry microfiber cloth is used to wipe the dust from the module glass. For the wet cleaning, the cloth is first soaked in distilled water and then used to wipe of the dust, starting from the top of the module. The cloth is used a second time to wipe the modules to remove the surplus water from the surface.

The anti-soiling product used is *RPS Eco-Coat Glass* provided by *Revolutionary Protective Solutions Ltd.* This is a hydrophobic product, which means it increases the water repellence of the glass. Because of the water repellence, the contact area between glass and water is minimized and the water forms into spherical drops, which easily roll down the module, picking up the dust in their path. The liquid product is spread over a clean surface with a cloth, and according to the producer it should be reapplied every 18th month. It generates an invisible surface coating which is supposed to remove dust more efficiently when it is raining because of its hydrophobic property, and increase the smoothness of the glass surface, which should make it harder for dirt and water to mark it.

3.3 Data analysis

In this analysis, measurement data from the test station in Kalkbult in the period from 04.05.2016 to 04.11.2016 is used.

The short circuit current is often used as an indicator for PV-module performance. However, for the case of non-uniform soiling, which may be the case in many natural environments, power output measurements may give a more accurate result, especially for crystalline silicon modules. (Gostein et al. 2013) The effect of soiling may be estimated by comparing how the power output and the efficiency of uncleaned modules and of modules cleaned on regularly basis changes with time.

As discussed earlier, the efficiency of a photovoltaic module is also dependent on other factors, as cell temperature, light intensity, and angle of incidence of incoming light. The following section describes the strategies used to compensate for these other factors influencing the efficiency to extract the effect of soiling from the measurements, and how the efficiency and power output is calculated and compared. In the first section the selection of data is presented. In the second and third section, methods for correcting the data and presenting the results are presented.

In the discussion of the results, the measurements from the test station of the amount of precipitation (natural cleaning) wind speed and relative humidity is considered.

3.3.1 Data selection

To reduce the effect of changes in light intensity and angle of incidence, the analysis is limited to data measured at midday, when the irradiance is at maximum and as constant as possible. As there are no objects in the surroundings close to the front side of the modules, there should also be no shading of the solar cells in this period.

The time when the irradiance is at maximum changes through the year, as shown in Figure 3.14. For the data used in this analysis, the measurements from 12:00 – 12:50 were selected as the midday values, as these measurements for most days are from the almost constant part of the irradiance curve, except for in the last month of the dataset. In October, the 12:50 irradiance measurement is on the decreasing part of the curve. A smaller interval would more likely contain values only from the constant part of the curve, but using fewer values would increase the uncertainty in the calculation of the midday average efficiency or power output. The 12:00 – 12:50 interval was considered as accurate enough for most of the dataset, but in an analysis with data from a whole year, changing the midday time period could be important.

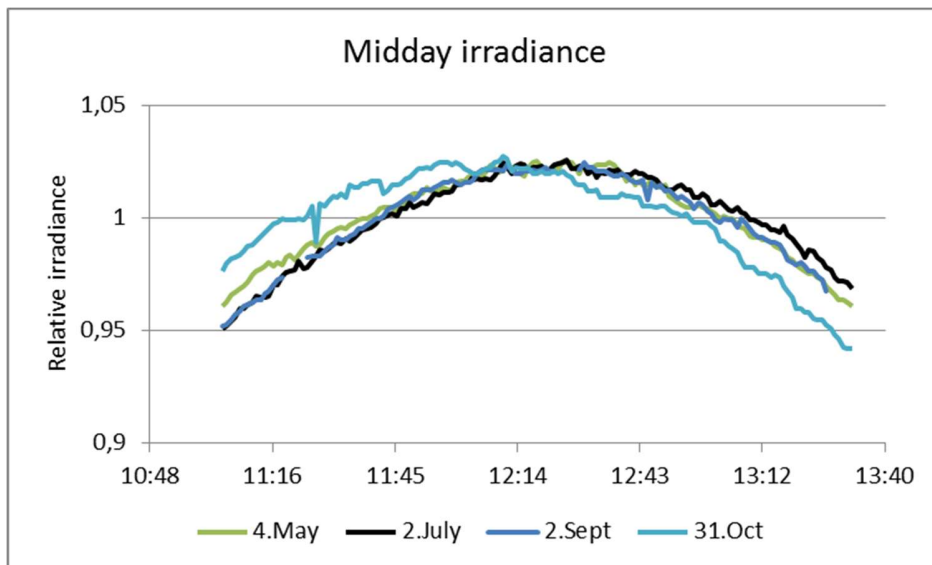


Figure 3.14: The irradiance at midday, relative to the average irradiance in the same period for four days in the time period used in the analysis.

The efficiency is calculated from the maximum power point of the measured IV -curve, and the irradiance measured at the same time by the pyranometer. This requires very accurate measurements. When the efficiency for the whole dataset was calculated, unlikely high efficiencies ($> 17\%$ for the poly Si-modules) were sometimes observed. This occurred when there was a relatively large change in the incoming radiation (relatively big difference between the instantaneous irradiance value used and the minimum or maximum measurement for the minute the value was logged). An explanation for this could be delay in the

pyranometer measurements. The response time of the pyranometer is given as < 2 seconds. If the instantaneous value is taken when there are fast changes in the irradiance, this delay could be large enough to cause significant errors. Another possible explanation is that the clouds are not shadowing the modules and the pyranometer at the exact same time.

To avoid these effects caused by clouds, only clear days are used in the analysis. It was observed that when the standard deviation of the midday measurement for the irradiance exceeded 11 W/m^2 , the standard deviation of the efficiencies for the same period could increase above 0.1. To avoid this large variation in efficiency, a standard deviation below 11 W/m^2 for the irradiance measurements at midday was defined as a clear day. As an example, from 04.05.2016 to 09.05.2016, only the three first days are used (Figure 3.15). In the period from 04.05.2016 to 04.11.2016, 91 of 185 days were considered as clear days.

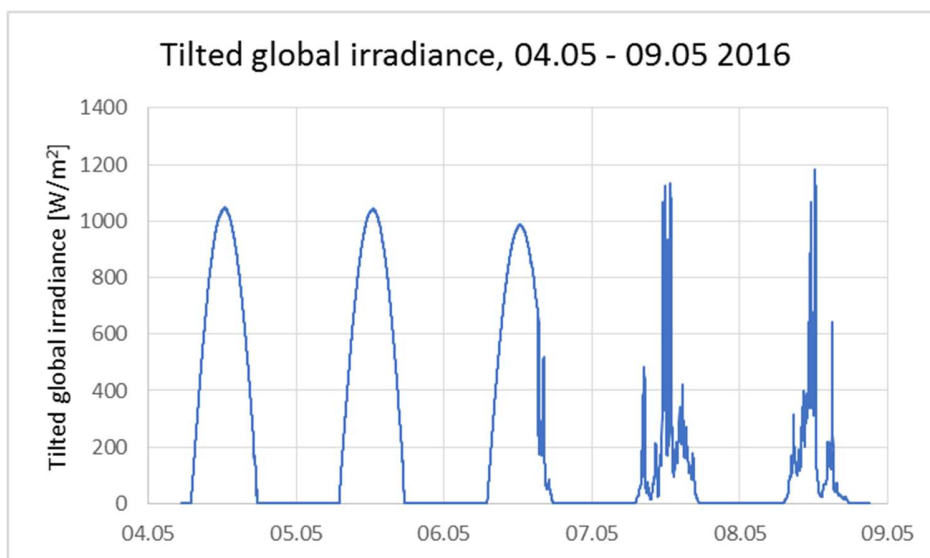


Figure 3.15: Tilted global irradiance in the beginning of May, 2016.

3.3.2 Data correction

3.3.2.1 Estimate of maximum power point

Figure 3.16 shows the distribution of the 20 measured IV -pairs for module number 3, at 12:00 02.09.2016. The red points mark in which part of the curve the maximum power point may be located. To secure an accurate identification of the maximum power point, an IV -curve is fitted to the 20 measured points using the ECN IV -curve fitting program *ivfit*, based on the two-diode model. The two-diode model is shown to be applicable for both polycrystalline silicon solar cells and CdTe thin film cells. (Prorok et al. 2006) The power output (P_{\max}) used in the calculations in the analysis, is the maximum power point of the fitted curve.

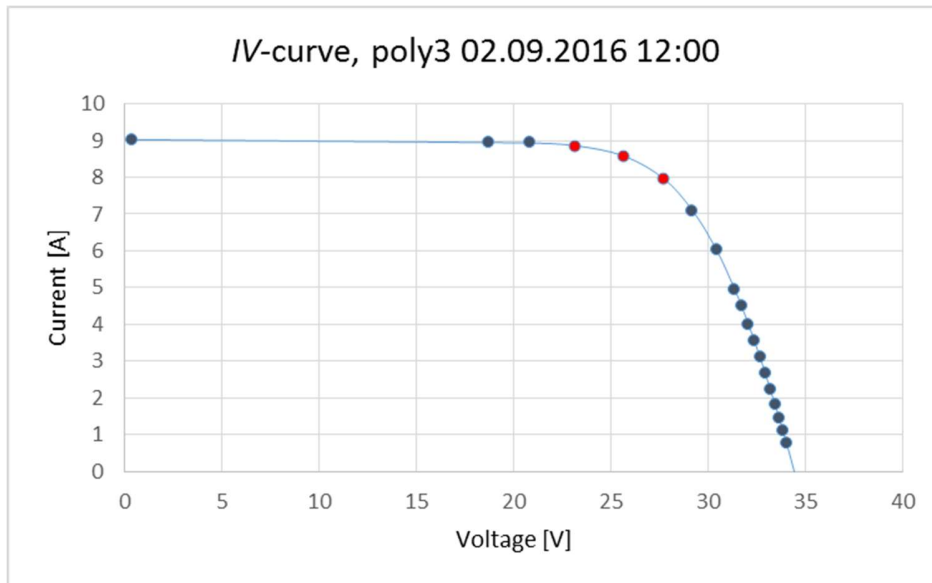


Figure 3.16: IV-curve at 12:00, 02.09.2016, for polycrystalline silicon module 3. The red points mark in which part of the curve the maximum power point may be located.

3.3.2.2 Temperature corrections

As mentioned in section 2.3.4.1, the effect of temperature on the power output is well known, and to avoid these effects the power output should be corrected for the cell temperature. For this correction, an estimate of the cell temperature is necessary, as the temperature of the cell is assumed to be higher than the measured back-surface module temperature.

Cell temperature estimate

To estimate the cell temperature, both the models presented in section 2.3.2 are considered. The cell temperature estimate from the model presented in equation 5 is referred to as the estimate based on measured module temperature, and the temperature estimate from equation 6 is the estimate based on the ambient temperature.

King et al. (2004) found the difference between the cell temperature and the back-surface module temperature at an irradiance level of 1000 W/m^2 to be $3 \text{ }^\circ\text{C}$ for modules with a polymer sheet back cover (as the poly Si-modules) and thin film modules with a steel back cover (as the CdTe-modules) in an open rack.

According to the datasheet, the nominal operational cell temperature for the poly Si-modules is $(45 \pm 2) \text{ }^\circ\text{C}$. Not using the measured back-surface temperature, the estimate based on the ambient temperature will be the same for all the modules.

The two estimates of the cell temperature are plotted with the measured back-surface module temperature for one of the poly Si-modules in Figure 3.17.

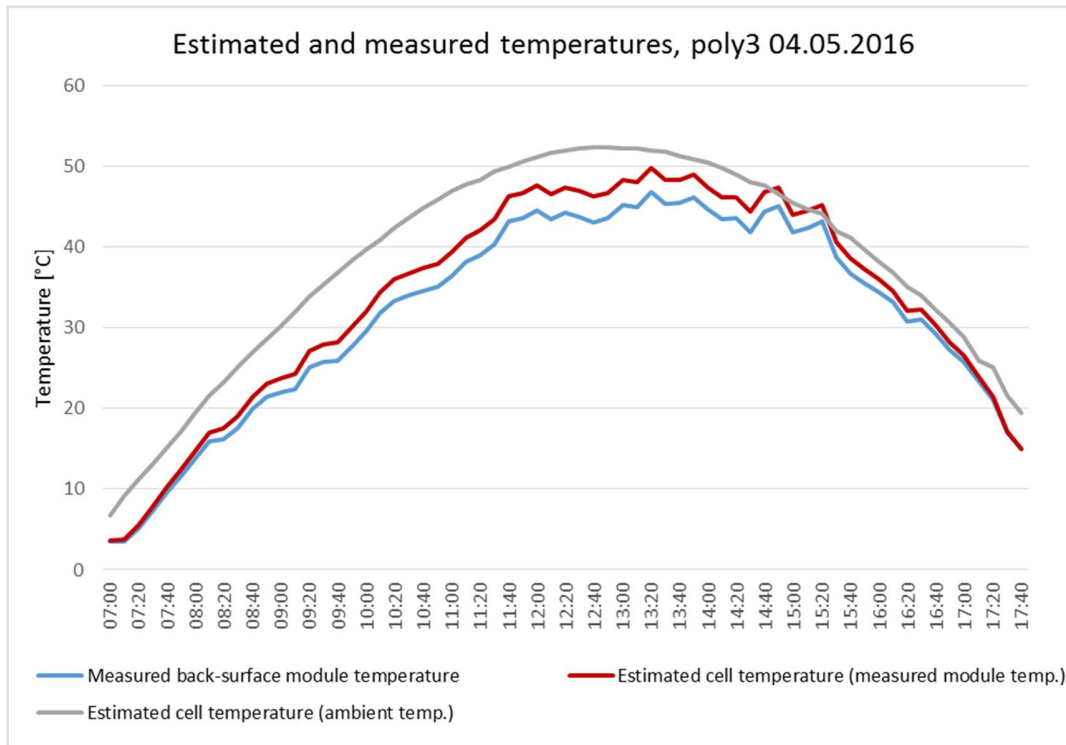


Figure 3.17: Two different estimates of the cell temperature plotted with the measured back-surface module temperature of poly3 on 04.05.2016.

The cell temperature estimates are both proportional with the irradiance, and consequently the largest difference between the measured temperature and the estimates is at midday, when the solar irradiance is at its highest. The estimate based on the ambient temperature is giving a smoother curve than the estimate based on the measured back-surface module temperature.

Temperature corrected efficiency

The temperature corrected power output (P^*) is calculated from equation 8 presented in section 2.3.4.1. In the datasheet for the polycrystalline modules, the material dependent constant is given as $-0.40\ \%/^{\circ}\text{C}$. For the thin film modules, this constant is $-0.29\ \%/^{\circ}\text{C}$.

Figure 3.18 shows the temperature corrected efficiencies (η^*) using the two temperature estimates and the measured temperature for poly 3 on 04.05.2016. The temperature corrected efficiency is calculated from the following equation:

$$\eta^* = \frac{P^*}{I_L \cdot A} \quad (14)$$

where A is the active area of the PV-module. The solar cells of the polycrystalline modules are composed of 60 solar cells of $156 \times 156\ \text{mm}$, giving a total area of $1.46\ \text{m}^2$. The active area is in practice lower because of the surface contacts covering a small part of the solar cells. The thin film modules consist of 216 active cells, and the total area is given as $0.72\ \text{m}^2$.

The uncorrected efficiency, using P_{\max} instead of P^* , is also included in Figure 3.18.

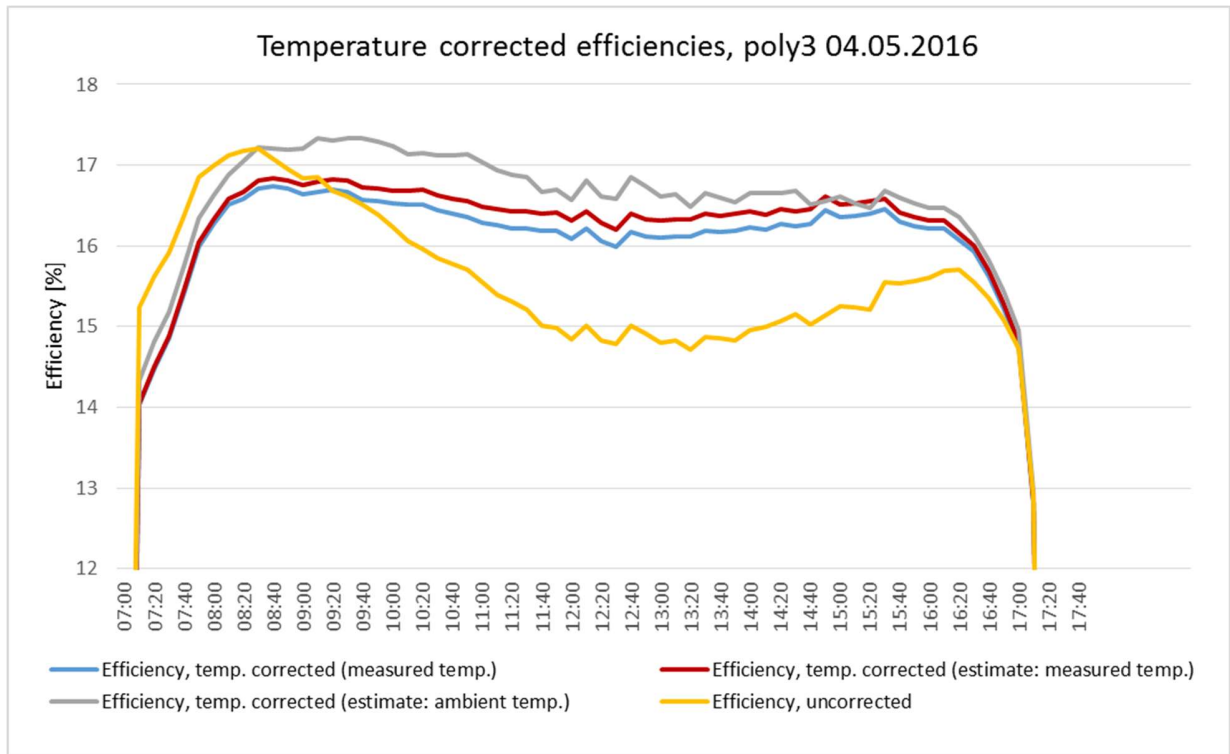


Figure 3.18: Temperature corrected efficiency based on measured back-surface module temperature and two different cell temperature estimates, plotted with the uncorrected efficiency.

As shown in Figure 3.18 the uncorrected efficiency has a decrease in the middle of the day. This decrease can be related to the increase in temperature shown in Figure 3.17, as the temperature corrected efficiencies are more constant. Further, in accordance with equation 8, we get the highest efficiency using the cell temperature estimate based on the ambient temperature, as a high temperature estimate gives higher temperature corrected power output.

From the plot of the uncorrected efficiency in Figure 3.18, it is clear that when comparing efficiencies for different days, temperature correction is necessary. Another reason that cell temperature correction is important is that the temperature of the modules depend on the position at the test site, as illustrated in Figure 3.19. As discussed earlier, an estimate of the cell temperature should be used, as the back-surface module temperature is measured in the shadow and is lower than the actual cell temperature. Even for the corrected values, the efficiencies are still higher in the beginning of the day than in the afternoon. This may indicate that the temperature correction is not a perfect compensation.

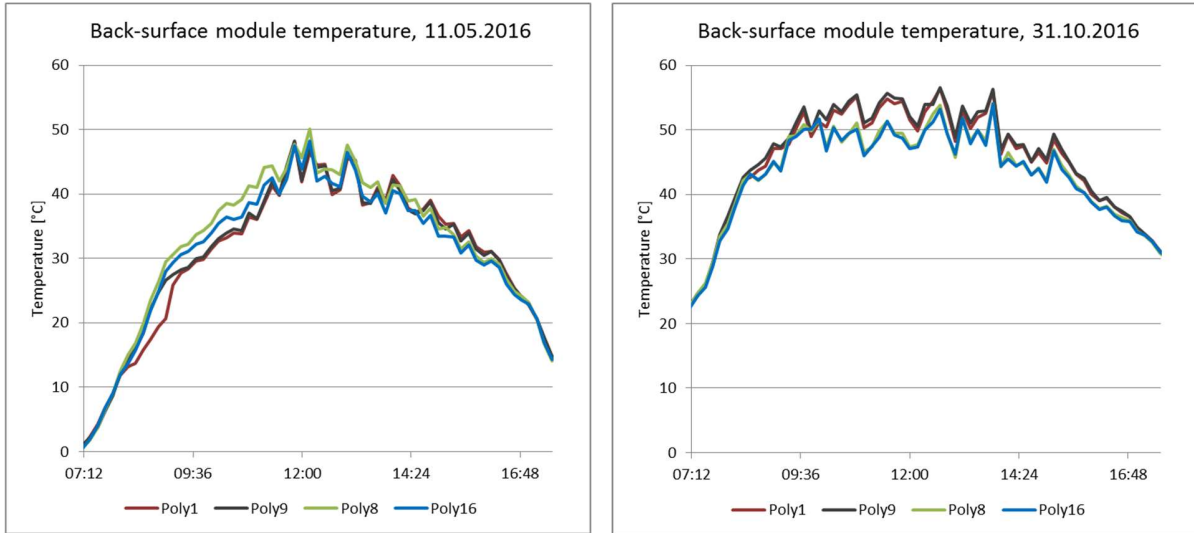


Figure 3.19: The measured back-surface module temperature for four different poly Si-modules 11.05.2016 and 31.10.2016. Poly1 and poly9 is located at the eastern side of the test site, and poly8 and poly16 is located at the western side.

The estimate based on the ambient temperature is higher than the estimate based on the measured back-surface module temperature. For the first estimate, a wind speed of 1 m/s is assumed. Normally the wind speed in Kalkbult is higher. As shown in Figure 3.7 is the daily average of the wind speed recorded at the test site never below 1 m/s. Higher wind speeds cools down the modules, consequently there is a probability that the estimate based on the ambient temperature is too high. The fact that the estimate based on the ambient temperature is unaffected by changes in wind speed may be an explanation for why this estimate is smoother than the estimate based on the measured temperature. Another source of error is that the ambient temperature is measured about 3 meters above the ground.

For the efficiencies showed in Figure 3.18 the estimate based on ambient temperature leads to a larger difference between the efficiency values in the morning and in the afternoon than for the efficiencies corrected by the measured temperature. This may indicate that the temperature estimate based on measured back-surface module temperature leads to better temperature correction. Because of this, and because the estimate based on ambient temperature does not distinguish between the modules, the temperature estimate based on the measured back-surface module temperature is considered as the better choice, and used in the analysis.

The uncertainty in the temperature estimate calculated from equation 5 is approximately equal to the uncertainty in the temperature measurement:

$$\partial T_c = \sqrt{\left(\frac{\partial I \cdot 3 \text{ }^\circ\text{C}}{1000 \text{ W/m}^2}\right)^2 + (\partial T_m)^2} \approx \partial T_m$$

The relative uncertainty in the temperature corrected power output calculated by equation 8, is given by the relative uncertainty of the cell temperature multiplied with the temperature coefficient, when assuming the unknown uncertainty of the maximum power point is negligible:

$$\frac{\partial P^*}{|P^*|} = \frac{\partial T_c \cdot \gamma}{|T_c|}$$

With an accuracy in the cell temperature of 0.5 °C, a cell temperature at midday in the range of 40 – 60 °C, corresponding to 313 – 333 K, and a temperature coefficient of 0.0040 for the poly Si-modules and 0.0029 for the thin film modules, the uncertainty in the temperature power point is insignificant. The unknown uncertainty in the maximum power point will increase the uncertainty in the temperature corrected power output. This uncertainty is attempted minimized by fitting an *IV*-curve to the measured points, and is thereby assumed insignificant.

3.3.3 Presentation of results

3.3.3.1 Yield ratio

Modules of the same type will not be identical, and they might have differences in their initial performance. To compare the performance of different technologies, and modules with different initial performance, the change in power output for the modules is compared with a reference power output. The most accurate method for finding the reference power output would be to characterize each module at STC. Another possibility would be to use the power output from the time when the modules were initially installed and cleaned. Because of missing data, the power output for each module at midday on 11.05.2016, a day with irradiance conditions close to STC, low wind speed, and after a heavy rainfall, is used as reference power output. For this it is assumed that the rainfall completely cleans all the modules. The average weather conditions and average back-surface module temperature at midday 11.05.2016 are presented in Table 3-2.

An advantage of using a reference day close to the analyzed period, is that the differences due to degradation of the modules will be reduced.

Table 3-2: The tilted global irradiance (G_t), wind speed (WS), relative humidity (RH), ambient temperature (T_{amb}) and the back-surface module temperature for both types of modules on 11.05.2016, given as the midday (12:00 – 12:50) average. The given back-surface module temperature is the average for all the modules of the same type.

Date	G_t [W/m ²]	WS [m/s]	RH [%]	T_{amb} [°C]	$T_{m, poly}$ [°C]	$T_{m, TF}$ [°C]
11.05	983.8	1.7	56.2	17.0	48	41

The change in module performance is described by their yield ratio, defined by the following equation:

$$Y_R = \frac{(P^*/G_t)_{measured}}{(P^*/G_t)_{ref}} \quad (15)$$

As the uncertainty in one single irradiance measurement is above 3 %, the uncertainty in the yield ratio will be above 4 %, assuming the uncertainty in the temperature corrected power output as insignificant.

To reduce the effect of random errors, the yield ratio will be presented as the midday average, i.e. the average of the six yield ratio values from 12:00 – 12:50.

3.3.3.2 Soiling ratio

The soiling ratio may be estimated by comparing the yield ratio of the uncleaned module (1) to an identical clean module (2):

$$S_R = \frac{P_1^*/P_{ref1}^*}{P_2^*/P_{ref2}^*} \quad (16)$$

The measured power output is divided by the reference power output to compensate for the modules not being identically. With no losses due to soiling $S_R = 1$. $S_R < 1$ indicates reduced efficiency due to soiling. As the uncertainty in the temperature corrected power output is assumed insignificant, the uncertainty in the soiling ratio is minimal.

To reduce the effect of random errors, the soiling ratio will be presented as the midday average, i.e. the average of the six soiling ratio values from 12:00 – 12:50.

3.3.3.3 Efficiency comparison

When the change in performance of one single module is investigated, the efficiency may be used. The temperature corrected efficiency is calculated by equation 14. Investigating the efficiency of one module to estimate the soiling losses may be useful after a heavy rainfall, where the rain is assumed to clean the module completely. A disadvantage with using the efficiency, is that there are large uncertainties in the calculations due to uncertainties in the irradiance measurements above 3 %. The uncertainty in the temperature corrected efficiency is even larger, because of the unknown uncertainty in the temperature corrected power output and the active area. Especially the uncertainty in the active area will increase the total uncertainty in the temperature corrected efficiency.

To reduce the effect of random errors, the efficiencies will be presented as the midday average, i.e. the average of the six efficiency values from 12:00 – 12:50.

3.3.4 Summary of analysis procedure

The summary of the analysis procedure is presented in Figure 3.20.

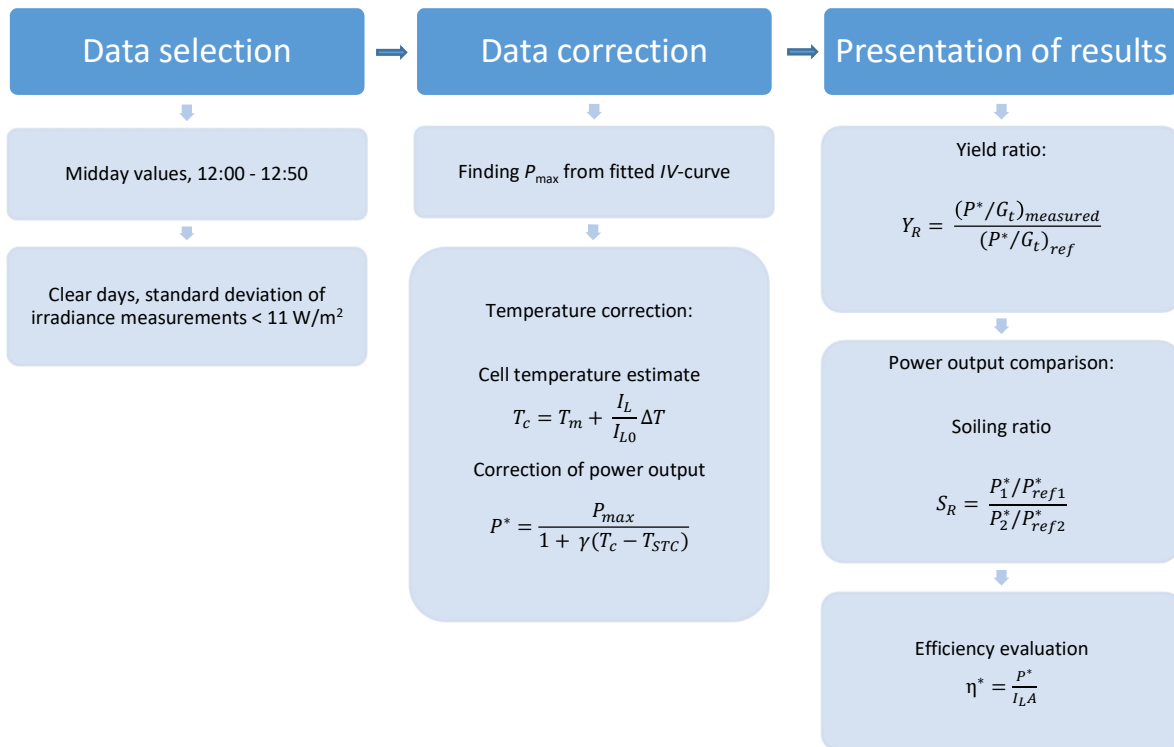


Figure 3.20: Summary of analysis procedure.

3.4 Experimental methodology

3.4.1 Quantified accumulation of dust

14.10.2016, 15.10.2016 and 17.10.2016, between 8:40 and 10:15 in the morning, a cloth was used to wipe of the dust from the 12 lower cells of poly3 – 6 to quantify the accumulation of dust through mass measurements. An additional motivation for doing this was to see if there was a difference in the amount of dust accumulating on the modules with and without the anti-soiling treatment. After the dust sample was taken, the whole module surface was cleaned. The weather conditions in the period when the experiments were conducted are presented in Table 3-3.

Table 3-3: The weather conditions in the period when the experiments investigating daily soiling were conducted, given as daily average.

Date	G_t [W/m^2]	WS [m/s]	RH [%]	T_{amb} [$^{\circ}C$]
12.10	649	2.65	23.41	15.97
13.10	658	2.65	23.61	17.99
14.10	652	2.95	21.81	19.57
15.10	518	3.65	10.36	22.44
16.10	325	3.86	19.99	18.09
17.10	645	3.06	36.07	15.67

3.4.1.1 Radwag AS 220/C/2 and Mettler Toledo Excellence Plus scale

The on-site measurements of the cloths in Kalkbult were conducted using a Radwag AS 220/C/2 scale (Figure 3.21), with a maximum capacity of 220 g, and an error of 1 mg. The scale has moveable glass walls and roof around the measure area. The Radwag scale measurements done on site were compared with measurements at IFE, Kjeller, using a Mettler Toledo Excellence Plus scale, with an accuracy of 0.1 mg.

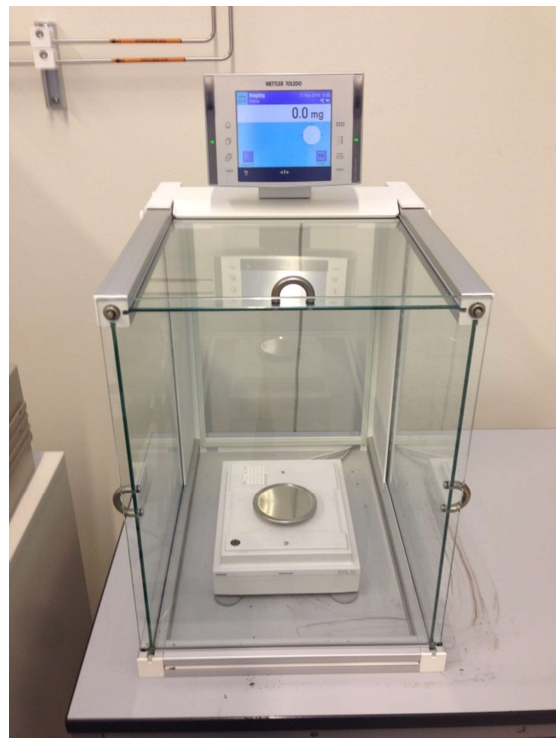
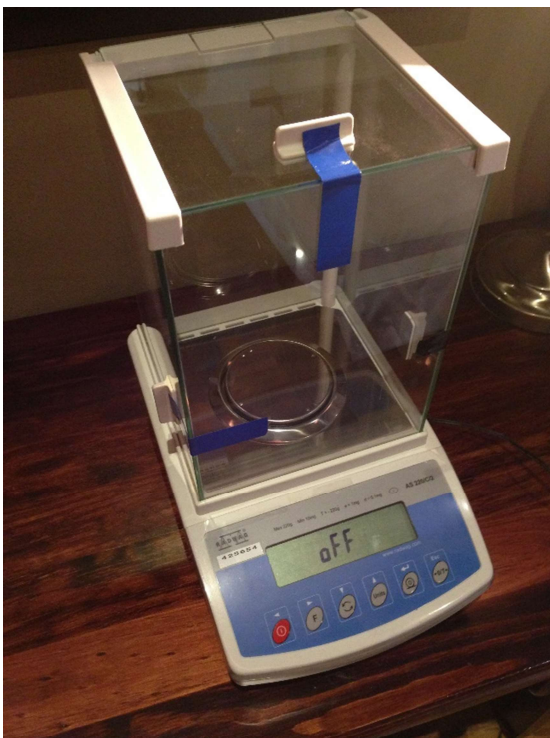


Figure 3.21: Left: the Radwag AS 220/C/2 scale, right: the Mettler Toledo Excellence Plus scale.

3.4.1.2 *Experimental procedure and calculations*

A dry cloth was used to wipe the dust of the 12 lower cells of the modules. The cloth was weighed before and after the cleaning. The mass difference between the second and first cleaning is the estimate of the amount of dust on the 12 cells. The cells are 156 x 156 mm, giving a total area of the 12 cells of 0.3 m². The soiling levels are defined the following way:

$$\text{Soiling levels} = \frac{m_2 - m_1}{A} = \frac{\Delta m}{0.3 \text{ m}^2} \quad (17)$$

where m_1 is the mass of the cloth before cleaning, m_2 is the mass of the cloth after cleaning, and A is the area of the cleaned cells. The accumulated dust per day is given as the soiling level divided by days since last cleaning.

The uncertainty in the soiling level is given as the uncertainty in the mass difference before and after cleaning, divided by the area. As the exact area is unknown, the actual uncertainty is greater. The uncertainty of dust accumulation per day is given as the uncertainty of the soiling levels divided by number of days since last cleaning.

3.4.2 Transmittance measurements

The effect of soiling was also investigated through transmittance measurements, conducted by measuring the spectral irradiance through clean and dirty glass.

3.4.2.1 *Spectroradiometer*

The spectral irradiance was measured using a portable PSR-1100F spectroradiometer provided by Spectral Evolution. The instrument measures spectral irradiance in the range 320 – 1100 nm, and the measurement uncertainty at 350 nm, 654.6 nm and 900 nm is respectively 3.2 %, 3.1 % and 3.2 %. (Brekke 2016) The fiber optic cable supplied with the spectroradiometer has a 25° field of view. To avoid the dependence of direction when measuring, the optical input was adjusted using a diffuser with a 180° field of view.

3.4.2.2 *Experimental procedure*

A module glass equal to the glass on the thin film modules was installed on the test site in the frame shown in Figure 3.22, with approximately the same tilt angle and in the same direction as the PV modules on the test site, but higher up. The glass was installed and cleaned 14.10.2016 in the afternoon, and the transmittance measurements were conducted 17.10.2016, after two and a half days. The day was chosen because it was a clear day, with no clouds.

When the measurements were conducted, the module glass was covered by a thin, visible layer of dust. One half of the glass was cleaned, while the other half was kept dirty. The light spectrum was then measured by the spectroradiometer with the diffuser in the same angle as the module glass for different times of the day. For each of the following positions (illustrated in Figure 3.22), the spectrum was measured three times within approximately 10 seconds:

1. No glass (diffuser located above the frame)
2. Through dirty glass (diffuser held close to the glass)
3. Through clean glass (diffuser held close to the glass)
1. No glass (diffuser located above the frame)

To detect changes in irradiance within the measuring time, and to verify that the measurements are within the expected value, the spectral irradiance was measured in the same angle without glass before and after the measurements through the glass.

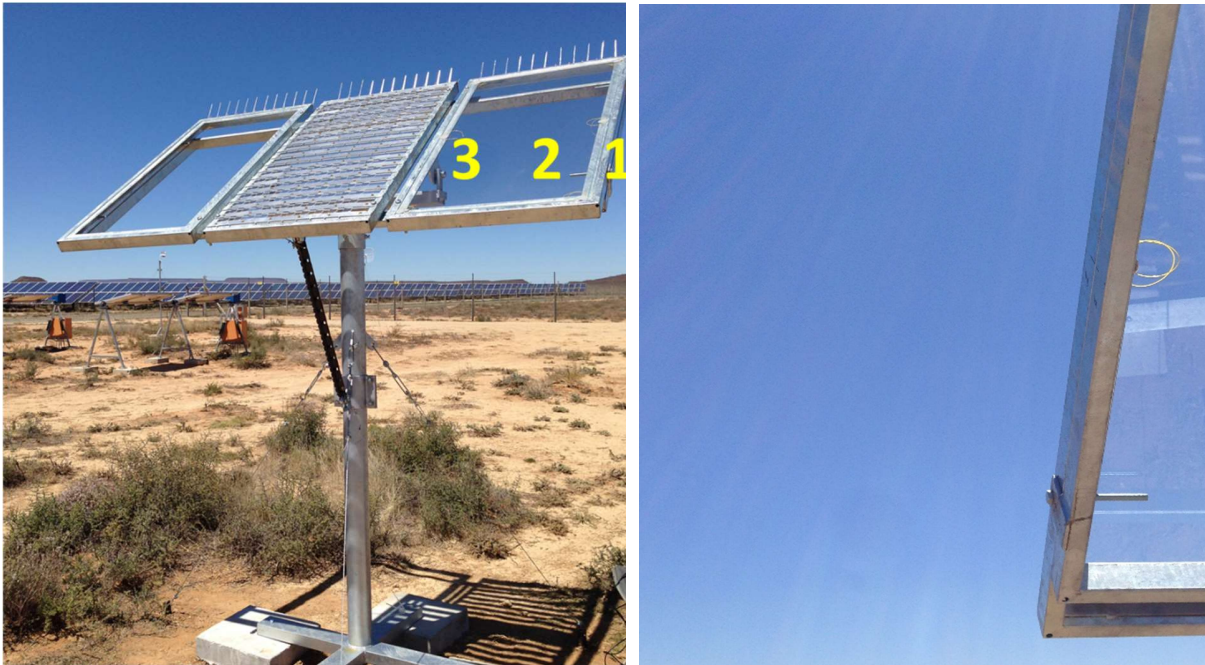


Figure 3.22: Set up for the transmittance measurement. Left: the module glass in the tilted frame. The positions where the measurements are conducted are numbered as follows: 1: no glass, 2: dirty glass, 3: clean glass. Right: The sky conditions when the measurements were taken.

4 Results and discussion

In the first part of this chapter, the analytical estimation of the effect of soiling is presented. The changes in yield ratio are presented to compare different modules and different technologies, and the energy losses due to soiling are estimated by calculating the soiling ratio and comparing the module efficiency before and after heavy rain. The performance of modules cleaned every second week, modules cleaned after one week of soiling, and modules cleaned after nine months of soiling is investigated to discuss the effect of cleaning. The irradiance dependence of the efficiency is also discussed, as this seems to be an important factor increasing the uncertainties in the analysis.

In the last part of the chapter the results from quantification of dust accumulation and the effect of the dust accumulation on the transmittance are presented.

In the interpretation of the results, amount of precipitation, wind speed and relative humidity are discussed.

4.1 Analytical estimation of the effect of soiling

4.1.1 Changes in yield ratio

The average yield ratio at midday for the six different cleaning strategies in the period from 04.05.2016 to 04.11.2016 is presented in Figure 4.1, to illustrate how the performance of the modules changes over time. The yield ratio for the thin film modules is shown in Figure 4.2. Only a selection of the thin film modules is presented due to missing data. The yield ratio is defined in section 3.3.3.1 as the efficiency of a module relative to a reference efficiency. As mentioned earlier, the modules of same type may not be identical, and because of this the yield ratio is used rather than the efficiency when the performance of different modules and different technologies are compared.

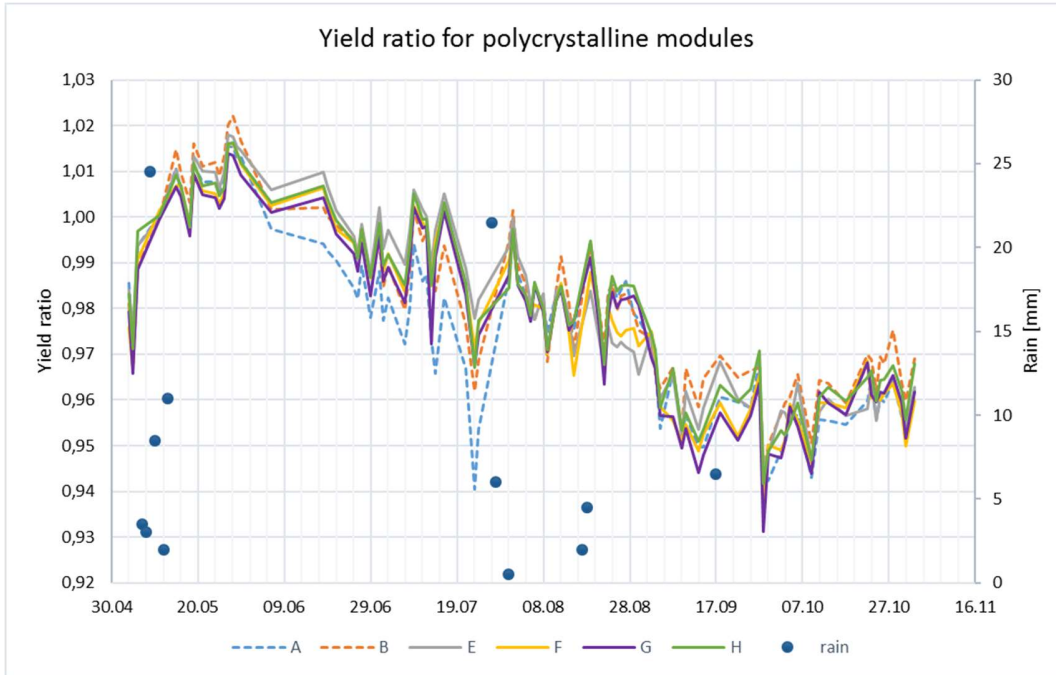


Figure 4.1: The average yield ratio at midday (12:00 – 12:50) for modules with the same cleaning strategy in the period 04.05.2016 - 04.11.2016, plotted with the amount of precipitation. A and B are the uncleaned reference modules.

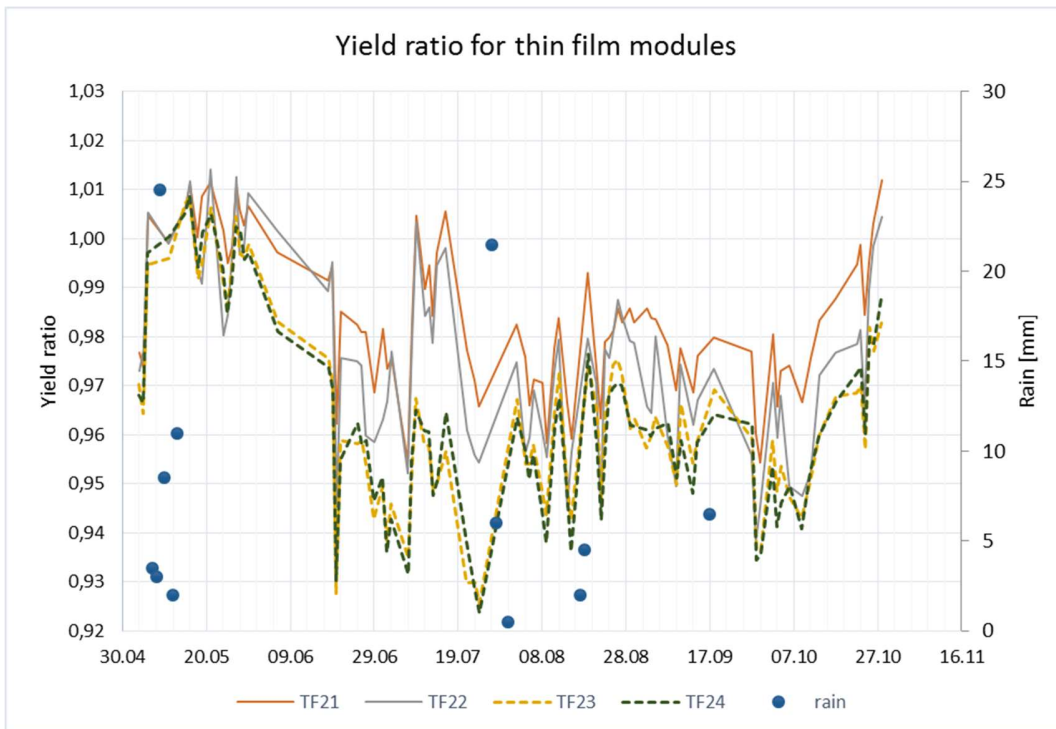


Figure 4.2: The average yield ratio at midday (12:00 – 12:50) for a selection of the thin film modules without anti-reflective coating in the period 04.05.2016 - 04.11.2016, plotted with the amount of precipitation. All the modules are treated with the anti-soiling product. TF21-22 are cleaned regularly every second week, TF21 with distilled water and TF22 is dry-cleaned. TF23-24 are uncleaned.

For all the modules, both thin film and poly Si, the yield ratio is increasing in the beginning of May, and then following a downward trend, which may seem to turn in the beginning of October. Changes in irradiance, degradation of modules and soiling are important factors that may explain the changes in performance, and are discussed more closely in the following subsections.

4.1.1.1 Irradiance dependence

The yield ratio is not corrected for dependency of light intensity. As showed in Figure 4.3 there is a correlation between the yield ratio of the regularly cleaned poly Si-modules and the irradiance at the modules. For the midday values in the period from 04.05.2016 to 04.11.2016 yield ratio is on average reduced by 0.0002 when the irradiance is increased by 1 W/m². This indicates that the decrease in yield ratio in the winter months May – July for the regularly cleaned modules (shown in Figure 4.1 and Figure 4.2) is primarily due to changes in irradiance. This is also confirmed by comparing the midday irradiance (given in Figure 4.4) with the yield ratio plots; when the irradiance is increasing the yield ratio is decreasing, and when the irradiance is decreasing the yield ratio is increasing.

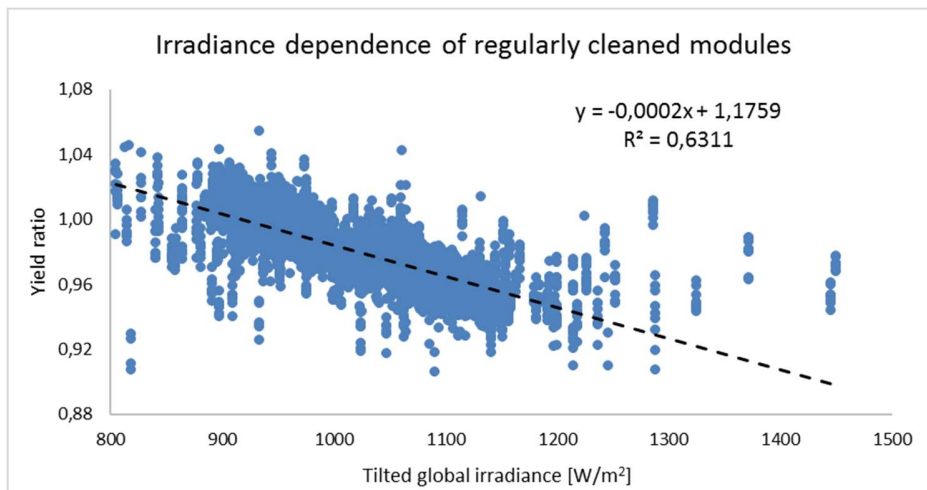


Figure 4.3: The midday yield ratio values for all the regularly cleaned poly Si-modules plotted over the tilted global irradiance. Irradiance values below 800 W/m², and yield ratio values where the corresponding efficiency is below 15 % or above 17 % are excluded. The equation for the linear fit and R² are included in the diagram.

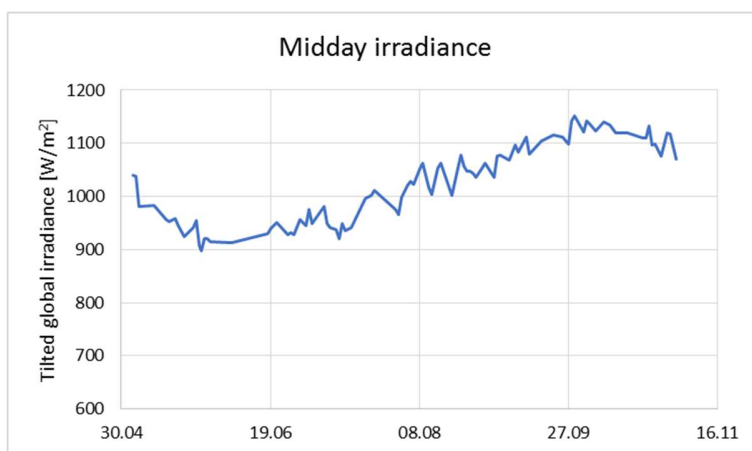


Figure 4.4: The average midday (12:00-12:50) tilted global irradiance, for clear days in the period 04.05.2016 – 04.11.2016.

The increase in yield ratio in October and May is thus also explained by irradiance dependence. In May it is reasonable that the midday irradiance decreases. However, in October the irradiance in South Africa should be increasing. An explanation for the unexpected decrease is the selection of data. As discussed in section 3.3.1, the time of the peak value of the irradiance curve is changing through the year. In October, even though the standard deviations of the irradiance values at midday do not exceed the earlier defined limit, all the values are no longer from the flat part of the irradiance curve, some of them are from the part of the curve where the decreasing trend is beginning, resulting in a lower average.

The plot in Figure 4.3 also illustrates that using the measuring data to correct for irradiance dependence will increase the uncertainty in the calculations, as the variations for a given irradiance value are large and R^2 is only 63 %.

4.1.1.2 *Degradation of modules*

The guarantee of the poly Si-modules states that the performance of the modules may be reduced from 100 % to 97.5 % due to degradation within the first year, and that the reduction is fastest in the beginning. After the first year, the degradation is slower. Light induced degeneration, an important factor for fast degradation in the period after the modules are installed and exposed to sunlight, is one of the biggest challenges for thin film solar cells. (Jäger et al. 2016) The thin film modules are consequently also experiencing fast reduction of efficiency right after they are installed.

When comparing changes in yield ratio, it is assumed that the degradation is equal for all the modules. However, it is possible that some modules are degrading faster than others, resulting in power output differences that may lead to underrating or overrating of the soiling losses. On the other side, as the modules were installed in July 2015, the most significant changes in performance due to degradation have most likely happened before 11.05.2016, when the reference power output was calculated. The influence of degradation on the comparison of the power output of the modules in May – October with the reference value should thus be minimal.

4.1.1.3 *Soiling*

After the rainfall in the middle of May, the yield ratio for all the modules are at approximately the same level. In the period from 13.05.2016 to 27.07.2016, when there is no precipitation, the yield ratio of the uncleaned modules (A and B in Figure 4.1, TF23 and TF24 in Figure 4.2) is decreasing more than the yield ratio of the regularly cleaned modules, indicating reduced power output because of soiling. Another indication of soiling, is that the differences are reduced after the rainfall in the end of July, implying that the rainfall restores the performance by cleaning the module surface. After 17.09.2016 there is also data for one and a half month without precipitation. However, in this period this difference between regularly cleaned and uncleaned modules are not distinct.

As mentioned earlier, there are several factors influencing the accumulation of dust on PV-modules. Two factors that may be important in Kalkbult, is the wind speed and the humidity. As shown in Figure 4.5, the winter months May – July have higher relative humidity and lower wind speed than September and October. The average relative humidity is 54 % in the first period, and 27 % in the second. The wind speed in the first period is mainly between 1 – 3 m/s, with some peaks at 5 m/s. In the second period the wind speed is more stable between 2 – 4 m/s. Both high relative humidity and low wind speed may increase the dust accumulation. (Guo et al. 2015; Mani & Pillai 2010; Naeem et al. 2015)

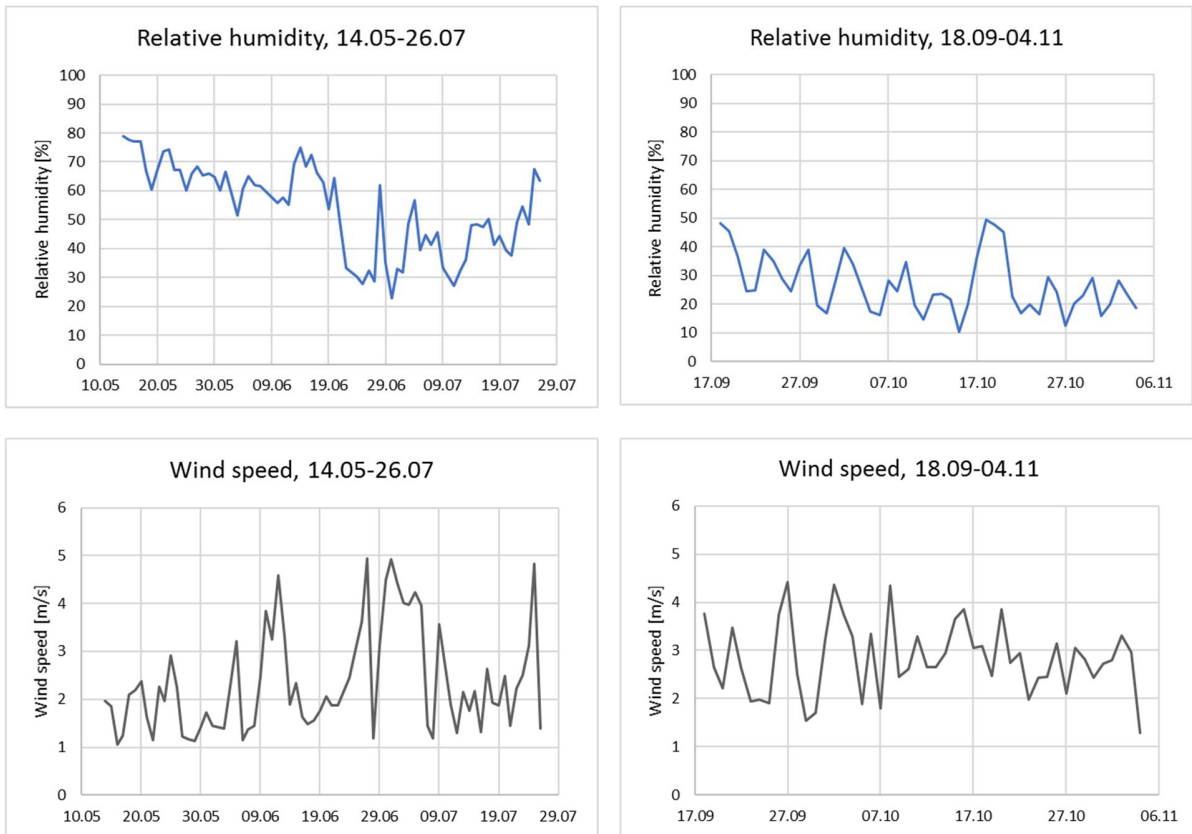


Figure 4.5: The daily average of relative humidity and wind speed 14.05.2016 - 26.07.2016 and 18.09.2016 - 04.11.2016, two periods without precipitation.

4.1.1.4 Summary of subsection

The plot of the yield ratio of the regularly cleaned and uncleaned modules in Figure 4.1 and Figure 4.2 may indicate that the yield ratio calculations, and thus also the efficiency calculations, in this analysis are highly dependent of the irradiance, and that the losses due to soiling is only significant in the winter months, where the weather conditions are unfortunate with little precipitation, high humidity and low wind speed. As mentioned in section 3.1.3, the winter months (June – August) is the period with the on average lowest number of days with precipitation in the Northern Cape.

4.1.2 Estimation of the effect of soiling on PV-module performance

In the following sections, the effect of soiling on the performance of the PV-modules and losses due to soiling are estimated using the following two methods:

One possible way to estimate the effect of soiling is to compare the uncleaned modules with the regularly cleaned modules, and investigate how the difference in power output changes. A disadvantage with this method is that the modules are cleaned only every second week, and therefore only completely clean two times every month. The actual difference between the power output of a clean module and a dirty module

will consequently be greater than the difference between the regularly cleaned modules and the dirty modules at the test site. This will result in an underestimation of the effect of soiling. On the other hand, as dust seem to attract more dust (Mani & Pillai 2010), it is possible that the uncleaned modules collect more dust per day than the regularly cleaned modules, and that the accumulated dust in two weeks on an initially clean surface is not enough to make a significant difference in the power output.

Another approach of estimating the soiling effect is to investigate how the performance of one single module changes over time. To get a useful result from this, the efficiency should be corrected for all the other different factors influencing the efficiency of the solar cell. Some of these factors are not possible to correct for because data is not available. Using the measuring data from the test site to correct for i.e. changes in irradiance and wind speed would be possible, this would on the other side increase the uncertainty in the calculated as mentioned in section 4.1.1.1. To avoid increasing the uncertainty, measurements from days with similar weather conditions may be compared. A disadvantage with this type of comparison where few data points are used, is that there may be other unknown sources of errors influencing the efficiency on the specific time for when the comparison is conducted.

4.1.2.1 Comparing regularly cleaned and dirty modules

The power output of the regularly cleaned modules and the reference modules are in the following section compared by calculating the soiling ratio, defined in section 3.3.3.2 as the ratio of the power output of a module exposed to soiling and the power output of a clean module. The regularly cleaned modules are in this calculation used as clean modules. As mentioned earlier, this assumption may lead to an underestimation of the soiling effect.

The soiling ratio for the poly Si-modules are shown in Figure 4.6, where the averages of the power outputs for four different cleaning strategies are compared with the average values of the uncleaned modules. The cleaned modules with anti-soiling treatment are compared with uncleaned modules with the treatment, and the cleaned modules without treatment are compared with uncleaned modules without the treatment. The averages are presented, as the modules with the same cleaning strategy are assumed to have the same soiling levels. Figure 4.7 shows the soiling ratio for the thin film modules for two different cleaning strategies. With an increased dust accumulation on the uncleaned modules, the power output would be reduced compared to the clean modules, and a decrease in the soiling ratio would be expected.

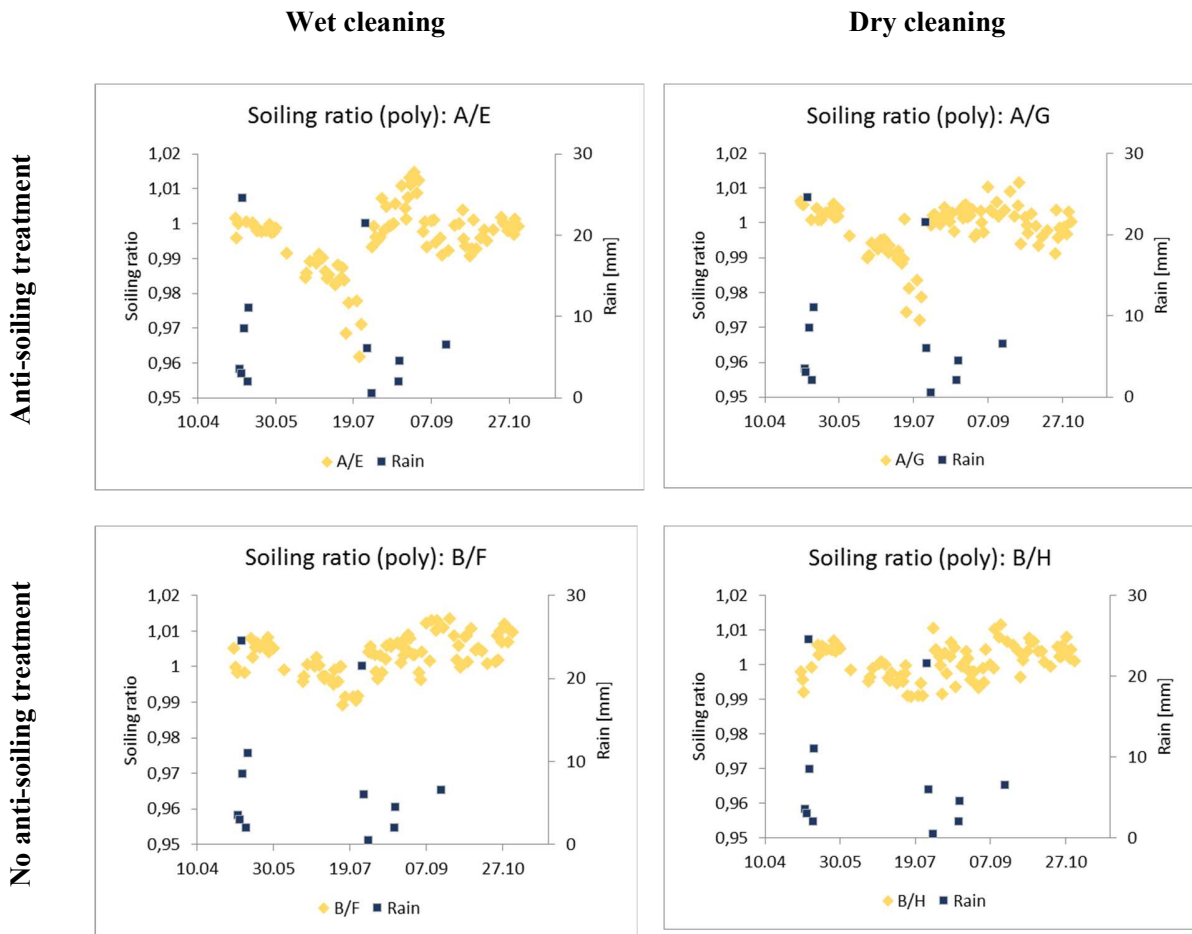


Figure 4.6: The average soiling ratio at midday (12:00 – 12:50) for the uncleaned and regularly cleaned poly Si-modules. The ratio is calculated as an average for the modules with the same cleaning strategy, and plotted with the amount of precipitation.

Ideally the maximum soiling ratio should be 1. The explanation for why it in some cases is larger than 1, is the uncertainty in the reference value used to correct the power output. However, in this comparison this is not essential, as it is the changes in the soiling ratio that are discussed.

Anti-soiling treatment

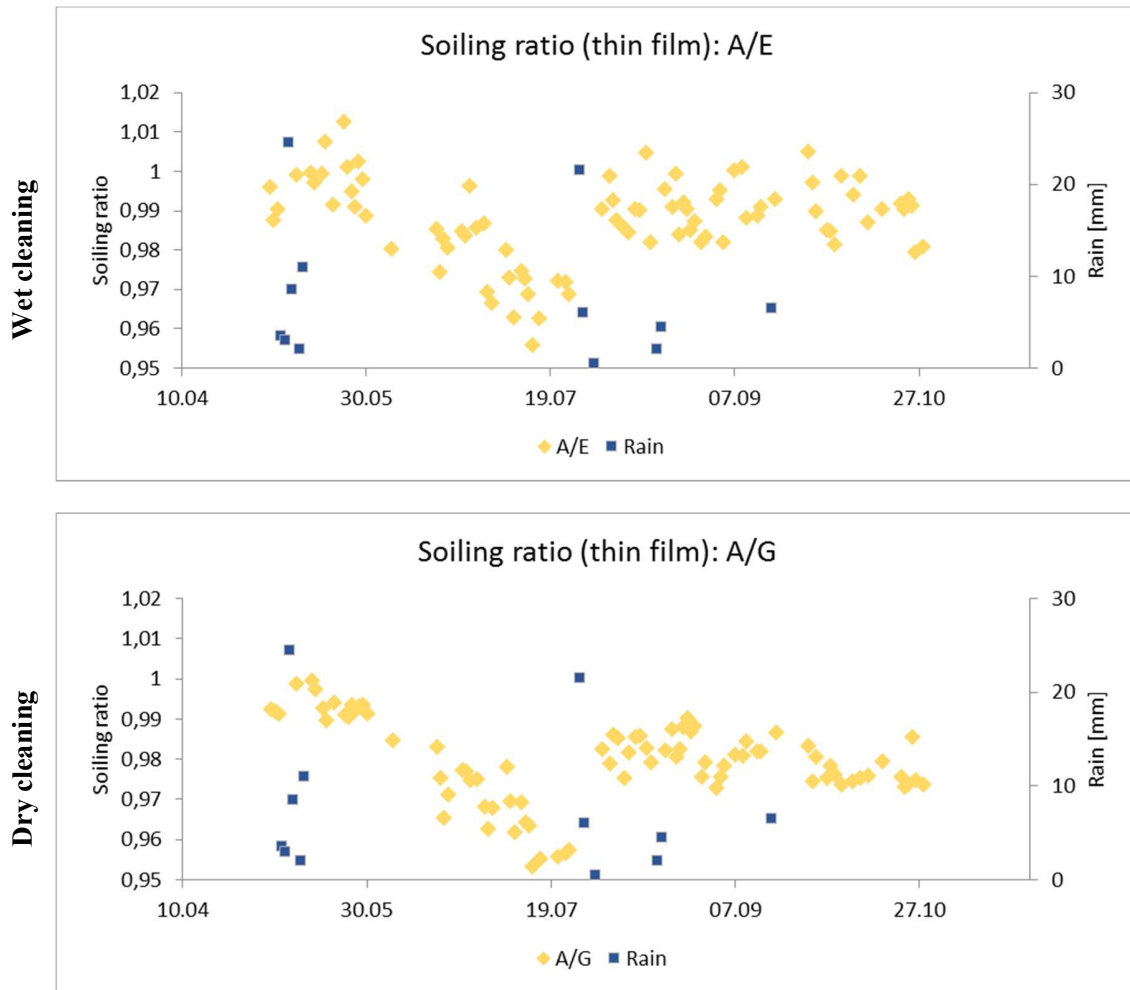


Figure 4.7: The average soiling ratio at midday (12:00 – 12:50) for the uncleaned and regularly cleaned thin film modules. The ratio is plotted with the amount of precipitation. Cleaning strategy E is represented by TF22, G by TF21, and A is an average of the power output values for TF23 and TF24.

For the modules (both thin film and poly Si) with the anti-soiling treatment, the soiling ratio in the winter months is decreasing in greater extent than for the modules without anti-soiling treatment, for both the wet- and dry-cleaned modules. From the end of September, the changes in the ratio is more random for all the cleaning strategies, showing that the accumulation of dust is not as prominent as in June and July, as earlier discussed. After the rainfall in the end of July, the soiling ratio for the poly Si-modules are restored to the values after the rainfall in May, indicating that the rainfalls are cleaning the modules in equal extent. For the thin film modules, the soiling ratio is not perfectly restored after the rain in July, implying that the cleaning effect of the rain is not as good as for the poly Si-modules. An explanation for this may be different properties of the module surface.

In the period with no precipitation during the winter months, the soiling ratio calculated for the poly Si-modules is reduced by 0.04 for the modules with anti-soiling treatment, and 0.02 for the modules without the treatment. For the thin film modules with anti-soiling treatment the soiling ratio is reduced by 0.05. All

three reductions apply for both cleaning strategies, indicating that that the cleaning techniques are equally effective, and that the factor causing differences in soiling levels is the anti-soiling treatment.

The slow decrease in soiling ratio for the modules without anti-soiling treatment could mean that the modules without the treatment are collecting less dust than the modules with the treatment. Another explanation is that the cleaned modules without the treatment are collecting more dust, reducing the difference to the uncleaned modules.

The average yield ratio and the power output ratio (calculated as soiling ratio) for the uncleaned poly Si-modules with and without anti-soiling treatment are given in Figure 4.8.

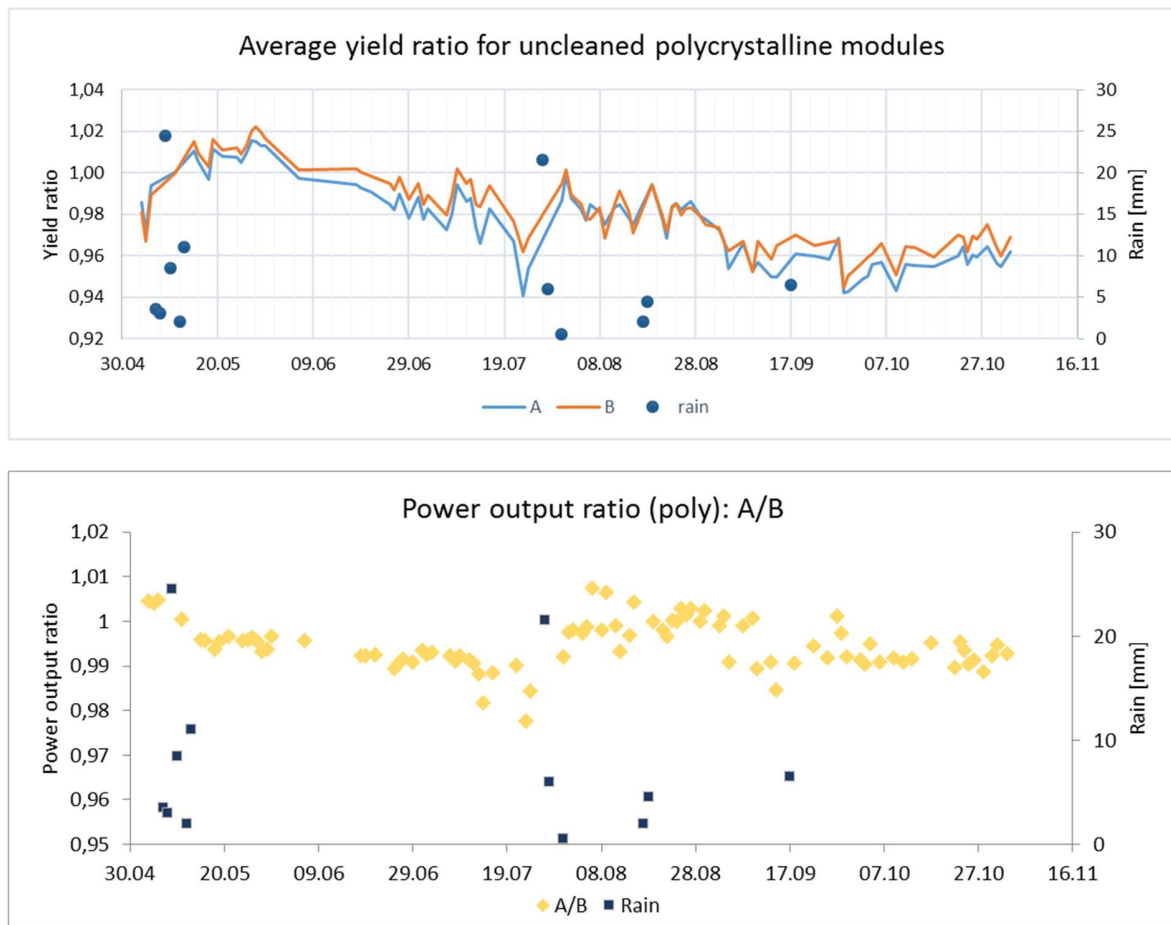


Figure 4.8: The average yield ratio at midday for the uncleaned polycrystalline silicon modules with (A) and without (B) anti-soiling treatment, and their power output ratio (calculated as soiling ratio).

Figure 4.8 shows that the power output ratio for the uncleaned modules with and without anti-soiling treatment is decreasing, implying that the power output of the modules with anti-soiling treatment is reduced relative to the power output of the modules without the treatment. When the power output of the cleaned modules with and without treatment is compared, no changes in power output ratio is observed. This indicates that the reason for the decreasing soiling ratio for the modules with anti-soiling treatment is that the uncleaned modules with the treatment are collecting more dust, and not that the cleaned modules with the anti-soiling treatment are collecting less dust than the cleaned modules without the treatment.

As mentioned in section 3.3.3.2, the uncertainty in the soiling ratio, and thus also the uncertainty in the power output ratio, is minimal. The losses in power output for the modules with the anti-soiling treatment might consequently be considered as significant.

4.1.2.2 Changes in performance for each module due to soiling

For the investigation of the changes in performance for each module presented in the following section, the average midday efficiency is used, to include modules without measurements on the day the reference value was calculated. Another reason for using the efficiency is to avoid the uncertainties of the reference value, as it is a chance that the modules were not completely clean on the reference day.

To estimate the maximum losses due to soiling in the winter months, the average midday module efficiency on days with similar weather conditions before and after heavy rain is compared. The rainfall 27.07.2016 is used because the soiling levels in the analyzed time period are at its highest before this event, as seen in section 4.1.2.1, and because the total amount of rain was 21.5 mm, which is one of the highest values recorded at the test station (Figure 3.6). The midday efficiency on 21.07.2016 represents the conditions where the soiling levels are at its highest, and the efficiency on 02.08.2016 is assumed to be the efficiency of a completely cleaned module. The difference in efficiency between the two days may consequently be interpreted as maximum efficiency reduction due to soiling. The weather conditions for the two days used in the comparison are given in Table 4-1.

Table 4-1: The average and standard deviation for the midday (12:00 – 12:50) tilted global irradiance (G_t), wind speed (WS) and ambient temperature (T_{amb}) on 21.07.2016 and 02.08.2016.

Date	Avg. G_t [W/m ²]	St.d. G_t [W/m ²]	Avg. WS [m/s]	St.d. WS [m/s]	Avg. T_{amb} [°C]	St.d. T_{amb} [°C]
21.07	997.2	2.9	2.8	0.4	16.9	0.5
02.08	998.2	3.6	3.4	0.2	15.4	0.4

The uncertainty in the midday efficiency can be estimated from the standard deviation of the measurements. The standard deviation should describe random uncertainties in irradiance and maximum power point measurements, and the uncertainty caused by variation in power output because of factors not corrected for in the calculation, such as small changes in weather conditions. The largest standard deviation for the midday efficiencies used in the following comparison is 0.1 %. There are six efficiency values at midday, giving a maximum standard deviation of the mean equal to $\frac{0.1}{\sqrt{6}} = 0.04$ %. As discussed in section 3.3.3.3 the uncertainty in the calculated efficiency is above 3 %. Using this percentage, the uncertainty would be about 10 times the value given from the standard deviation of the mean. If the 3 % error is due to constant systematic errors in the measurement equipment, this would not affect the comparison in great extent. However, if the error in the measurements of e.g. the pyranometer is changing for different temperature or irradiance levels, this could lead to significant errors in the comparison.

The temperature corrected midday efficiencies on 21.07.2016 and 02.08.2016 for the poly Si-modules and the thin film modules are given in Figure 4.9 and Figure 4.10, respectively. The regularly cleaned modules are marked, and the maximum standard deviation of the mean is included.

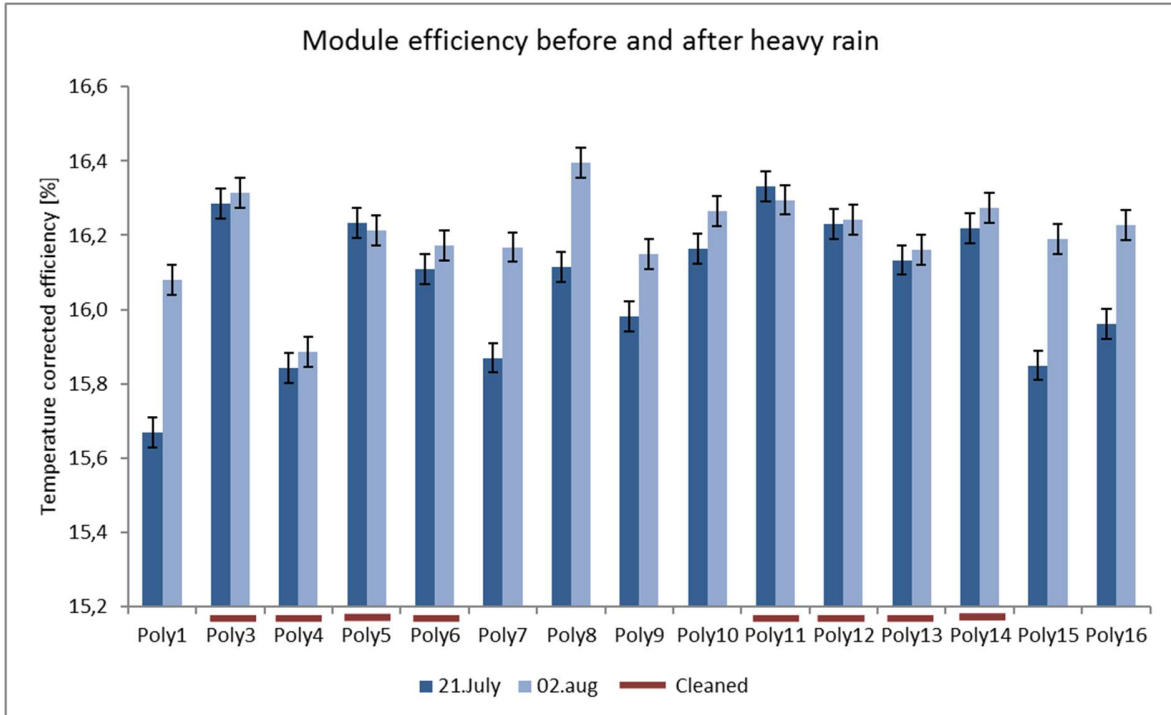


Figure 4.9: The temperature corrected average midday efficiency 21.07.2016 and 02.08.2016 for the poly Si-modules, before and after a heavy rainfall. The regularly cleaned modules are marked, and all the efficiencies are plotted with the maximum standard deviation of the mean.

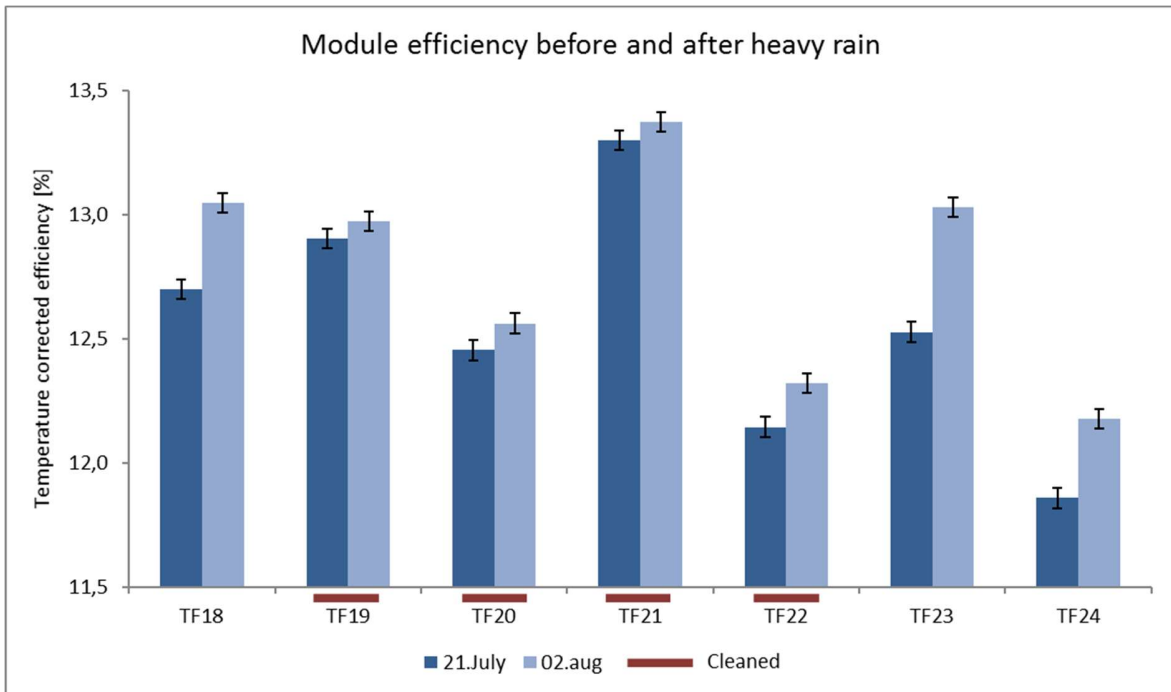


Figure 4.10: The temperature corrected average midday efficiency 21.07.2016 and 02.08.2016 for the thin film modules, before and after a heavy rainfall. The regularly cleaned modules are marked, and all the efficiencies are plotted with the maximum standard deviation of the mean.

All the modules that are cleaned every second week have either a lower increase in efficiency than all the dirty reference modules, or no significant difference at all.

The module efficiencies before and after the rain are compared by calculating their difference in percentage points, as presented in Table 4-2. The differences are given as the average value for each cleaning strategy.

Table 4-2: Comparison of the module efficiencies before (21.07.2016) and after (02.08.2016) heavy rain. The average difference in percentage points is calculated for the four cleaning strategies (E – H) and the two reference strategies (A, B). The number of modules for each cleaning strategy (n) is given in column 3 and 5. A, E and G is treated with anti-soiling product.

Poly Si-modules			Thin film modules	
Cleaning strategy	n	Difference ($\eta_{02.08}^* - \eta_{21.07}^*$) [p.p.]	n	Difference ($\eta_{02.08}^* - \eta_{21.07}^*$) [p.p.]
<i>A</i>	3	0.34	2	0.41
<i>B</i>	4	0.21	1	0.35
<u><i>E</i></u>	2	0.04	1	0.18
<u><i>F</i></u>	2	0.01	1	0.07
<u><i>G</i></u>	2	0.04	1	0.07
<u><i>H</i></u>	2	0.00	1	0.11

Using the maximum standard deviation of the mean as the maximum uncertainty for the calculated efficiency, the uncertainty in the difference is $\sqrt{0.04^2 + 0.04^2} = 0.06$ percentage points. For the uncleaned modules, the differences exceed this value, meaning there is a significant increase in efficiency from 21.07.2016 to 02.08.2016, and thus also significant losses due to soiling. The modules treated with anti-soiling product (A) is increasing more than the untreated modules (B). The increase in efficiency for the regularly cleaned modules is significant for the thin film modules. The increase in efficiency for the poly Si-modules are not significant when using the maximum standard deviation. However, it may seem like the efficiency of poly Si-modules with anti-soiling is increasing in greater extent than the modules without the treatment. The result that thin film modules and modules with anti-soiling treatment are more affected by soiling is consistent with the results presented in section 4.1.2.1.

Most likely these differences are underestimating the effect of soiling. Firstly, this estimation requires that the rainfall completely cleans the modules. Whether this may be the case will be discussed further in section 4.1.3 regarding the long-term cleaning. Secondly, after the rain, due to the wet surface, dust may stick more easily to the module glass. A result of this is that even though the rain completely cleans the PV-module, the dust accumulation may be large in the hours after, and reduce the efficiency calculated for the assumed clean modules. The maximum decrease in efficiency before the rainfall is also higher, as there is almost a week from the day the minimum efficiency is calculated (21.07.2016) to the rainfall.

4.1.2.3 Losses

The average power losses per month, calculated by $1 - S_{R, \text{monthly average}}$, where the soiling ratio is adjusted so that the maximum value is equal to 1, is given for June and July in Table 4-3 and Table 4-4, respectively. The reduction in efficiency and the corresponding energy loss are also presented in the tables. The average

midday efficiency for the clean poly-Si modules is 16.4 % in June and 16.3 % in July. The average efficiency for the clean thin film modules is 12.9 % for both months. For a plane with the same orientation as the PV-modules at the test station, the average insolation is 167 kWh/m² in June and 184 kWh/m² in July (Figure 3.4). For the energy loss calculation, the efficiency and power loss is assumed constant for the whole day.

Table 4-3: The average power loss in June calculated by comparing the uncleaned reference modules with the regularly cleaned modules, the resulting reduction in efficiency given in percentage points (based on the average efficiency of the clean modules) and total energy loss for one module (based on the normal insolation for the month).

June	A / \underline{E}, A / \underline{G} (poly Si)	B / \underline{E}, B / \underline{G} (poly Si)	A / \underline{E} (thin film)	A / \underline{G} (thin film)
Power loss [%]	1	1	2	4
Reduction in efficiency [p.p.]	0.2	0.2	0.3	0.5
Energy loss [kWh/month]	0.5	0.5	0.7	1.2

Table 4-4: The average power loss in July calculated by comparing the uncleaned reference modules with the regularly cleaned modules, the resulting reduction in efficiency given in percentage points (based on the average efficiency of the clean modules) and total energy loss for one module (based on the normal insolation for the month).

July	A / \underline{E}, A / \underline{G} (poly Si)	B / \underline{E}, B / \underline{G} (poly Si)	A / \underline{E} (thin film)	A / \underline{G} (thin film)
Power loss [%]	2	1	3	4
Reduction in efficiency [p.p.]	0.3	0.2	0.4	0.5
Energy loss [kWh/month]	0.8	0.5	1.1	1.3

The efficiency will not be constant through the day, as assumed in the energy loss estimate. Because the efficiency is lower in the beginning and end of the day, this could lead to an overestimation of monthly energy losses. However, in the morning and afternoon, the total insolation is low compared to the daily insolation, and the efficiency reduction will be applicable to the largest part of the insolation. Additionally, as mentioned in section 2.4.1, the soiling losses are larger at higher angle of incidence, meaning that higher losses in the morning and evening may compensate for the lower efficiency.

In Kalkbult the average daily insolation on a surface with the same orientation as the test site modules in July is 5.9 kWh/m² (Figure 3.4). The maximum efficiency decrease presented in Table 4-2, will lead to maximum daily losses as presented in Table 4-5, assuming the efficiency and loss is constant the whole day.

Table 4-5: The maximum daily loss in July for poly Si-modules and thin film modules with and without anti-soiling treatment, calculated from the maximum efficiency difference, given in percentage points.

Poly Si-modules			Thin film modules	
Strategy	Difference [p.p.] ($\eta_{02.08}^* - \eta_{21.07}^*$)	Daily loss [kWh/day]	Difference [p.p.] ($\eta_{02.08}^* - \eta_{21.07}^*$)	Daily loss [kWh/ day]
A	0.34	0.03	0.41	0.04
B	0.21	0.02	0.35	0.03

As for the losses calculated from the average soiling ratio (Table 4-3 and Table 4-4), the losses are largest for the modules with anti-soiling treatment, and the thin film modules are more affected than the poly Si-modules. John et al. (2016) also showed that cadmium telluride modules are more affected by dust than polycrystalline modules, and related this to measurements showing that the dust used in their experiments in greatest extent affected the light spectra for the wavelengths best utilized by CdTe solar cells, and had least impact on the wavelengths in the part of the light spectra where the crystalline silicon solar cells best utilize the incoming light. Another possible explanation is that the glass surface of the modules may be different. For the module glass used for the transmittance measurements, which is of the same type as the thin film modules, it was observed that the dust was sticking to the surface in greater extent than for the poly Si-modules. This could also explain that the modules are not fully recovered after rain, as shown in Figure 4.7.

The average reduction in efficiency for July (calculated by comparing clean and dirty modules, Table 4-4) is equal to the estimated maximum efficiency reduction in July (calculated by comparing the module efficiency before and after rain, Table 4-5). As discussed earlier are both values underestimated. This may indicate that the maximum efficiency reduction is underestimated to a greater extent than the average monthly soiling ratio. On the other hand, the energy losses may in both cases be overestimated, as the efficiency is assumed as constant for the whole day, when it actually is lower in the morning and the evening than in the middle of the day.

4.1.2.4 Summary of subsection

For both the thin film and poly Si-modules, the performance of modules with anti-soiling treatment is reduced by soiling in greater extent than modules without the treatment, meaning that the anti-soiling product is working against its purpose. No significant difference in the performance of modules cleaned with distilled water or dry-cleaned modules were identified. In July, when the losses are most distinct, the average losses in power output is 1 % for poly Si-modules without anti-soiling treatment, 2 % for poly Si-modules with treatment, and 4 % for thin film modules with treatment, corresponding to monthly energy losses for one module of 0.5, 0.8 and 1.2 kWh respectively. In solar parks with more than 100.000 modules, this may lead to monthly losses of several MWh. The estimate of maximum reduction in efficiency in the winter months based on the comparison of performance before and after rain is most likely underestimated, as it is the same as the average monthly reduction calculated from the soiling ratio.

4.1.3 Effect of cleaning

To investigate the effect of cleaning, the changes in efficiency of the regularly cleaned modules is compared with the changes in efficiency of uncleaned modules in the period with no precipitation from May to July. In this period the dust accumulation is at its maximum, and the effect of cleaning should be most evident. The efficiency is used to include the modules without data on the reference day. Correlated to the experiments conducted to quantify the dust accumulation, half of the regularly cleaned modules were cleaned approximately one week after the scheduled cleaning. In an attempt to isolate the effect of cleaning, the changes in performance of the poly Si-modules cleaned after one week are compared with the regularly cleaned modules. The effect of long term cleaning for the poly Si-modules is also discussed.

4.1.3.1 Regular cleaning

Figure 4.11 - Figure 4.14 shows the midday efficiency of 8 different regularly cleaned modules in the period from 15.05.2016 to 24.07.2016. The efficiency calculations after a cleaning are marked in red. In all figures modules cleaned with distilled water, dry cleaned modules, and uncleaned modules are compared. Because the efficiency is used, the changes in performance should be used for comparison and not the absolute value of the efficiency, as all the modules are initially different. Figure 4.11 and Figure 4.12 shows poly Si-modules, the first with and the second without anti-soiling treatment. Figure 4.13 and Figure 4.14 shows the thin film modules with and without anti-soiling treatment, respectively. The period from 15.05.2016 to 24.07.2016 is chosen because in this period there is no precipitation, and the soiling levels are at maximum.

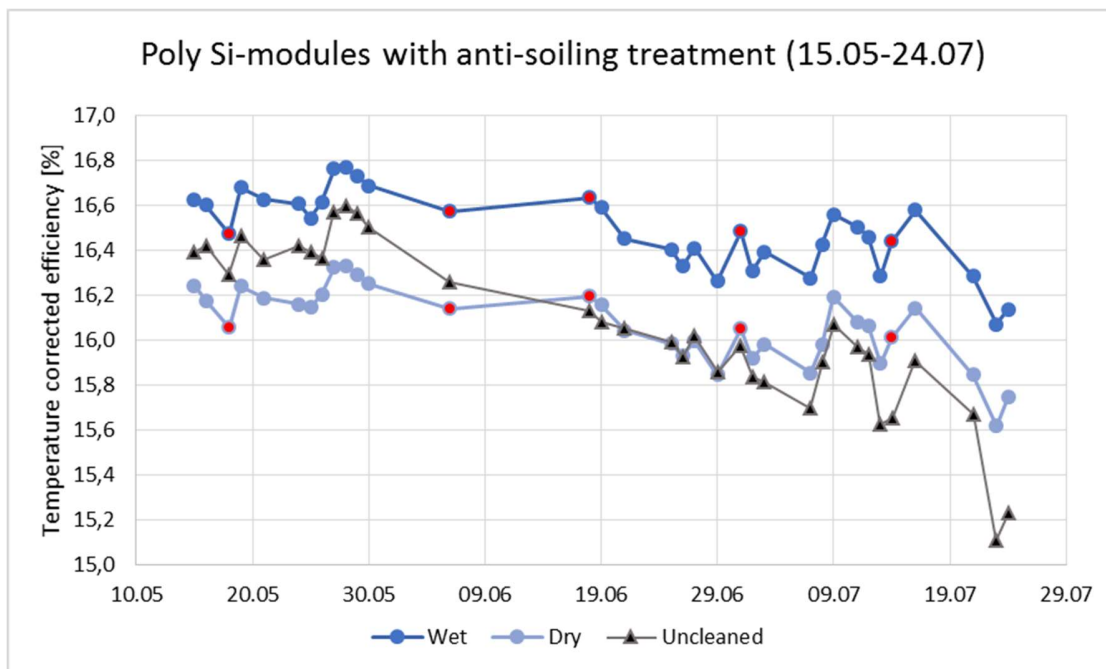


Figure 4.11: The midday (12:00 – 12:50) efficiency of poly3 (wet cleaning), poly4 (dry cleaning) and poly1 (uncleaned), all treated with anti-soiling product, in the period from 15.05.2016 to 24.07.2016. The red points mark when the modules have been cleaned prior to the measurement.

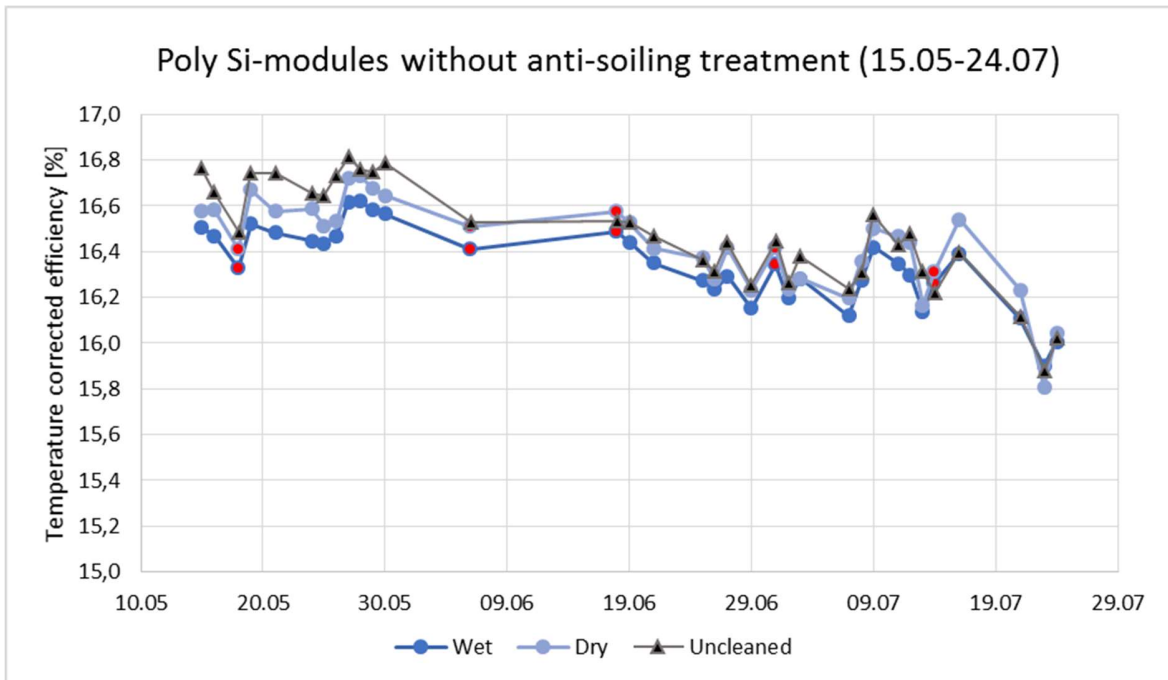


Figure 4.12: The midday (12:00 – 12:50) efficiency of poly6 (wet cleaning), poly5 (dry cleaning) and poly8 (uncleaned), all without anti-soiling treatment, in the period from 15.05.2016 to 24.07.2016. The red points mark when the modules have been cleaned prior to the measurements.

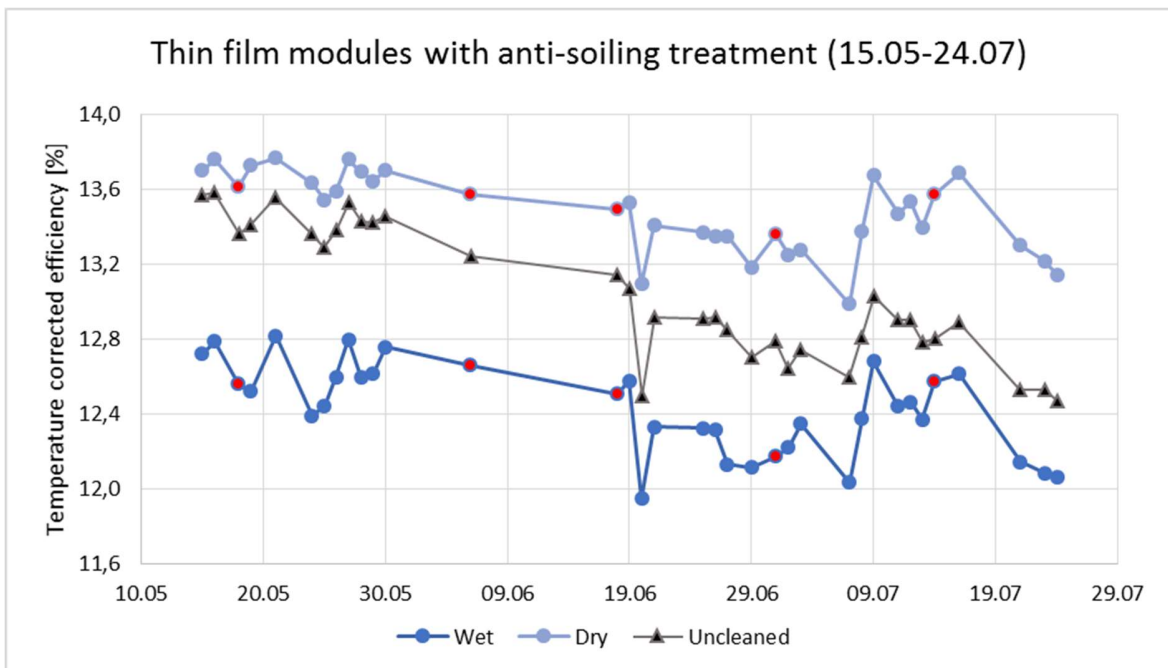


Figure 4.13: The midday (12:00 – 12:50) efficiency of TF21 (dry cleaning), TF22 (wet cleaning) and TF23 (uncleaned), all with anti-soiling treatment and without anti-reflective coating, in the period from 15.05.2016 to 24.07.2016. The red points mark when the modules have been cleaned prior to the measurements.

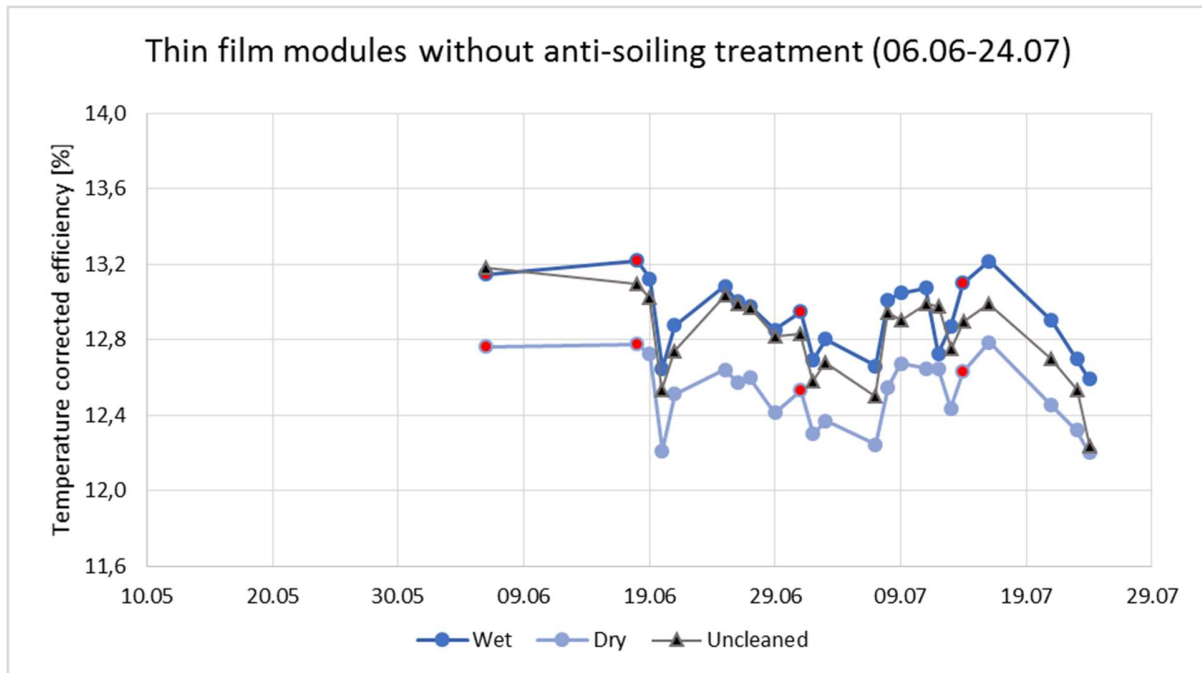


Figure 4.14: The midday (12:00 – 12:50) efficiency of TF19 (wet cleaning), TF20 (dry cleaning) and TF18 (uncleaned), all without anti-soiling treatment and with anti-reflective coating, in the period from 15.05.2016 to 24.07.2016. The red points mark when the modules have been cleaned prior to the measurements.

For some cases, it may seem like the efficiency is increasing more for the cleaned modules than for the uncleaned modules. This is however not consistently, and the differences are not greater after the cleaning than it can be on other days. For both the poly Si-modules and the thin film modules there are also no significant difference after cleaning between the dry-cleaned modules and the modules cleaned with distilled water. From this it may be concluded that both cleaning techniques are equally efficient, and that the dust accumulated over two weeks is not enough to significantly reduce the efficiency, even in the winter months, supporting the assumption that the regularly cleaned modules in the calculations may be treated as a clean module.

For more accurate comparisons, the data should have been corrected for changes in light intensity or the efficiency should have been compared for days with similar weather conditions. However, the correlation between efficiency and light intensity is not known well enough to do a correction without increasing the uncertainty. In this period, it is also too much variation in the weather to compare the efficiency right before and right after a cleaning. This is however done for a period in October in the following section.

4.1.3.2 Increased cleaning frequency

On 17.10.2016 four of the regularly cleaned modules (poly3 – 6) were cleaned after only one week of exposure to soiling, i.e. outside the scheduled cleaning. The efficiencies of all the regularly cleaned poly Si-modules before and after the extra cleaning are given in Table 4-6. The dates 13.10.16 and 17.10.16 are chosen for the comparison because of similar weather conditions, as shown in Table 4-7.

Table 4-6: The temperature corrected efficiencies before (13.10.2016) and after (17.10.2016) the additional cleaning of poly3 – 6 for all the regularly cleaned poly Si-modules, given as the midday (12:00 – 12:50) average. The ratios of the efficiencies for each module are shown in the bottom. The modules with anti-soiling treatment are marked with AS.

	<i>Poly3_{AS}</i>	<i>Poly4_{AS}</i>	<i>Poly5</i>	<i>Poly6</i>	<i>Poly11</i>	<i>Poly12</i>	<i>Poly13_{AS}</i>	<i>Poly14_{AS}</i>
$\eta^*_{13.10}$ [%]	15.92	15.48	15.88	15.69	15.92	15.83	15.72	15.65
$\eta^*_{17.10}$ [%]	15.84	15.48	15.74	15.75	15.82	15.87	15.64	15.60
Ratio ($\eta^*_{17.10} / \eta^*_{13.10}$)	<i>0.99</i>	<i>1.00</i>	<i>0.99</i>	<i>1.00</i>	<i>0.99</i>	<i>1.00</i>	<i>0.99</i>	<i>1.00</i>

Table 4-7: The weather conditions (tilted global irradiance, wind speed and ambient temperature) before and after the additional cleaning of poly3 – 6, given as the midday (12:00 – 12:50) average.

Date	G_t [W/m ²]	WS [m/s]	T_{amb} [°C]
13.10	1120	2.5	25
17.10	1119	2.7	21

The calculated efficiency ratio for the day where all the modules should be in the same condition (13.10.16) and the day where half of them were cleaned after approximately one week with soiling (17.10.16) shows no difference between the cleaned modules and the uncleaned modules. This supports the earlier results showing that the soiling in the spring is small, and that the accumulation of dust on regularly cleaned modules is not large enough to significantly reduce the efficiency.

4.1.3.3 Long term cleaning

Half of the reference poly Si-modules (poly2, poly7, poly10 and poly15) were cleaned 28.10.2016 in the afternoon, 9 months after they were cleaned with distilled water (21.01.2016). In Figure 4.15 the yield ratios of poly7, poly10 and poly15 in October are compared with the average yield ratio of the uncleaned reference modules. The yield ratio is chosen to reduce the uncertainty in the comparison. For poly2 the efficiency is compared to the average efficiency of the uncleaned reference modules because of missing data.

Anti-soiling treatment

No anti-soiling treatment

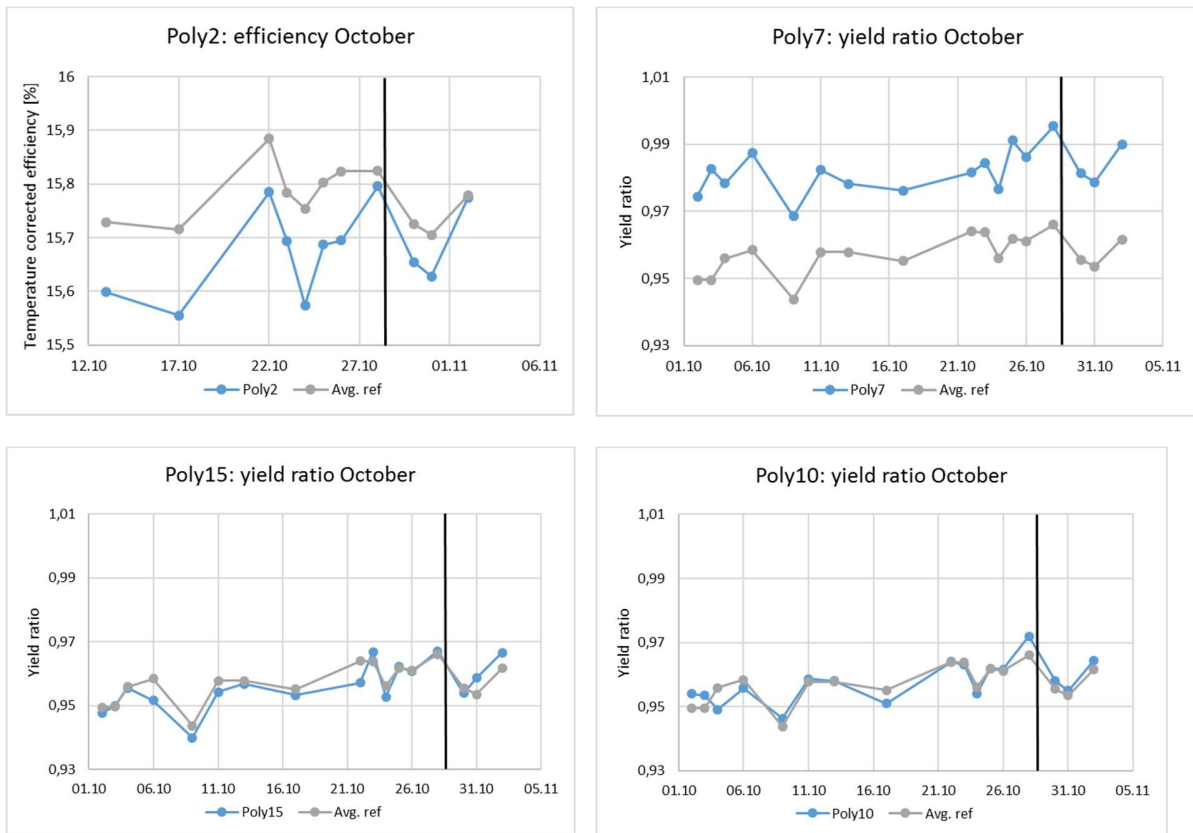


Figure 4.15: Yield ratio/efficiency for the cleaned poly Si-reference modules in October compared to the average yield ratio/efficiency (Avg. ref) of the uncleaned reference modules. The black line shows where modules number 2, 7, 10 and 15 were cleaned for the first time since 21.01.2016.

For all four modules, the yield ratio or efficiency follows the same trend as the efficiency or yield ratio for the uncleaned reference modules from 28.10.2016 to 30.10.2016. There is no indication that their performance is increasing after the cleaning compared to the uncleaned modules.

With six weeks without precipitation, it would be expected that the cleaning would increase the performance of the cleaned modules relative to the uncleaned modules. In this case, there is no increase in performance, suggesting that the modules are almost perfectly cleaned after the heavy rainfall, and that the dust accumulation in the spring is so low that six weeks with dust accumulation on a clean surface is not enough to reduce the performance.

4.1.3.4 Summary of subsection

From the efficiency changes in the period of regular cleaning and in the period of increased cleaning frequency, there is not identified any significant change in efficiency due to cleaning, for both cleaning techniques and for modules with and without anti-soiling treatment. This indicates that the soiling levels after two weeks of dust accumulation is not enough to significantly reduce the efficiency. From this it may be concluded that for the modules in Kalkbult, cleaning every two weeks is often enough to avoid significant losses. Cleaning four of the reference modules did not cause any significant changes in the efficiency of the

modules compared to the uncleaned reference modules. This result suggests that the modules are completely cleaned after a heavy rainfall, and confirms that the soiling in the spring months is low.

4.2 Irradiance dependence and temperature effects

In this section the irradiance dependence of the efficiency and yield ratio calculations are discussed, as this seems to be a considerable source of error in the dataset.

As mentioned in section 2.3.4 the efficiency of solar cells is dependent of the light intensity. The dependency of irradiance for the poly Si-modules, according to the data sheet, is shown in Figure 4.16.

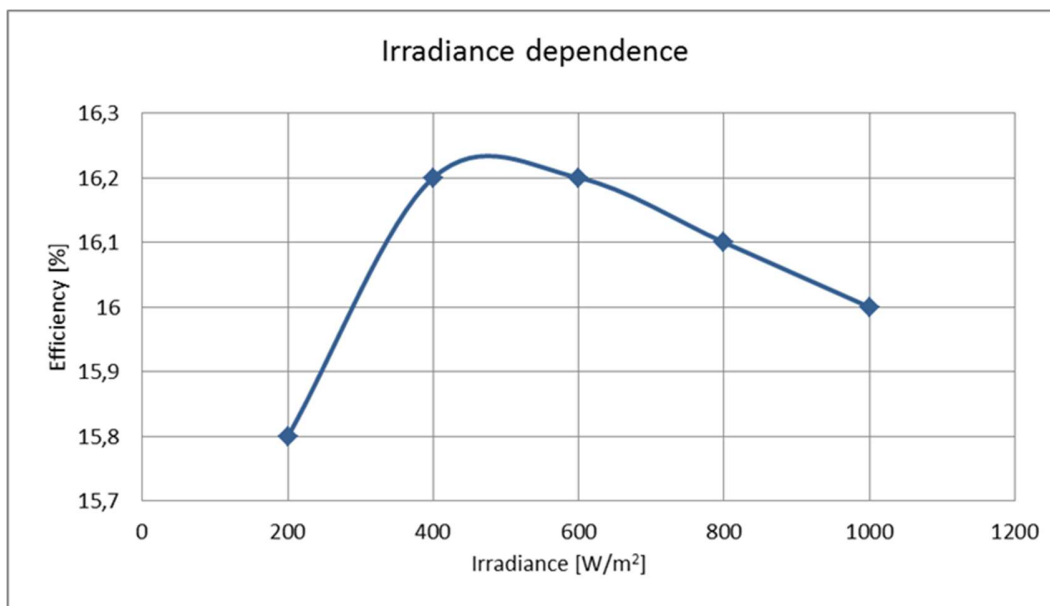


Figure 4.16: The irradiance dependence of the efficiency for the poly Si-modules, based on data from the datasheet of the modules.

The linear trend from 600 W/m² to 1000 W/m² can be described by the following relationship:

$$Efficiency = -0.0005 \cdot Irradiance + 16.5 \quad (18)$$

Figure 4.17 shows the temperature corrected efficiencies values for poly14 plotted over the irradiance for the whole data period (04.05.2016 – 04.11.2016). Efficiency values above 17 % and below 15 % are excluded.

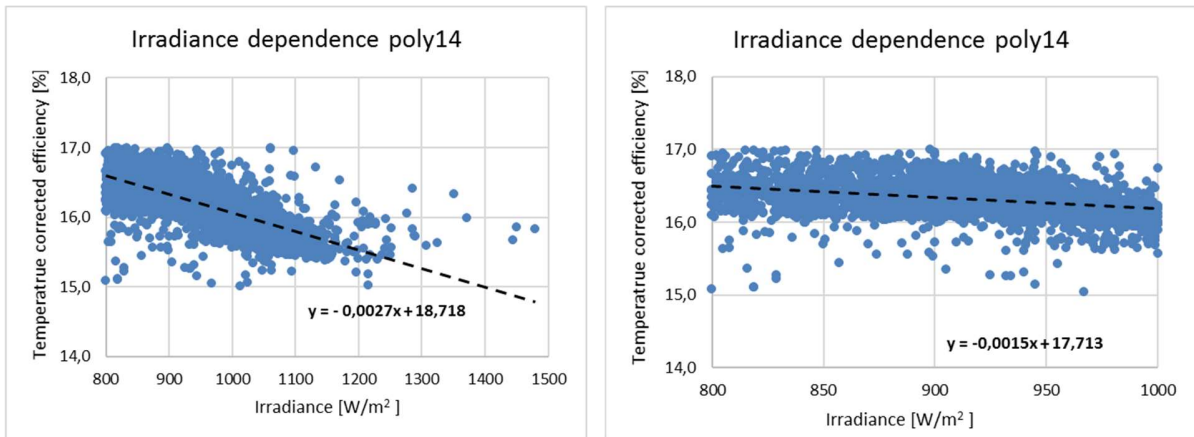


Figure 4.17: The irradiance dependence for poly14, calculated for the whole data period (04.05.2016 - 04.11.2016), for irradiance above 800 W/m² and efficiencies between 15 % and 17 %. The equation for the linear fit is included in the diagram. Left: All irradiance measurements above 800 W/m². Right: Irradiance measurements between 800 W/m² and 1000 W/m².

Figure 4.17 shows that the efficiency is decreasing more exponentially at higher irradiance, as the slope for linear fit for the 800 – 1500 W/m² range is about twice the slope of the linear fit for 800 – 1000 W/m². In the range from 800 W/m² to 1000 W/m² the efficiency is decreased by 0.0015 when the irradiance is increased by 1 W/m². This is three times the expected decrease presented in equation 18.

For all the regularly cleaned poly Si-modules, for the whole data period (04.05.2016 – 04.11.2016), for all the values where the irradiance is above 800 W/m², and when the efficiency values above 17 % and below 15 % are removed, the temperature corrected efficiency on average decreases by 0.003 percentage points when the irradiance is increased by 1 W/m². Poly14 is thus an average module.

An explanation for irradiance dependence could be higher series resistance in the modules than normal, resulting in a high dependence of irradiance at high light intensities. That this should be the case for all the modules seems unlikely, and it could be more appropriate to explain this deviation with a systematic error. The measured temperature is a factor that has great influence on the calculated power output, and as earlier discussed it may seem that the efficiency is not perfectly corrected for temperature changes. This may be due to the way the temperature is measured, and the way the power output is corrected.

As described in section 3.1.4.3 the back-surface module temperature is measured in the middle of the module, and there is an aluminum plate between the sensor and the back surface. Firstly, the temperature on the module surface may vary. The temperature in the middle of the module will probably be representative for most of the module, but it is possible that other parts of the module may have a different temperature. With large differences, this could mean that the temperature measurement would not give the exact temperature correction. Secondly, the aluminum plate could lead to losses and delay in the measurement. Another factor that could cause a difference between the temperature of the solar cells and the aluminum plate at the back of the modules, is the wind speed and direction.

In the cell temperature estimation, it is assumed for all the modules that the temperature difference between the solar cell and the back-surface is 3 °C when the irradiance is 1000 W/m². In the temperature correction of power output, it is also assumed that all the modules of the same type have the same temperature coefficient. The modules of the same type are supposed to be identical. However, as shown earlier, the power output for the same type of modules may differ at similar conditions, indicating differences in the

modules. These differences may also affect the material properties of the module, and result in variations of the temperature coefficient. The temperature difference between the solar cell and the back-surface at 1000 W/m² of the module may also be affected by this.

From this it may be concluded that the temperature measurements and correction could cause significant errors in the result, and that to obtain more accurate results, the temperature effects should be investigated closer. It is especially interesting to know if these effects are changing through the year, as this could cause changes in yield ratio and efficiency that could be interpreted as losses due to soiling. To minimize the uncertainty, the temperature coefficient of each module and the temperature difference between the solar cell and the back of the aluminum plate should be verified.

4.3 Quantified dust accumulation

4.3.1 Verification of weighing method

When quantifying the dust accumulation by on-site mass measurements, there are many factors reducing the reliability of the result. Most important may be the uncontrolled conditions on site. Between measurements there were changes in humidity, and when the samples were taken the wind speed was at some days high. The cloths were folded together, with the dust inside, and transported to the scale in a closed box. Losses of dust could still occur before weighing. Another factor leading to underestimating of soiling levels is that all the dust may not be cleaned of the modules.

The mass of the cloths used 17.10.2016 for cleaning the 12 lower cells of poly3 – 6 and two test cloths are given in Table 4-8. The given value is the average of three mass measurements. The test cloths are not used to clean. At the test site the box they were transported in was just opened and closed. The test cloths were weighed at the same time as the cloths used to clean. The uncertainty in the mass given from the accuracy of the scale is ± 1 , and is chosen rather than the standard deviation of the mean to describe uncertainty, to include systematic errors and to not underestimate the errors.

Table 4-8: The mass of two test cloths and the cloths used to clean poly3 – 6 on 17.10.2016, m_1 is the mass before cleaning and m_2 is the mass after. The amount of dust on the 12 cells is estimated by adding the average of the mass reduction of the test cloths to the measured mass difference of the cloths used to clean. The uncertainty in mass given from the uncertainty of the scale is ± 1 mg, resulting in an uncertainty in the difference and estimated amount of dust of respectively ± 1 and ± 2 mg.

17.10.2016	m_1 [mg]	m_2 [mg]	Difference [mg]	Estimated amount of dust (diff+6.5 mg) [mg]
Poly3	685	686	1	8
Poly4	701	708	7	14
Poly5	716	722	6	13
Poly6	756	759	3	10
Test1	720	713	-7	-
Test2	690	684	-6	-

The 6 mg and 7 mg reduction in mass of the two test samples would indicate that the mass difference is underestimating the amount of dust on the cells. This reduction could be due to changes in humidity. As the mass of both the test samples is reduced by 6 – 7 mg, it may be assumed that all the cloths are experiencing the same absolute mass loss. In this case the amount of dust may be estimated by adding 6.5 mg to the measured mass difference. An increase in mass of 6.5 mg, will lead to an increase in soiling levels (calculated by equation 17) for all the modules of 22 mg/m².

Table 4-9 shows the mass measurements of six cloths, conducted at IFE, Kjeller, before and after the cleaning experiments in Kalkbult. The given value for the mass before cleaning is the average of three measurements, and the value for the mass after cleaning is the average of two measurements. Four of the samples are with dust, and were also weighed twice in Kalkbult. Two samples are without dust, and the box they were transported in was only opened and closed at the test site. The uncertainty given from the accuracy of the scale is ± 0.1

Table 4-9: The cloths measured at IFE, Kjeller, before (m_1 , 29.09.2016) and after (m_2 , 01.11.2016) the cleaning experiments in Kalkbult. Sample 1 – 4 were used to clean the modules in Kalkbult, and were also weighed on site 14.10.2016. For test 3 – 4 the box was transported to Kalkbult, opened, and transported back to Kjeller. The average mass reduction of test 3 and 4 is added to the mass difference of the other samples to estimate the amount of dust on the 12 cells. The differences before and after cleaning with the same samples in Kalkbult is included in the last column. The uncertainty in mass given from the uncertainty of the scale is ± 0.1 mg, resulting in an uncertainty in the difference and estimated amount of dust of respectively ± 0.1 and ± 0.2 mg. The uncertainty in the Kalkbult difference is ± 1 mg.

	m_1 [mg]	m_2 [mg]	Difference [mg]	Estimated amount of dust (diff+8.6 mg)	Difference, Kalkbult, [mg]
Sample1	689.1	693.7	4.6	13.2	11
Sample2	682.5	694.1	11.6	20.2	17
Sample3	686.6	691.4	4.8	13.4	10
Sample4	710.0	714.6	4.6	13.3	9
Test3	678.3	669.4	-8.9	-	-
Test4	695.0	686.7	-8.3	-	-

An increase in the estimated mass difference of 3 – 4 mg would lead to an increase in soiling levels of 10 – 13 mg/m². Due to the long transportation and the weighing procedure in Kalkbult, it is likely that some of the dust may have fallen off before the last weighing at Kjeller. Considering this underestimation, both the test samples measured on site and the measurements conducted at Kjeller indicate that the on-site measurements of the mass difference are underestimating the soiling levels by about 20 mg/m².

The underestimation due to uncontrolled measurement conditions will reduce the reliability of the quantification of soiling levels. If the mass loss is due to changes in relative humidity, the loss in the mass of the cloths could be different on a day with other weather conditions. However, if the error is due to weather conditions, it may be assumed that it is the same for all module measurements for one day, and it may still be possible to compare the dust levels on different modules to see if some type of modules (i.e. with and without anti-soiling treatment) collect more dust than others. Additionally, the estimated error of 20 mg/m² may be used to partly correct the measured soiling levels.

4.3.2 Soiling level measurements

The accumulated dust on four different modules for three different days is given in Table 4-10, both the soiling levels and the daily dust accumulation (both defined in section 3.4.1) are presented. Each cloth was weighed one to three times before and after cleaning, and the average mass value was used in the calculations. The soiling levels for each day are also illustrated in Figure 4.18. The cloths used the 14.10.2016 is showed in Figure 4.19. To compensate for the underestimation discussed in the previous section, 20 mg/m² are added to the measured soiling levels.

Table 4-10: Measured soiling levels for four different polycrystalline modules on three different days. Dust accumulation per day is the soiling levels divided by number of days since last cleaning. The modules were cleaned after the soiling levels were measured. Before 14.10 the modules were cleaned between 08.10 and 12.10, the exact date is unknown. For all measured soiling levels 20 mg/m² is added to compensate for underestimation. Poly3 and poly4 are with anti-soiling treatment, and poly5 and poly6 without. The uncertainty in the soiling levels based on the accuracy of the scale is ± 5 mg/m². The uncertainty in the daily dust accumulation is ± 5 and ± 2 mg/m²/day for 15.10 and 17.10 respectively.

	Soiling levels 14.10 [mg/m ²]	Soiling levels 15.10 [mg/m ²]	Daily dust accumulation [mg/m ² /day]	Soiling levels 17.10 [mg/m ²]	Daily dust accumulation [mg/m ² /day]
Poly3	57	46	46	25	13
Poly4	79	39	39	43	22
Poly5	54	43	43	41	21
Poly6	50	33	33	31	16

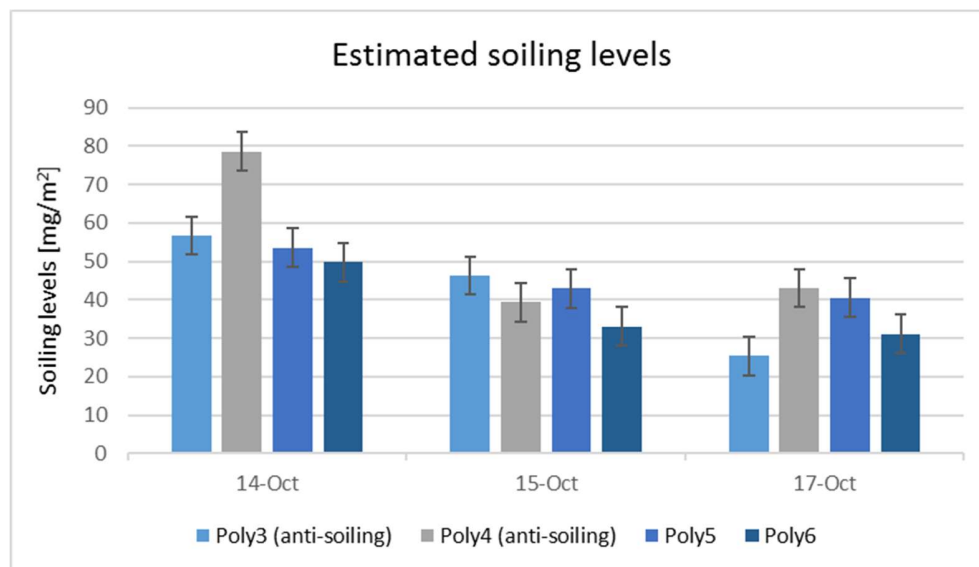


Figure 4.18: Estimated soiling levels for four different poly Si-modules 14.10, 15.10 and 17.10 2016. 20 mg/m² is added to the measured soiling levels to compensate for underestimation. Poly3 and poly4 are treated with anti-soiling product, and poly5 and poly6 are without treatment. The uncertainty based on the accuracy of the scale is ± 5 mg/m².

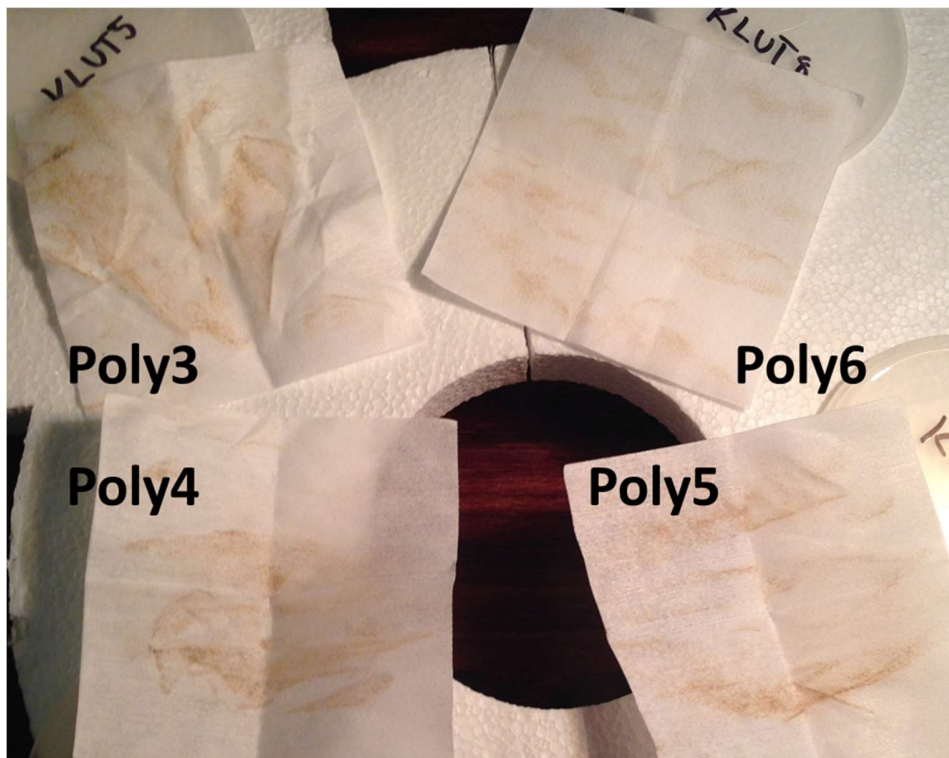


Figure 4.19: The cloths used to wipe of the 12 lower cells of the polycrystalline modules 3-6 14.10.2016.

As illustrated in Figure 4.18, there is no clear pattern based on these measurements showing that some of the modules collect more dust than others. This indicates that in this period, the modules with the anti-soiling treatment do not significantly collect more or less dust than the modules without the treatment. The measurements also do not indicate a significant difference in the efficiency of the wet and dry cleaning, or that the modules cleaned with wet cloths collect more dust in the period after cleaning because of the humidity on the surface. It may seem like other factors, i.e. the wind conditions, have more influence on which modules collect more dust than if they are treated with anti-soiling product or not, or if they are cleaned with wet or dry cloth.

On 15.10, for two of the modules the soiling levels are higher after one day of soiling than on 17.10 after two days of soiling. In the afternoon on 14.10, the gravel road on the west side of the test site was graded causing more dust in the air than normal, at the same time as the wind was blowing in the direction of the test site. This event is a plausible explanation for the higher values.

In Kathmandu, Nepal, a dust deposition of 9.67 g/m^2 lead to a reduction in efficiency of 29.76 %. (Paudyal & Shakya 2016) In Kjeller, Norway, soiling levels up to 0.113 g/m^2 gave a reduction in efficiency of 0.3 percentage points. (Pedersen 2015) In Portland, Oregon, it was shown that a soiling level of 0.85 g/m^2 resulted in a power loss of 4 %. (Smith et al. 2013) In the study from Portland the average daily dust accumulation was shown to be 0.045 g/m^2 . It is important to remember that the soiling levels at different places cannot be compared directly, as the losses are dependent of type of dust. In India it was shown that a soiling level of 3 g/m^2 lead to losses of 17.1 % with dust from Mumbai, and 9.8 % with dust from

Jodhpur. (John et al. 2016) However, with the low estimated daily dust accumulation of $0.013 - 0.022 \text{ g/m}^2$, soiling levels at the day when the gravel road was graded excluded, it seems reasonable that no significant change in efficiency was observed in October.

Based on earlier results a difference in the soiling levels of the modules with and without anti-soiling treatment would be expected. The reason this difference is not confirmed by these measurements, may be the in general low soiling levels in October.

4.3.3 Summary of subsection

The verification of the weighing method implies that the measured soiling levels are underestimated due to the uncontrolled measuring conditions. However, even when this is considered, the soiling levels would still be low enough to justify that the soiling losses in October are insignificant. The measurements performed indicate a daily dust accumulation of $13 - 22 \text{ mg/m}^2$. For a more reliable estimate, more days should be used, as the soiling most likely is not uniform.

4.4 Transmittance measurements

4.4.1 Measurements and uncertainty discussion

The spectral irradiance measurements conducted 17.10.2016 through clean glass, dirty glass and directly at the sky, are given in Figure 4.20 for three different times of the day, and consequently three different angles of incidence of the sunlight. The given values are an average of three measurements taken within approximately 10 seconds. If the soiling losses are significant, the measurement through the dirty glass is expected to give lower spectral irradiance values than the measurement through the clean glass.

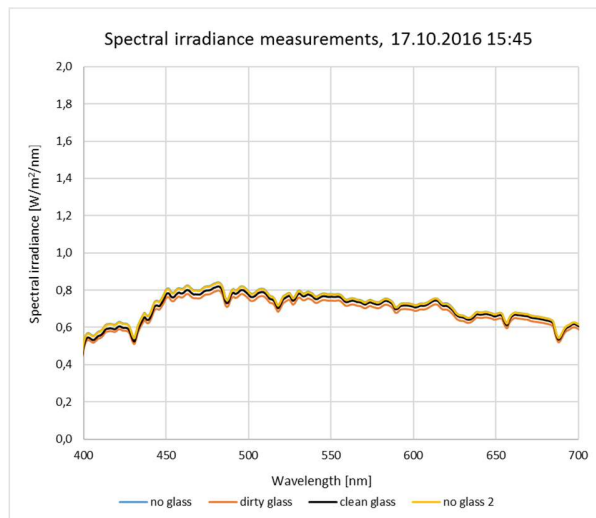
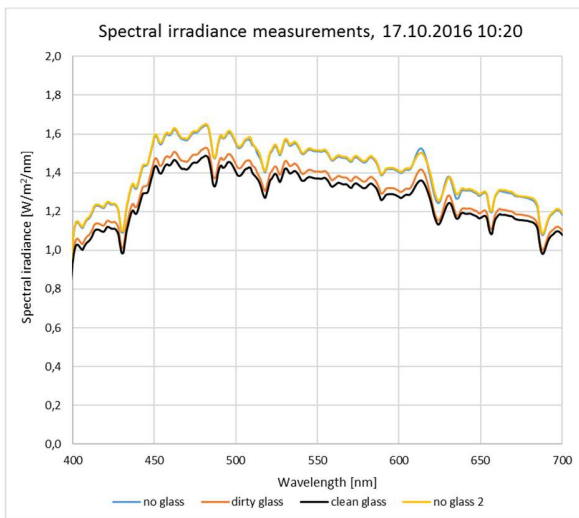
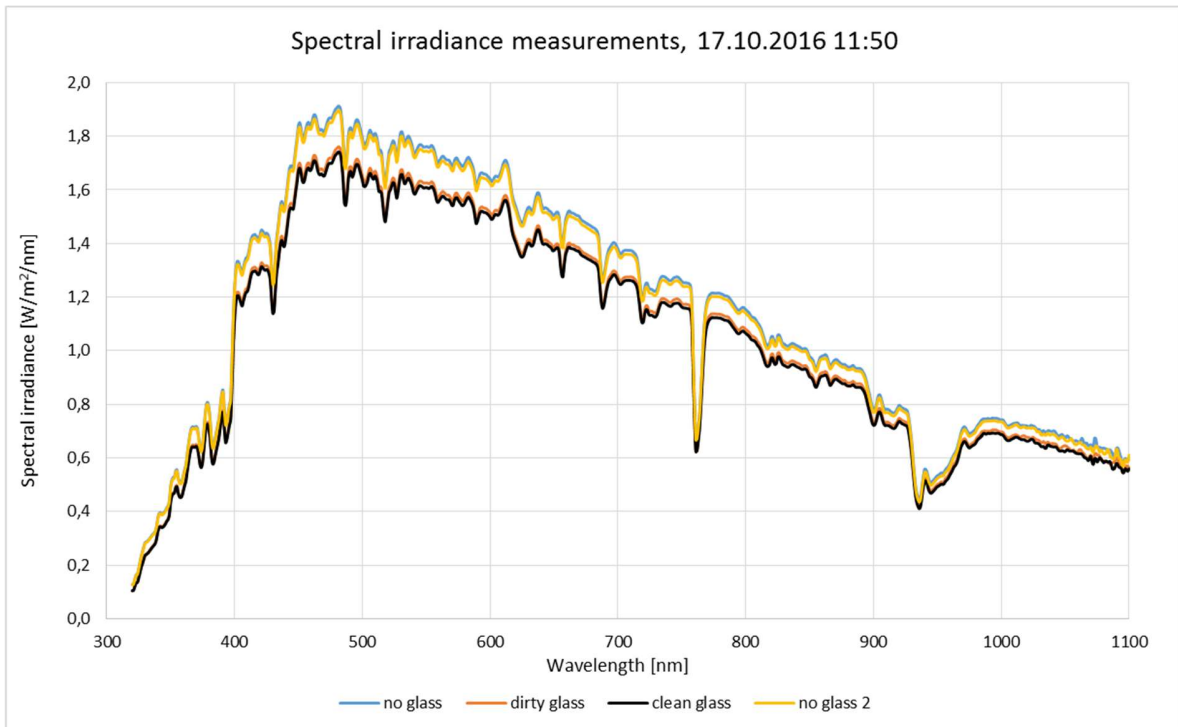


Figure 4.20: Spectral irradiance measurements through clean and dirty glass and no glass 17.10.2016 at 10:20, 11:50 and 15:45. For the measurements at 10:20 and 15:45 the wavelength range in the figure is reduced to 400 – 700 nm to show the part of the spectrum where the difference between the measurements is greatest.

The spectral irradiance is as expected higher for the measurement without glass, due to reflection in the glass. The amount of reflected light is also expected to change through the day, as the angle of incidence changes.

At 11.50 the spectral irradiance through the dirty glass has slightly higher measurement values than through the clean glass. The difference is not larger than the difference between the two measurements outside the glass, and it is not more than 3 %, so this is within the uncertainty of the measurement equipment. In the

morning (10:20) the values for the dirty glass is higher, and in the afternoon (15:45) the values for the clean glass is higher. Both the differences are within the measurement uncertainty of 3 %. However, this could indicate a dependence of the position of the diffuser relative to the sun when the measurement is taken. The dependency of position could also explain why the difference between the values with and without glass are minimal in the afternoon.

If the transmittance was measured with the diffuser pointed directly at the sun and in the same position for all the measurements (i.e. if the clean and dirty glass was moved and the spectroradiometer was fixed), the measurements would be more comparable than when measured through a fixed frame.

For this comparison of measurements, uniform soiling is assumed. Most likely the soiling will not be perfectly uniform, and there is a chance that the part of the glass where the spectral irradiance is measured does not give a good representation of the total soiling levels. An additional source of errors is that the diffuser did not have a fixed position, and there might be small differences in angles and distance to the glass influencing the measurements. If the diffuser is not close enough to the glass, it might also measure reflected light from the metal frame.

A study at Kjeller, Norway, showed an approximately linear correlation between the reduction in transmittance and dust density, giving a reduction in transmittance of 0.09 % per 10 mg/m². (Pedersen 2015) Based on the dust measurements presented in section 4.3.2, the maximum soiling level on the modules glass, obtained by adding the maximum soiling levels 15.10.2016 and 17.10.2016, is 89 mg/m². Using the correlation found at Kjeller, this would lead to a maximum reduction in the transmittance of 0.8 %, which is less than the uncertainty of the spectroradiometer. These results are not directly comparable, as the correlation between reduction in transmittance and soiling levels depends on type of dust. However, this supports that at the given soiling levels, minimal changes in transmittance is expected.

4.4.2 Summary of subsection

For two and a half days, no significant difference between the transmittance through the clean glass and dirty glass was observed that could be explained by soiling. This is consistent with the results from section 4.1 indicating that the soiling in the spring months is low. The time period between the glass was installed and the transmittance measurements were conducted was reduced because of the weather conditions, a longer time period might have given a significant difference. Measuring the transmittance through the glass with the spectroradiometer in a fixed position might increase the accuracy of the measurements, and measuring at different positions of the glass could give a more reliable result if the soiling is not perfectly uniform.

4.5 Summary of results in a non-site-specific perspective

Important results from this study which is of value for other locations than desolated sites in the Northern Cape are as follows:

- The dust accumulation on PV-modules is probably not uniform at one site, as it is very dependent on weather conditions and activity in the surroundings. The soiling levels through the year is dependent

on how the precipitation is distributed, and also how the wind speed and humidity changes through the year. The non-uniformity may be increased by irregular human activity, as discussed in section 4.3.2.

- When using a spectroradiometer to perform on-site measurements of reduction in transmittance, measuring at different positions on a fixed glass might not be ideal, as the measurements showed a possible dependency of the position of the instrument.

5 Conclusions

In the time period considered in this analysis (04.05.2016 – 04.11.2016), it seems like the losses due to soiling are only significant in the winter months May-July, where the weather conditions are unfortunate with little precipitation, low wind speed and high relative humidity. Thin film modules experienced higher losses due to soiling than poly Si-modules, and modules with anti-soiling treatment had higher losses than the modules without anti-soiling treatment, meaning that the anti-soiling product worked against its purpose. In July, when the losses due to soiling were most distinct, the average power loss due to soiling was 1 % for poly Si-modules without anti-soiling treatment, 2 % for poly Si-modules with anti-soiling treatment, and 4 % for thin film modules with anti-soiling treatment.

Based on the changes in efficiency for modules cleaned every second week, it may seem like two weeks of soiling is not enough to reduce the efficiency significantly, even in the winter months. However, as it may be that dust attracts more dust, it is possible that the soiling levels of the uncleaned modules are increasing faster than for the regularly cleaned modules.

For the poly Si-modules, it was shown that heavy rainfall cleaned the module surface to the extent that the performance was recovered. For the thin film modules, the performance also increased after heavy rain, although it may seem like the module surface was not completely cleaned.

The measurements conducted at the test site confirmed that the soiling levels are low in October. The measurements of the soiling levels suggest a daily dust accumulation of 13 – 22 mg/m². Compared with other studies it seems reasonable that these soiling levels did not cause any reduction in the efficiency. The transmittance measurements confirm that two and a half days with soiling in October is not enough to reduce the incoming light on the solar cells.

6 Further work

- Expand the analysis with a longer time period. Using data recorded for a whole year would give a deeper insight in the total yearly losses due to soiling, and with data for more than a year a more reliable estimate of the monthly losses would be obtained.
- Use the expanded dataset to closer investigate how the weather conditions affect the soiling levels. Especially the relative humidity and dew formation, and also wind speed and wind direction is interesting. This requires thorough analysis as an increase in both relative humidity and wind speed might result in either an increase or decrease of soiling levels. With high relative humidity, the dust particles might easier stick to the surface, on the other side dew formation may lead to partial cleaning. Higher wind speed could have a cleaning effect on the surfaces, or lift more dust up in the air resulting in increased dust accumulation. This could also be related to the wind direction and i.e. the traffic in the area. This type on analysis would be more reliable with greater amount of data.
- Closer investigate the effect of natural cleaning by study the rain intensity, i.e. mm rain per hour, and not only the amount of rain (which is investigated in many other studies).
- Determine the size and type of dust at the test site. By predicting how this type of soiling would affect the transmittance of incoming light, and if it would easily be cleaned off by rain, this could be a supplement to the data analysis. With information about type of dust, the analysis would also be more comparable with other studies, and in greater extent be used to predict soiling losses at other locations.
- Conduct transmittance measurements over a longer time period, and test a measurement set up where the spectroradiometer is fixed and the glass is moved.
- The variations in the data could be reduced by correcting for irradiance and wind speed, and using a time interval which are more exact in the middle of the day.
- Investigate the losses due to soiling in the morning and evening, when the angle of incidence of incoming light is large.
- Use the soiling losses to estimate if it is economically beneficial to clean the modules in the solar park, and eventually when and how often.
- Improve the temperature corrections by measuring the actual temperature difference between the solar cells and the back of the aluminum plate.

7 References

- Adinoyi, M. J. & Said, S. A. M. (2013). Effect of dust accumulation on the power outputs of solar photovoltaic modules. *Renewable Energy*, 60: 633-636.
- Appels, R., Lefevre, B., Herteleer, B., Goverde, H., Beerten, A., Paesen, R., De Medts, K., Driesen, J. & Poortmans, J. (2013). Effect of soiling on photovoltaic modules. *Solar Energy*, 96: 283-291.
- Barstad, S. (2016). *En solskinnshistorie*. Available at: <http://www.aftenposten.no/okonomi/En-solskinnshistorie-10279b.html>.
- Brekke, T. A. (2016). *Nordic Irradiance Conditions and the Effects on Solar Module Efficiency*. Ås: Norwegian University of Life Sciences. 86 pp.
- Cano, J. (2011). *Photovoltaic Modules: Effect of Tilt Angle of soiling*: Arizona State University. 65 pp.
- Caron, J. R. & Littmann, B. (2013). Direct Monitoring of Energy Lost Due to Soiling on First Solar Modules in California. *IEEE Journal of Photovoltaics*, 3 (1): 336-340.
- Cook, K. H. (2013). *Climate dynamics*. 1. ed. Princeton, N.J.: Princeton University Press. 199 pp.
- Garcia, M., Marroyo, L., Lorenzo, E. & Perez, M. (2011). Soiling and other optical losses in solar-tracking PV plants in Navarra.
- Goossens, D. & Van Kerschaver, E. (1999). Aeolian dust deposition on photovoltaic solar cells: The effects of wind velocity and airborne dust concentration on cell performance. *Solar Energy*, 66 (4): 277-289.
- Gostein, M., Littmann, B., Caron, J. R. & Dunn, L. (2013, 16-21 June 2013). *Comparing PV power plant soiling measurements extracted from PV module irradiance and power measurements*. 2013 IEEE 39th Photovoltaic Specialists Conference (PVSC). 3004-3009 pp.
- Goswami, D. Y. & Besarati, S. M. (2013). *Solar*. Available at: https://www.worldenergy.org/wp-content/uploads/2013/10/WER_2013_8_Solar_revised.pdf (accessed: 14.11.2016).
- Green, M. A., Emery, K., Hishikawa, Y., Warta, W. & Dunlop, E. D. (2016). Solar cell efficiency tables (version 48). *Progress in Photovoltaics*, 24 (7): 905-913.
- Guo, B., Javed, W., Figgis, B. W., Mirza, T. & Ieee. (2015). Effect of Dust and Weather Conditions on Photovoltaic Performance in Doha, Qatar. *2015 First Workshop on Smart Grid and Renewable Energy (Sgre)*.
- Herteleer, B. (2015). *Normalized Efficiency*. Available at: <https://pvpmc.sandia.gov/modeling-steps/5-ac-system-output/pv-performance-metrics/normalized-efficiency/> (accessed: 18.09.2016).
- Honsberg, C. & Bowden, S. (2014). *PVeducation.org*. Available at: <http://www.pveducation.org/> (accessed: 28.10.2016).
- IEA. (2015). *Energy and Climate Change*: International Energy Agency.
- John, J. J., Warade, S., Tamizhmani, G. & Kottantharayil, A. (2016). Study of Soiling Loss on Photovoltaic Modules With Artificially Deposited Dust of Different Gravimetric Densities and Compositions Collected From Different Locations in India. *Ieee Journal of Photovoltaics*, 6 (1): 236-243.
- JRC EC. (2016). *Photovoltaic Geographical Information System - Interactive Maps*. Available at: <http://re.jrc.ec.europa.eu/pvgis/apps4/pvest.php?map=africa&lang=en> (accessed: 22.11.2016).

- Jäger, K. D., Isabella, O., Smets, A., Swaaij, R. V. & Zeman, M. (2016). *Solar energy : the physics and engineering of photovoltaic conversion, technologies and systems*. 1 ed. Cambridge, England: UIT Cambridge. 462 pp.
- King, D. L., Boyson, W. E. & Kratochvill, J. A. (2004). Photovoltaic Array Performance Model. Albuquerque, New Mexico: Sandia National Laboratories.
- Mani, M. & Pillai, R. (2010). Impact of dust on solar photovoltaic (PV) performance: Research status, challenges and recommendations. *Renewable & Sustainable Energy Reviews*, 14 (9): 3124-3131.
- More details about the agreement*. (2015). Available at: <http://www.cop21.gouv.fr/en/more-details-about-the-agreement/> (accessed: 12.11.2016).
- Naeem, M., Tamizhmani, G. & Ilee. (2015). Climatological Relevance to the Soiling Loss of Photovoltaic Modules. *2015 Saudi Arabia Smart Grid Conference (Sasg)*.
- NASA. *Incoming sunlight*. Available at: <http://earthobservatory.nasa.gov/Features/EnergyBalance/page2.php> (accessed: 26.10.2016).
- Ndapuka, A. T. (2015). *Design and Development of a Monitoring Station for the Long-Term Investigation of Dust Pollution Effects on the Performance of PV Panels* Master. Stellenbosch: Stellenbosch University. 155 pp.
- Paudyal, B. R. & Shakya, R. (2016). Dust accumulation effects on efficiency of solar PV modules for off grid purpose: A case study of Kathmandu. *Solar Energy*, 135: 103-110.
- Pedersen, H. B. (2015). *Experimental study of soiling on photovoltaic modules in a Nordic climate*. Master. Ås: Norwegian University of Life Sciences, Department of Mathematical Sciences and Technology. 134 pp.
- Philbert, C. (2014). Technology Roadmap - Solar Photovoltaic Energy: International Energy Agency.
- Prorok, M., Werner, B. & Zdanowicz, T. (2006). Applicability of equivalent diode models to modeling various thin-film photovoltaic (PV) modules in a wide range of temperature and irradiance conditions. *Electron Technology*, 37/38.
- PVPMC. (2014). *Global Horizontal Irradiance*. Available at: <https://pvpmc.sandia.gov/modeling-steps/1-weather-design-inputs/irradiance-and-insolation-2/global-horizontal-irradiance/> (accessed: 09.12.2016).
- Skoplaki, E. & Palyvos, J. A. (2009). On the temperature dependence of photovoltaic module electrical performance: A review of efficiency/power correlations. *Solar Energy*, 83 (5): 614-624.
- Smith, M. K., Wamser, C. C., James, K. E., Moody, S., Sailor, D. J. & Rosenstiel, T. N. (2013). Effects of Natural and Manual Cleaning on Photovoltaic Output. *Journal of Solar Energy Engineering-Transactions of the Asme*, 135 (3).
- Solargis. (2016). *Solar resource maps for Southern Africa*. Available at: <http://solargis.com/products/maps-and-gis-data/free/download/southern-africa> (accessed: 01.11.2016).
- The Shift Project. *Breakdown of Electricity Generation by Energy Source*. Available at: <http://www.tsp-data-portal.org/Breakdown-of-Electricity-Generation-by-Energy-Source#tspQvChart> (accessed: 31.10.2016).
- Veret som var New Kalkbult, Northern Cape (Sør-Afrika)*. (2016). Available at: http://www.yr.no/stad/Sør-Afrika/Northern_Cape/New_Kalkbult/statistikk.html (accessed: 02.11.2016).

- Woyte, A., Moser, D., Reich, N., Green, M., Mau, S. & Beyer, H. G. (2014). Analytical Monitoring of Grid-connected Photovoltaic Systems: IEA.
- Zorilla-Casanova, J., Piliougine, M., Carretero, J., Bernaola, P., Carpena, P., Mora-Lopez, L. & Sidrach-de-Cardona, M. (2011, 8-13 May 2011). *Analysis of dust losses in photovoltaic modules*. World Renewable Energy Congress 2011, Linköping, Sweden. 2985-29992 pp.

8 Appendix

Appendix A: PV-module specifications

Appendix B: Shading analysis

Appendix C: Yield ratio for the polycrystalline silicon modules


Appendix D: Mass measurements at Kalkbult and Kjeller

Appendix E: Transmittance measurements, Kalkbult 17.10.2016

Appendix A


Electrical and mechanical specifications for the PV-modules at the test site.


Datasheet for the polycrystalline modules, JC255-24/Bb:





Virtus® II Module


240W, 245W, 250W, 255W, 260W





- 

High Module Conversion Efficiencies
- 


Easy Installation and Handling for Various Applications
- 


Mechanical Load Capability of up to 5400 Pa
- 

Conforms with IEC 61215:2005, IEC 61730: 2004, UL 1703 PV Standards
- 

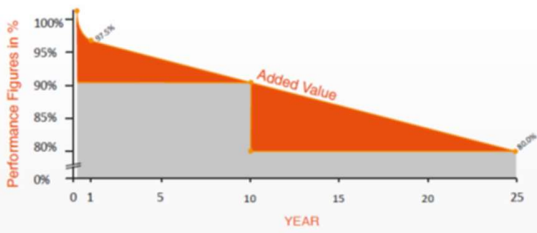
ISO9001, OHSAS18001, ISO14001 Certified
- 

Application Class A, Safety Class II, Fire Rating C





Guarantee




Year	Performance Figures in %
0	100%
10	90%
25	80.5%

10-year

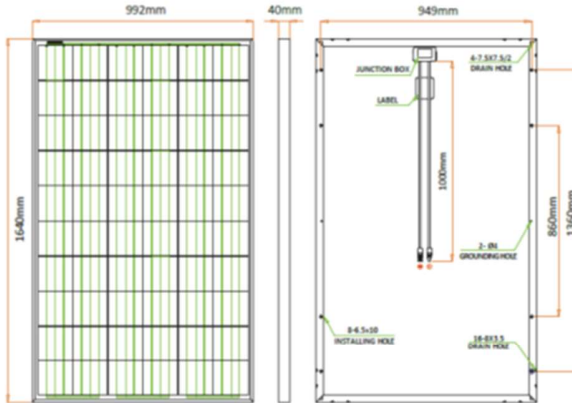
material & workmanship

25-year

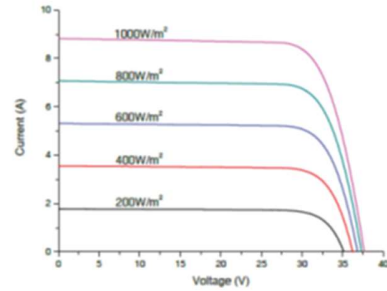
linear power output



Dimensions



I-V Curves



Varied Irradiation Efficiencies

Irradiance	200W/m ²	400W/m ²	600W/m ²	800W/m ²	1000W/m ²
Efficiency	15.8%	16.2%	16.2%	16.1%	16.0%

Electrical Characteristics STC

	JC240M-24/Bb	JC245M-24/Bb	JC250M-24/Bb	JC255M-24/Bb	JC260M-24/Bb
Maximum Power (P _{max})	240 W	245 W	250 W	255 W	260 W
Power Tolerance	0 - +5W	0 - +5W	0 - +5W	0 - +5W	0 - +5W
Module Efficiency	14.8%	15.1%	15.4%	15.7%	16.0%
Maximum Power Current (I _{mp})	8.08 A	8.19 A	8.31 A	8.39 A	8.53 A
Maximum Power Voltage (V _{mp})	29.7 V	29.9 V	30.1 V	30.4 V	30.5 V
Short Circuit Current (I _{sc})	8.64 A	8.73 A	8.83 A	8.86 A	8.95 A
Open Circuit Voltage (V _{oc})	37.2 V	37.3 V	37.4 V	37.5 V	37.6 V

Values at Standard Test Conditions STC (Air Mass AM1.5, Irradiance 1000W/m², Cell Temperature 25°C)

Electrical Characteristics NOCT

	JC240M-24/Bb	JC245M-24/Bb	JC250M-24/Bb	JC255M-24/Bb	JC260M-24/Bb
Maximum Power (P _{max})	178 W	182 W	185 W	189 W	193 W
Maximum Power Current (I _{mp})	6.51 A	6.53 A	6.57 A	6.63 A	6.74 A
Maximum Power Voltage (V _{mp})	27.4 V	27.9 V	28.2 V	28.5 V	28.6 V
Short Circuit Current (I _{sc})	6.97 A	7.04 A	7.12 A	7.20 A	7.27 A
Open Circuit Voltage (V _{oc})	34.7 V	35.0 V	35.0 V	35.1 V	35.2 V

Values at Normal Operating Cell Temperature, Irradiance of 800 W/m², spectrum AM 1.5, ambient temperature 20°C, wind speed 1 m/s

Mechanical Characteristics

Cell Type	156 x156 mm Polycrystalline, 60 (6x10) pcs in series
Glass	High Transmission, Low Iron, Tempered Glass
Frame	Anodized Aluminum Alloy
Junction Box	IP65/IP67 rated, with bypass diodes
Dimension	*1640 x 992 x 40 mm
Output Cable	4 mm ² (EU)/12 AWG (US), 1000 mm
Weight	18.5 Kg
Installation Hole Location	See Drawing Above

Characteristics

Temperature Coefficient of V _{oc}	-0.30%/°C
Temperature Coefficient of I _{sc}	0.04%/°C
Temperature Coefficient of P _{max}	-0.40%/°C
Nominal Operating Cell Temperature (NOCT)	45°C±2°C

Packing Information

	20' GP	40' GP	40' HQ
Container			
Pallets per Container	12	28	28
Pieces per Container	300	700	770

Maximum Ratings

Operating Temperature	-40°C - +85°C
Maximum System Voltage	1000VDC (EU) / 600VDC (US)
Maximum Series Fuse Rating	20A (EU) / 20A (US)

Rev No: JC705/2013.02 For TBA *Contact ReneSola for tolerance specification
CAUTION: All rights reserved. Design and specification are subject to change without prior notice.



First Solar Series 4™ PV Module

ADVANCED THIN FILM SOLAR TECHNOLOGY



INDUSTRY BENCHMARK SOLAR MODULES

As a global leader in PV energy, First Solar's advanced thin film solar modules have set the industry benchmark with over 10 gigawatts (GW) installed worldwide and a proven performance advantage over conventional crystalline silicon solar modules. Generating up to 8% more energy than competing modules with the same power rating, First Solar's Series 4™ and Series 4A™ PV Modules deliver superior performance and reliability to our customers.



PROVEN ENERGY YIELD ADVANTAGE

- Up to 8% more energy than conventional crystalline silicon solar modules with the same power
- Superior temperature coefficient (-0.29%/°C) resulting in greater energy yield in typical field operating temperatures
- Superior spectral response resulting in a proven energy yield advantage in humid environments
- Anti-reflective coated glass (Series 4A™) enhances energy production



ADVANCED PERFORMANCE & RELIABILITY

- Improved long-term power-output warranted for 25 years
- Compatible with advanced 1500V plant architectures
- Independently tested to pass accelerated life and stress tests beyond industry standards
- Highly predictable energy in all climates and applications
- Independently certified for reliable performance in high temperature, high humidity, extreme desert and coastal environments

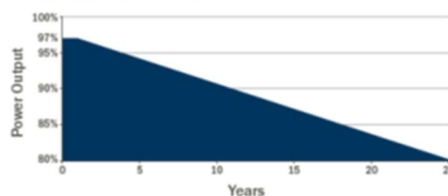


CERTIFICATIONS & TESTS

- Thresher Test, Long-Term Sequential Test, and PID-Free
- IEC 61646 1500V, IEC 61730 1500V, CE
- IEC 61701 Salt Mist Corrosion, IEC 60068-2-68 Dust and Sand Resistance
- ISO 9001:2008 and ISO 14001:2004
- UL 1703 and ULC 1703 Listed Class B Fire Rating (Class A Spread of Flame)
- CSI Eligible (CA-USA), FSEC (FL-USA), MCS (UK), CEC Listed (Australia), SII (Israel), InMetro (Brazil)¹



MODULE WARRANTY²



- 25-Year Linear Performance Warranty³
- 10-Year Limited Product Warranty

FIRST SOLAR SERIES 4™ PV MODULE

MECHANICAL DESCRIPTION

Length	1200mm
Width	600mm
Weight	12kg
Thickness	6.8mm
Area	0.72m ²
Leadwire	2.5mm ² , 610mm
Connectors	MC4 ⁴
Bypass Diode	None
Cell Type	Thin-film CdTe semiconductor, 216 active cells
Frame Material	None
Front Glass	3.2mm heat strengthened Series 4A™ includes anti-reflective coating
Back Glass	3.2mm tempered
Encapsulation	Series 3 Black Laminate material with edge seal

MODULE NUMBERS AND RATINGS AT STC^{5,6}

NOMINAL VALUES		FS-492	FS-495	FS-497	FS-4100	FS-4102	FS-4105A
		FS-492A	FS-495A	FS-497A	FS-4100A	FS-4102A	
Nominal Power (± 5%)	P _{MPP} (W)	92.5	95.0	97.5	100.0	102.5	105.0
Voltage at P _{MAX}	V _{MPP} (V)	67.0	67.9	68.7	69.4	70.0	70.4
Current at P _{MAX}	I _{MPP} (A)	1.38	1.40	1.42	1.44	1.47	1.49
Open Circuit Voltage	V _{OC} (V)	86.0	86.5	87.0	87.6	88.0	88.2
Short Circuit Current	I _{SC} (A)	1.54	1.55	1.55	1.57	1.57	1.58
Maximum System Voltage	V _{SYS} (V)	1500 ⁷ / (1000 UL)					
Limiting Reverse Current	I _R (A)	4.0					
Maximum Series Fuse	I _{CR} (A)	4.0					

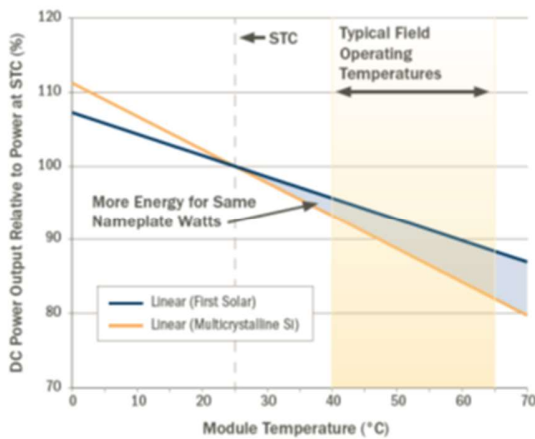
MODULE NUMBERS AND RATINGS AT 800W/m², NOCT⁸ 45°C, AM 1.5⁴

NOMINAL VALUES		FS-492	FS-495	FS-497	FS-4100	FS-4102	FS-4105A
Nominal Power (± 5%)	P _{MPP} (W)	69.7	71.6	73.5	75.4	77.3	79.1
Voltage at P _{MAX}	V _{MPP} (V)	62.8	63.4	63.9	65.0	65.5	65.7
Current at P _{MAX}	I _{MPP} (A)	1.11	1.13	1.15	1.16	1.18	1.20
Open Circuit Voltage	V _{OC} (V)	81.2	81.7	82.1	82.7	83.1	83.3
Short Circuit Current	I _{SC} (A)	1.24	1.25	1.25	1.27	1.27	1.27

TEMPERATURE CHARACTERISTICS

Module Operating Temperature Range	(°C)	-40 to +85
Temperature Coefficient of P _{MPP}	T _K (P _{MPP})	-0.29%/°C
Temperature Coefficient of V _{OC}	T _K (V _{OC})	-0.28%/°C
Temperature Coefficient of I _{SC}	T _K (I _{SC})	+0.04%/°C

SUPERIOR TEMPERATURE COEFFICIENT



END-OF-LIFE RECYCLING

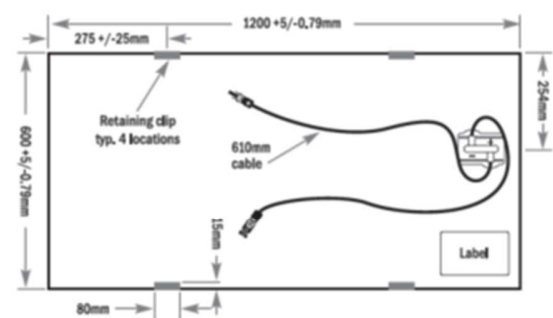
- Recycling services available through First Solar's industry-leading recycling program or customer-selected third party.

Disclaimer

The information included in this Module Datasheet is subject to change without notice and is provided for informational purposes only. No contractual rights are established or should be inferred because of user's reliance on the information contained in this Module Datasheet. Please refer to the appropriate Module User Guide and Module Product Specification document for more detailed technical information regarding module performance, installation and use.

The First Solar logo, First Solar™, and all products denoted with * are registered trademarks, and those denoted with a ™ are trademarks of First Solar, Inc.

MECHANICAL DRAWING



¹ InMetro Certification available on FS-495, FS-497, FS-4100, FS-4102, FS-495A, FS-497A, FS-4100A, FS-4102A

² Limited power output and product warranties subject to warranty terms and conditions.

³ Ensures 97% rated power in first year, -0.7%/year through year 25.

⁴ Multi-Contact MC4 (PV-KST4/PV-KBT4)

⁵ Standard Test Conditions (STC) 1000W/m², AM 1.5, 25°C

⁶ All ratings ±10%, unless specified otherwise. Specifications are subject to change.

⁷ Application Class A for 1000V (class II), Application Class B for 1500V (class O)

⁸ Nominal Operating Cell Temperature: Module operation temperature at 800W/m² irradiance, 20°C air temperature, 1m/s wind speed.

Appendix B

Shading analysis for the test station for three different positions. Performed by Armand du Plessis, reprinted with permission.

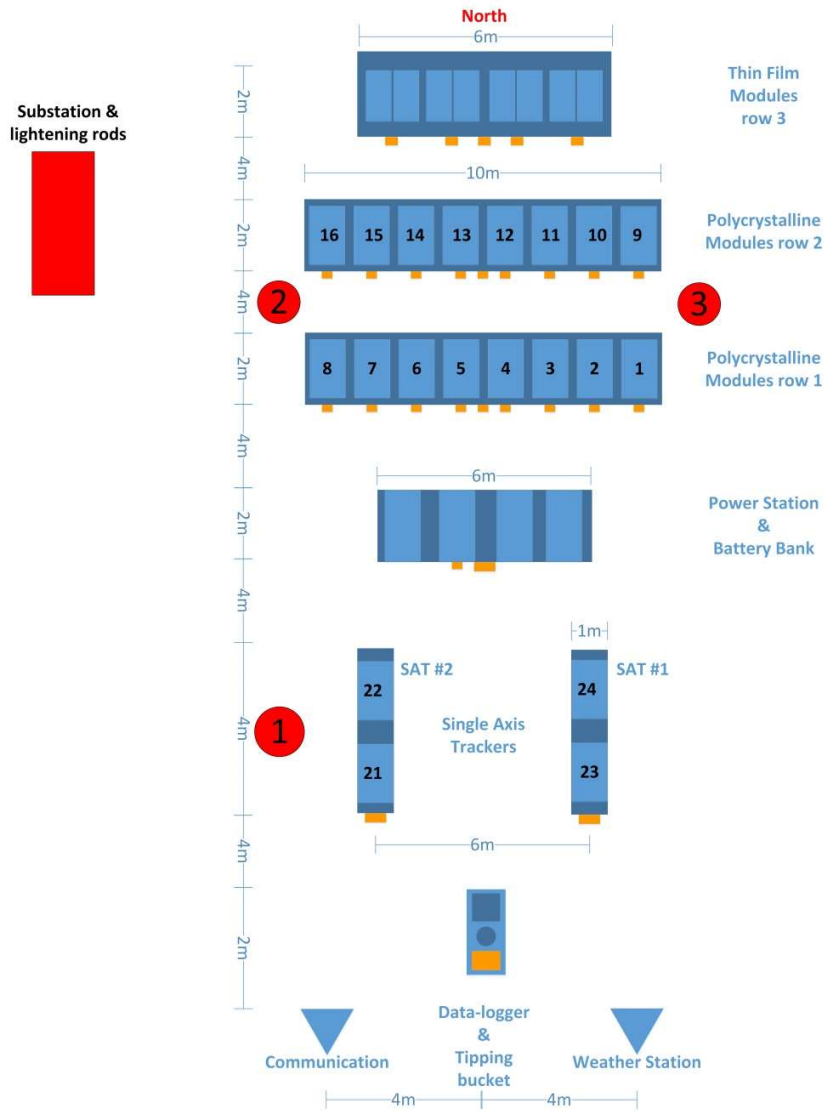


Figure 0.1: Facility layout.

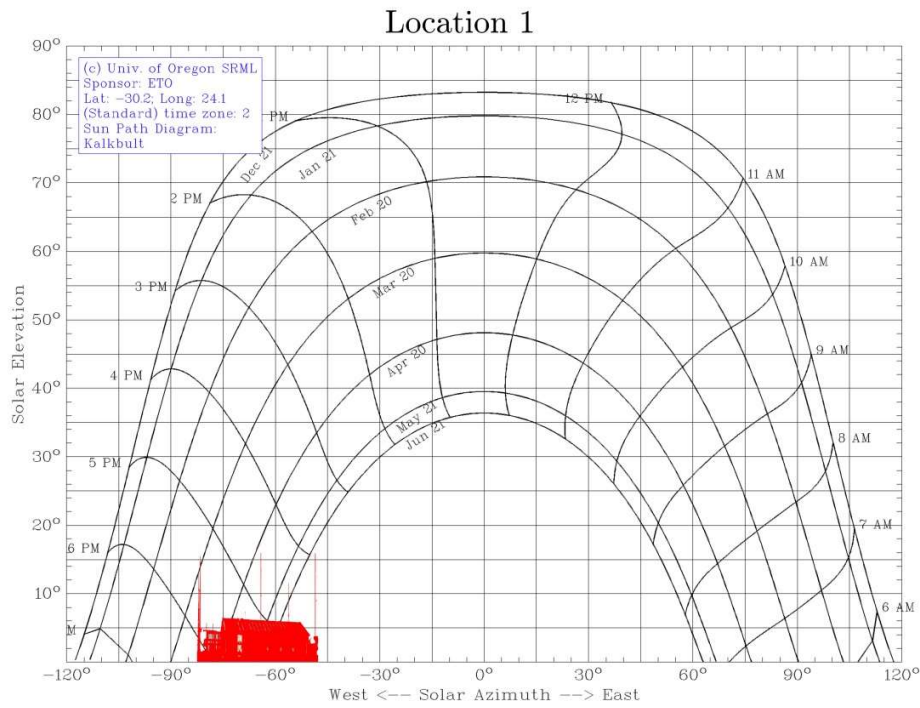


Figure 0.2: Shading diagram for position 1 at the facility layout (Figure 0.1).

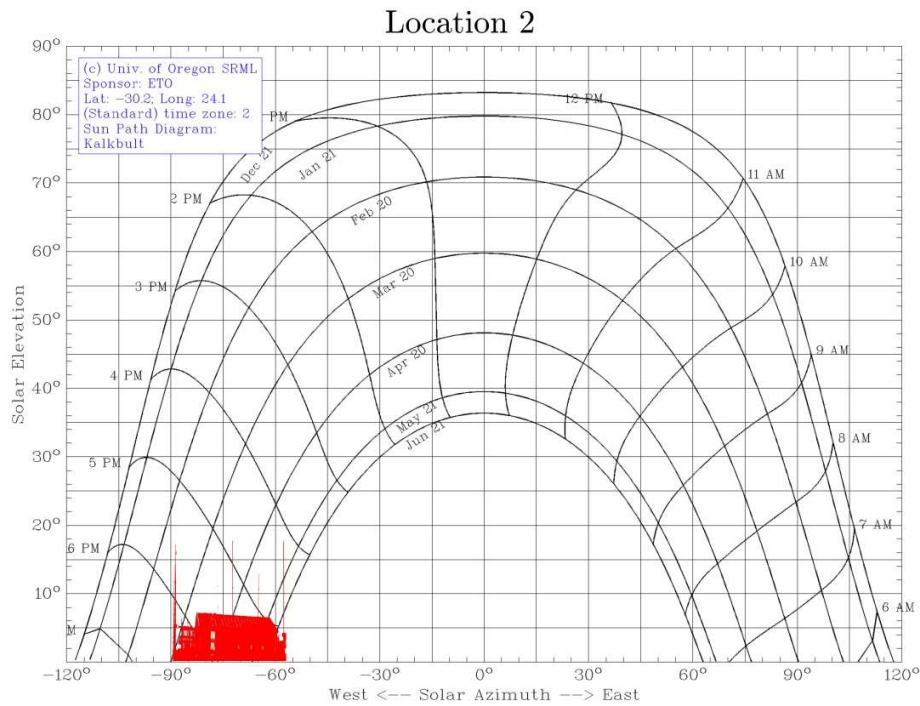


Figure 0.3: Shading diagram for position 2 at the facility layout (Figure 0.1).

Location 3

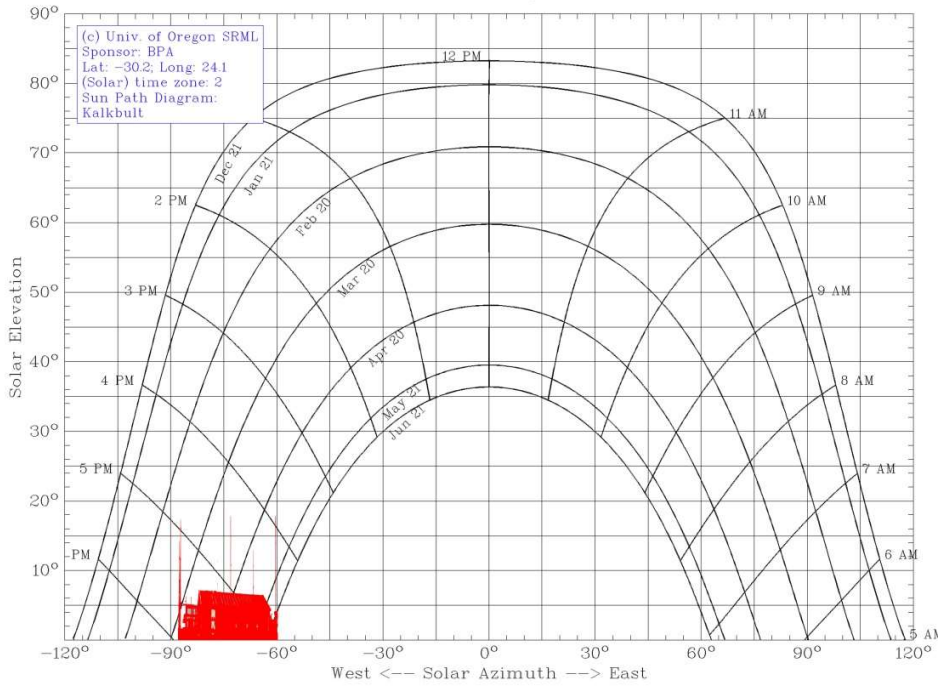


Figure 0.4: Shading diagram for position 3 at the facility layout (Figure 0.1).

Appendix C

The yield ratio for the polycrystalline modules 04.05.2016 – 04.11.2016.

The yield ratio for each poly Si-module distributed on cleaning strategy is presented in Figure 0.1 - Figure 0.6, showing the differences between the modules.

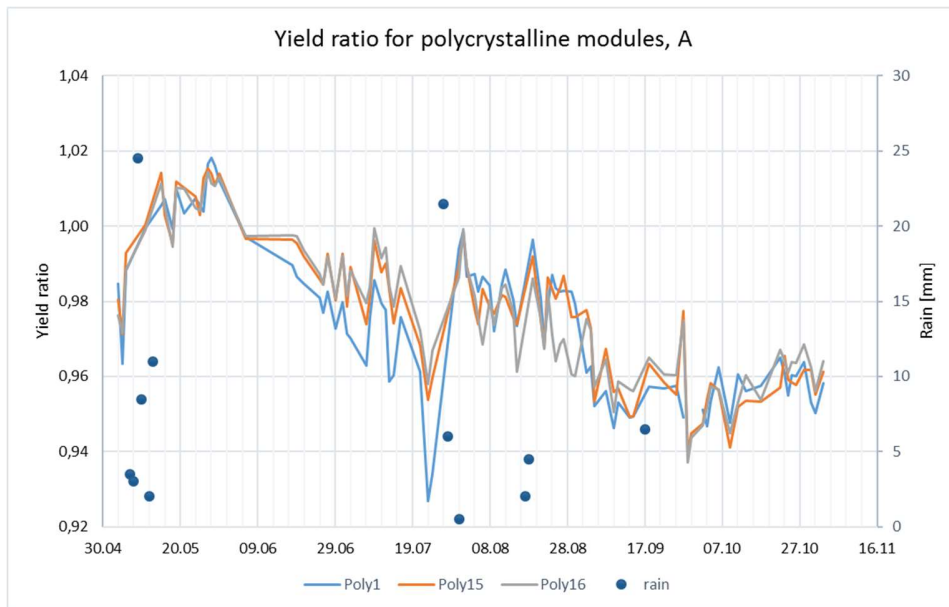


Figure 0.1: Yield ratio for poly Si-modules with cleaning strategy A.

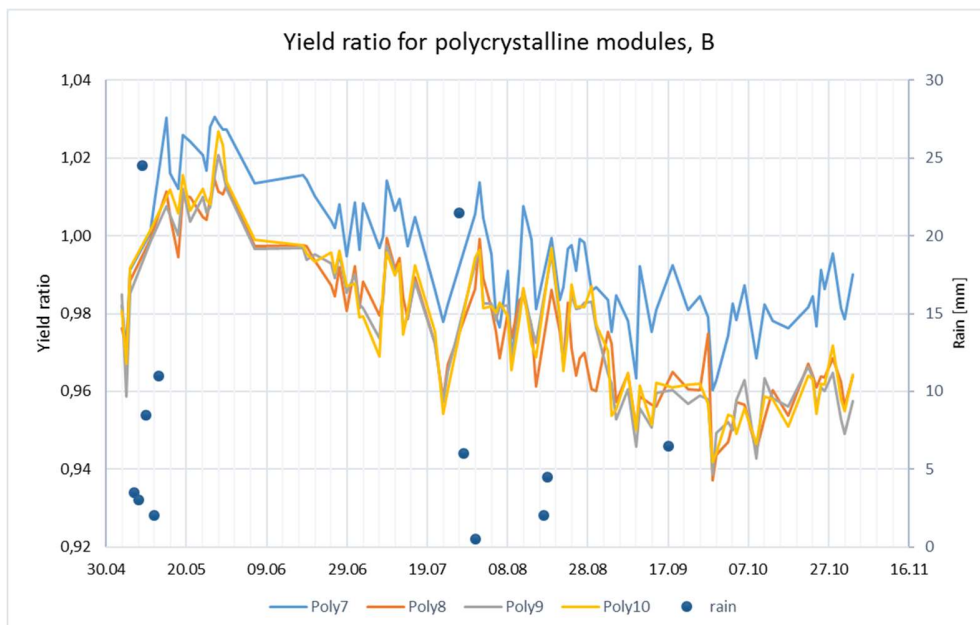


Figure 0.2: Yield ratio for poly Si-modules with cleaning strategy B.

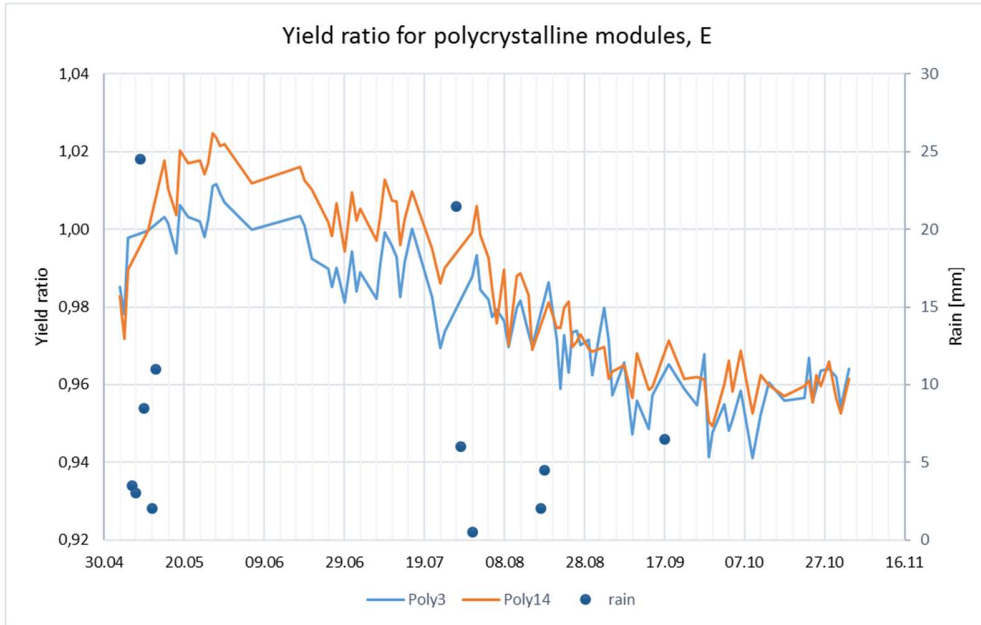


Figure 0.3: Yield ratio for poly Si-modules with cleaning strategy E.

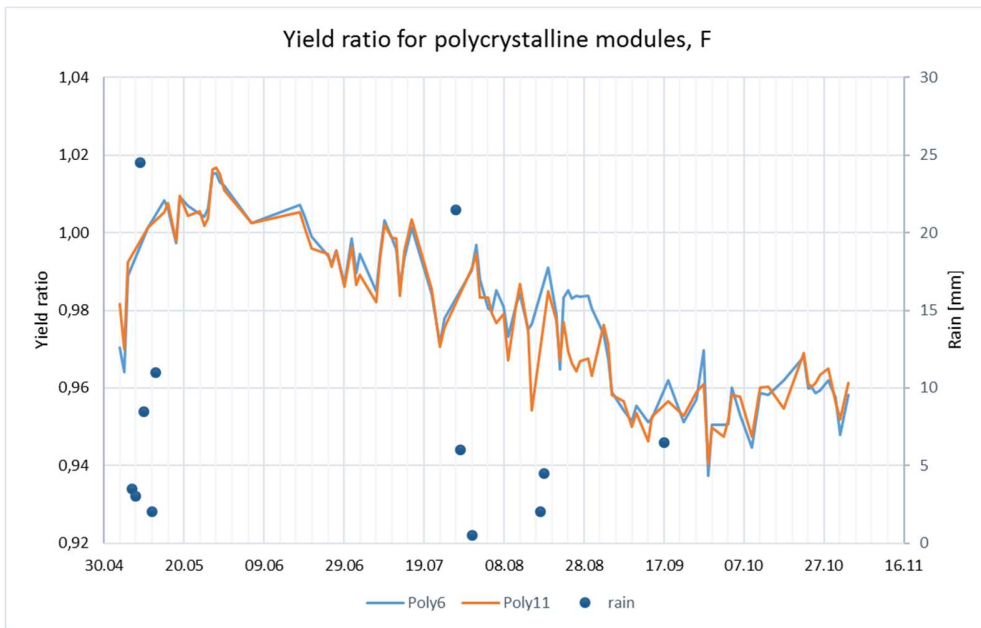


Figure 0.4: Yield ratio for poly Si-modules with cleaning strategy F.

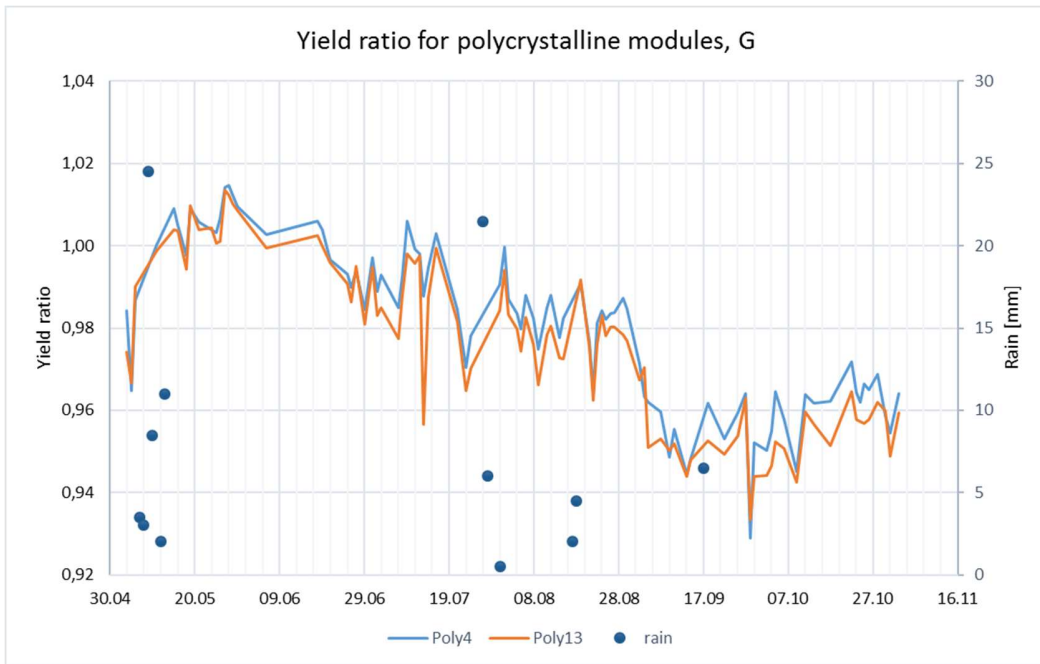


Figure 0.5: Yield ratio for poly Si-modules with cleaning strategy G.

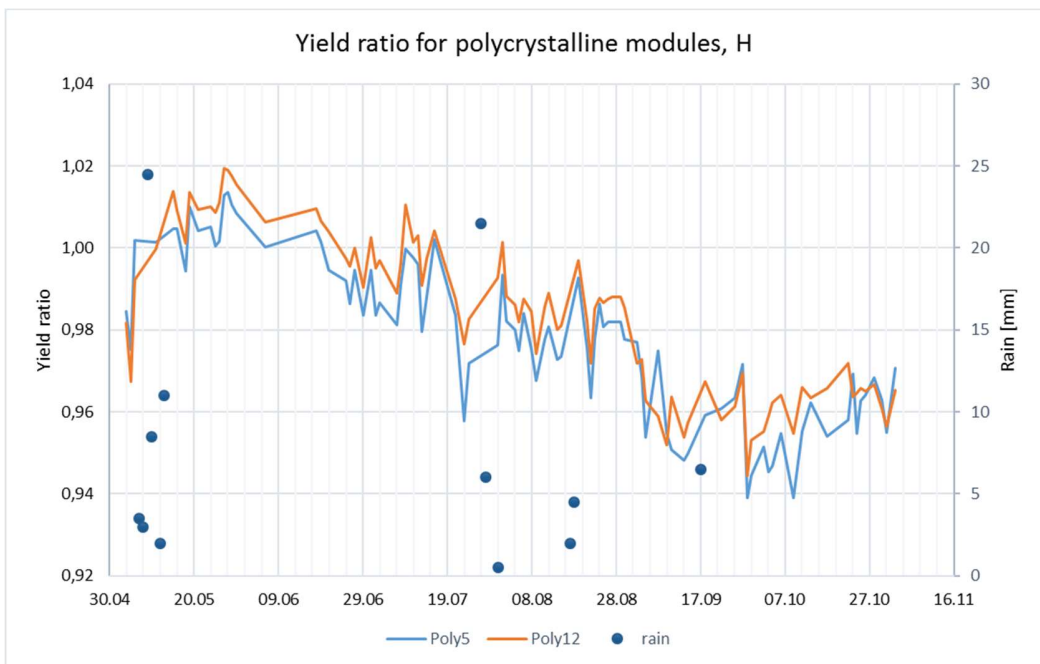


Figure 0.6: Yield ratio for poly Si-modules with cleaning strategy H.

Appendix D

Mass measurements conducted at Kalkbult and IFE, Kjeller.

The mass measurements conducted in Kalkbult are presented in Table 0-1 - Table 0-3. The cloths are weighed 1 – 3 times before ($m1$) and after ($m2$) cleaning. Four cloths are each day used to clean of the 12 – 18 lower cells of poly3 – 6. To verify the method, two unused cloths (test1 and test2) are on 17.10.2016 weighed at the same time as the cloths used to clean. The difference of the average mass before and after cleaning is also given ($m2 - m1$).

Table 0-4 shows the results of the weighing conducted at IFE, Kjeller, before and after the experiments in Kalkbult. Sample 1 – 4 were used to clean poly3 – 6 in Kalkbult 14.10.2016, and were also weighed two times on-site. Test 3 – 4 were brought to Kalkbult where the box they were transported in was opened and closed, before they were transported back to IFE, Kjeller.

14.10.2016

Dust sample taken: 9:31 – 9:35

Area, cleaned cells = 0.3 m²

On-site weighing, Kalkbult.

Table 0-1: Mass measurements conducted at Kalkbult, 14.10.2016.

Cloth	m1 ₁ [mg]	m1 ₂ [mg]	Avg. 1 [mg]	St.d. 1 [mg]	m2 [mg]	Diff [mg]
Poly3	682.5	682.1	682.3	0.3	693.0	10.7
Poly4	675.4	675	675.2	0.3	692.3	17.1
Poly5	679.8	679.2	679.5	0.4	689.3	9.8
Poly6	702.9	-	702.9	-	711.6	8.7

15.10.2016

Dust sample taken: 9:06 – 9:15

Area, cleaned cells = 0.3 m² (poly4 – 6), 0.4 m² (poly3)

Indoor weighing, Kalkbult.

Table 0-2: Mass measurements conducted at Kalkbult, 15.10.2016.

Cloth	m1 ₁ [mg]	m1 ₂ [mg]	m1 ₃ [mg]	Avg. 1 [mg]	St.d. 1 [mg]	m2 ₁ [mg]	m2 ₂ [mg]	m2 ₃ [mg]	Avg. 2 [mg]	St.d. 2 [mg]	Diff [mg]
Poly3	674.3	673	672.2	673.2	1.1	683.9	684.9	685.2	684.7	0.7	11.5
Poly4	673.1	671.7	672.3	672.4	0.7	677.7	678.3	-	678.0	0.4	5.6
Poly5	679.8	678.8	677.3	678.6	1.3	684.1	685.3	686.6	685.3	1.3	6.7
Poly6	686.1	-	-	686.1	-	690.9	688.9	-	689.9	1.4	3.8

17.10.2016

Dust sample taken: 8:42 – 8:52

Area, cleaned cells = 0.3 m²

Indoor weighing, Kalkbult.

Table 0-3: Mass measurements conducted at Kalkbult, 17.10.2016.

Cloth	m1₁ [mg]	m1₂ [mg]	m1₃ [mg]	Avg. 1 [mg]	St.d. 1 [mg]	m2₁ [mg]	m2₂ [mg]	m2₃ [mg]	Avg. 2 [mg]	St.d. 2 [mg]	Diff [mg]
Poly3	684.5	684.5	684.6	684.5	0.1	687.4	685.3	685.6	686.1	1.1	1.6
Poly4	701.9	700.7	701.5	701.4	0.6	708.1	708.4	707.8	708.1	0.3	6.7
Poly5	716.4	715.2	715	715.5	0.8	720.5	721.1	723	721.5	1.3	6.0
Poly6	755.7	755.4	755.6	755.6	0.2	759.1	758.1	759.2	758.8	0.6	3.2
Test 1	719.8	719.6	719.4	719.6	0.2	713.2	714.5	712.6	713.4	1.0	-6.2
Test 2	690.2	689	689.6	689.6	0.6	683.2	684.5	683.9	683.9	0.7	-5.7

IFE, Kjeller

m1: measured 29.09.2016

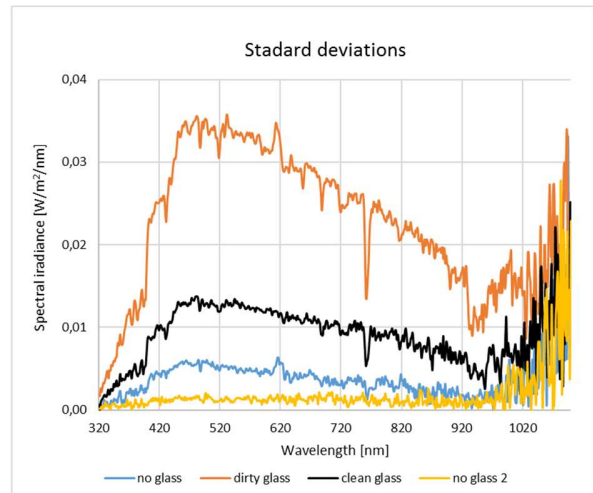
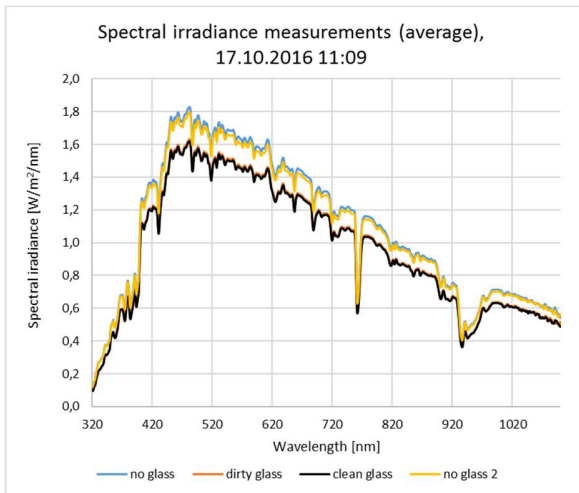
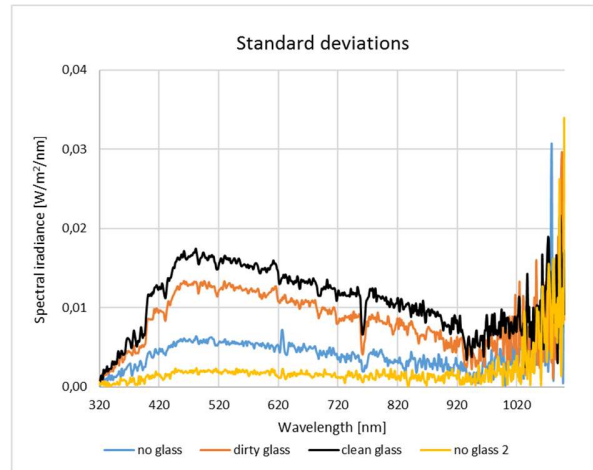
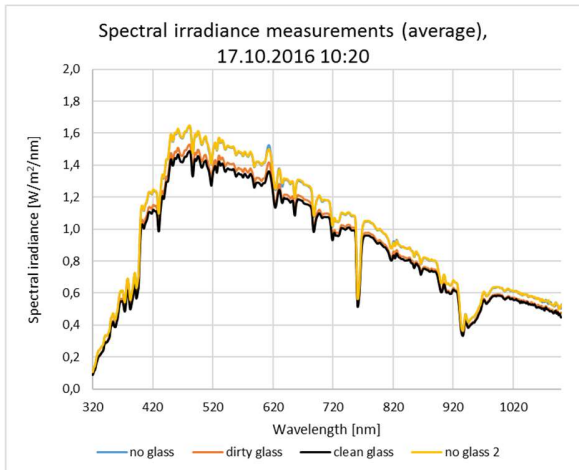
m2: measured 01.11.2016

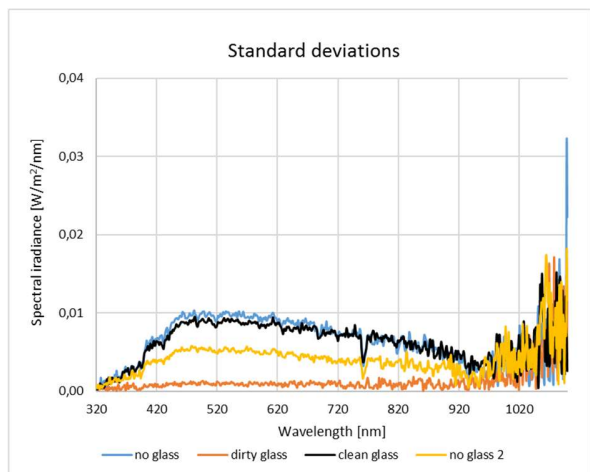
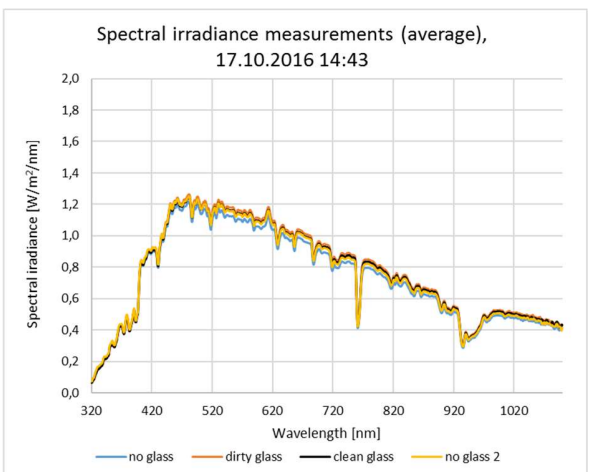
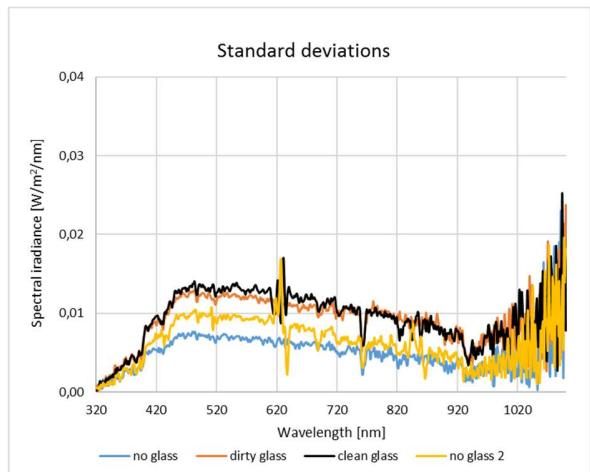
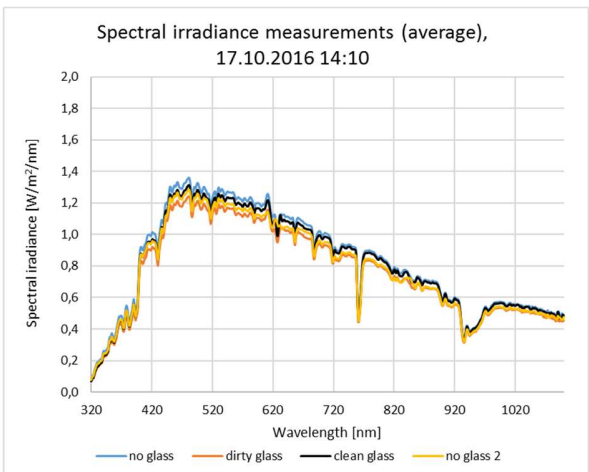
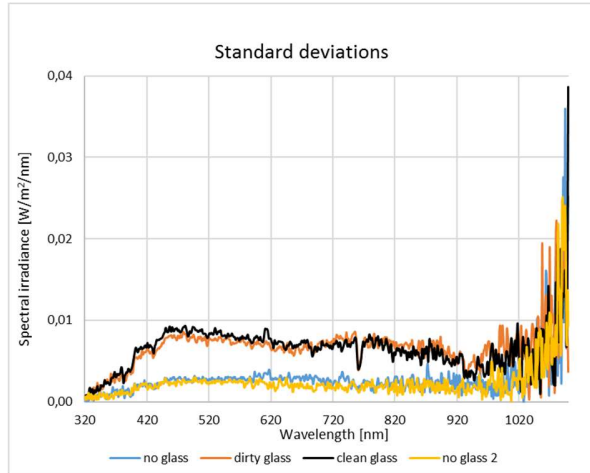
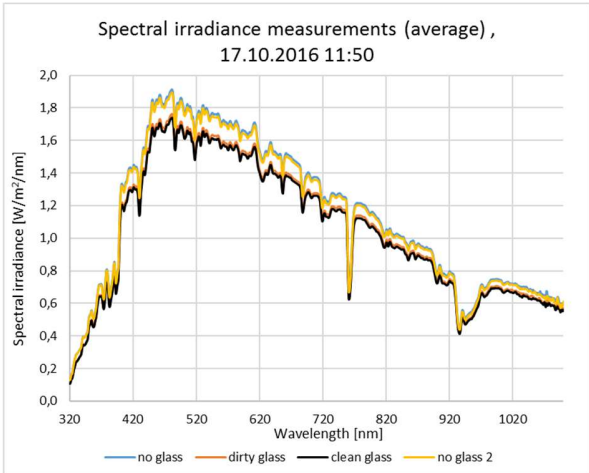
Table 0-4: Mass measurements conducted at IFE, Kjeller, 29.09.2016 and 01.11.2016.

Cloth	m1₁ [mg]	m1₂ [mg]	m1₃ [mg]	Avg. 1 [mg]	St.d. 1 [mg]	m2₁ [mg]	m2₂ [mg]	Avg. 2 [mg]	St.d. 2 [mg]	Diff [mg]
Sample 1	687.7	689.7	689.9	689.1	1.2	694.3	693.1	693.7	0.8	4.6
Sample 2	681.8	682.9	682.9	682.5	0.6	694.9	693.2	694.1	1.2	11.6
Sample 3	686.3	686.8	686.7	686.6	0.3	692.3	690.4	691.4	1.3	4.8
Sample 4	709.9	709.8	710.2	710.0	0.2	715.3	713.9	714.6	1.0	4.6
Test 3	678.1	678.2	678.7	678.3	0.3	670	668.8	669.4	0.8	-8.9
Test 4	694.4	695.5	695.2	695.0	0.6	687.7	685.7	686.7	1.4	-8.3

Appendix E

Transmittance measurements conducted at Kalkbult 17.10.2016 through clean glass, dirty glass and without glass for 7 different times of the day. The average and the standard deviation for the three measurements at each position are presented.





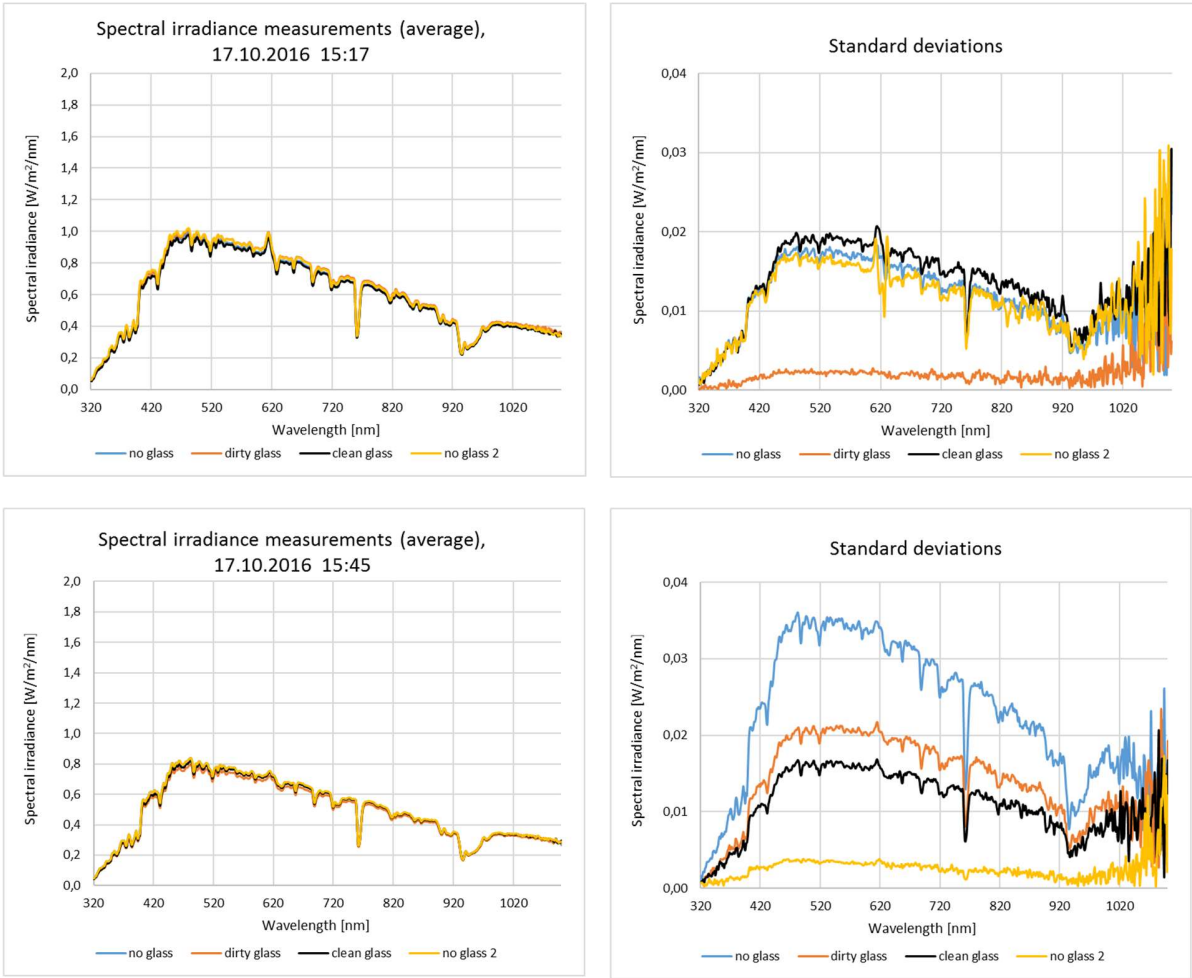


Figure 0.1: Average and standard deviations of the spectral irradiance measurements conducted 17.10.16 at Kalkbult.



Norges miljø- og biovitenskapelig universitet
Noregs miljø- og biovitenskapelige universitet
Norwegian University of Life Sciences

Postboks 5003
NO-1432 Ås
Norway